FRACTURE AND STRENGTH OF GLASSES AND GLASS FIBRES CONTAINING BISMUTH AND SILVER DISPERSOIDS

By

ANURADHA VENKATESWARAN

INTERDISCIPLINARY PROGRAMME IN MATERIALS SCIENCE

INDIAN INSTITUTE OF TECHNOLOGY KANPUR

AUGUST, 1979

FRACTURE AND STRENGTH OF GLASSES AND GLASS FIBRES CONTAINING BISMUTH AND SILVER DISPERSOIDS

A Thesis Submitted
In Partial Fulfilment of the Requirements
for the Degree of

MASTER OF TECHNOLOGY

By

ANURADHA VENKATESWARAN

to the

INTERDISCIPLINARY PROGRAMME IN MATERIALS SCIENCE

INDIAN INSTITUTE OF TECHNOLOGY KANPUR

AUGUST, 1979

to

my parents

CERTIFICATE

This is to certify that this work entitled 'Fracture and Strength of Glasses and Glass Fibres Containing Bismuth and Silver Dispersoids' by Ms. Anuradha Venkateswaran has been carried out under my supervision and that it has not been submitted elsewhere for a degree.

D. Chakravorty
Professor
Departments of Metallurgical Engg. and Materials Science
Indian Institute of Technology,
Kanpur

ACKNOWLEDGEMENTS

I am extremely grateful to Dr. D. Chakravorty for his unstinting and excellent guidance throughout the course of this work.

My thanks are due to Mr. B. Sharma, Mr. Nar Singh, Mr. Sagar Das, Mr. O. P. Malaviya, Mr. R. K. Prasad and Mr. V. P. Vohra for prompt help rendered whenever necessary.

I am very much obliged to Mr. Devendra Kumar, Mr. B. P. Kashyap, Mr. Syamal Chakrabarti, Mr. G. C. Das and Mr. Yogesh Chandra for helping with the experimentation.

I would also like to acknowledge the help rendered by Mr. M. H. Rehman, Mr. D. K. Sarkar, Mr. O. P. Bajaj and Mr. K. P. Mukherjee.

Thanks are due to Mr. N. Ahmad for his excellent typing, to Mr. V. P. Gupta for the superb drawings and to Mr. Vishwanath Singh for the cyclostyling.

CONTENTS

LIST OF TABLES

LIST OF FIGURES

LIST OF PHOTOGRAPHS

Photographs Page

SYNOPSIS

This is a study of the effect on the fracture and strength of glass compositions in the systems SiO_2-B_2O_3-Al_2O_3-K_2O and SiO_2-CaO-MgO-Na_2O-As_2O_3 due to the incorporation of Bismuth and silver dispersoids respectively.

In the Bismuth glass series the Rupture Modulus and Young's Modulus in bending for bulk glass containing metal are higher than those of the base glass. Tensile strengths and Young's Modulii of Bismuth containing glass fibres are also higher than values for the base glass fibres. Strengthening is attributed to modulus enhancement and flaw size limitation by the dispersions. Thermo-mechanical mismatch is also expected to play a positive role.

In the case of the silver glasses, there is no appreciable change in the modulus of the base glass due to the incorporation of the metal, because the intrinsic Modulii of silver and the base glass are very similar. The rupture Modulus for bulk, metal containing samples is higher than that of the base glass. This is due to thermomechanical stresses and also to flaw size limitation. The tensile strengths of fibres in this series are lower than that of the base glass. Optical microscopic evidence shows that whereas the crystalline phase is fairly regular in shape in the bulk silver glasses, in the silver glass fibres; the

crystalline phase shows up as sharp streaks parallel to the fibre axis, and probably acts as stress concentrators.

Transmission Electron Microscopy has been used to observe the microstructure of glasses and glass fibres and also to evaluate the shapes, sizes and volume fractions of the dispersed phase. Attempts have been made to correlate observed microstructure with measured mechanical properties.

X-ray Diffraction and selected Area Diffraction in TEM have been used to identify the crystalline phase. This is Bismuth in the case of glasses in the Bismuth series and silver and calcium magnesium silicate in the case of the silver series.

Fracture surfaces have been studied by a two stage replica process to compare the fracture in the metal containing and the base glasses. The fracture surface is much rougher in the case of the metal containing glasses; this is attributed to the fact that the crack front follows a more tortous path in such glasses. Replicas also show the interaction of the crack front with the second phase.

Chapter 1

INTRODUCTION

There is an increasing demand for high-performance materials for use in a very wide range of applications ranging from military and aerospace to biomedical and interest has been focussed on materials for limited or prolonged use at high temperatures. Originally metals were in the limelight but it was soon discovered that conventionally precipitation hardened metal alloys are not thermally stable and can undergo coarsening at temperatures even well below the softening point of the alloy, thus leading to a decrease in mechanical strength. Dispersion strengthened metals are found to lack adequate ductility at low and intermediate temperatures and are consequently prone to catastrophic failure. Metal matrix composites reinforced with ceramic fibres are rather prone to thermal degradation due to differences in the matrix-reinforcement thermal expansion coefficients. Many glasses and ceramics on the contrary exhibit fairly high strength and stability at elevated temperatures combined with a low density and chemical inertness. These are however brittle materials, subject to high notch sensitivity and thermal shock and fail catastrophically. It is in order to increase the

fracture toughness and the strength of such materials, that discrete particles with suitable thermal expansion coefficients and elastic moduli have been incorporated into the glass/ceramic matrix to act as barriers to crack propagation.

1.1 Dispersion Strengthened Glasses: Production

Dispersion strengthened glasses can be produced in a variety of ways. The second phase can be precipitated 'in situ' by a suitable choice of alloying additions and heat treatment and also by controlling the furnace atmosphere during the glass manufacture. Certain glasses can be induced to undergo phase separation to produce amosphous matrix - amorphous second phase composites or can be partially crystallized to form amorphous-crystalline composites. The latter includes low crystalline volume fraction glass ceramics. Standard powder metallurgy methods such as hot pressing have given rise to various glass/ceramic dispersion strengthened systems containing a fairly wide range of particle sizes and volume fractions of the second phase. Metals like Au, Ag and Cu can also be incorporated into glass by adding very small amounts of the metal in the glass batch along with a small amount of photosensitive nucleating agent and then subjecting the glass to a nucleation treatment by irradiating with X-rays, γ-rays or U.V. rays of a suitable wavelength followed by controlled heat treatment for their further growth.

1.2 Theories of Dispersion Strengthening

Glasses being brittle materials, once a crack is initiated in them, there is no resistance to its propagation and consequently the failure occurs with no warning whatsoever. The focus was originally on producing stronger and tougher glasses so that a higher fracture initiation stress exists at failure, but, nevertheless failure is still catastrophic. Since it is impossible to fabricate an absolutely flaw free brittle component, crack initiation is a 'built in' stage and the key to producing stronger and tougher ceramics and glasses lies therefore in prolonging or arresting the crack propagation stage.

Gupta[1] has shown by means of a qualitative model based on thermodynamic criteria that stronger and tougher glasses can only be produced by resorting to multiphase systems as opposed to single phase ones. The essence of stable crack propagation is that when crack arrestors are present in a brittle matrix, the energy demand curve for crack propagation is nonlinear in contrast to a linear demand curve for the ideal Griffith material. For a single phase homogenous brittle material, the energy demand is the same throughout the material and the crack initiation and propagation stages coincide. In multiphase materials there is however a distinct division in energy demand between various

phases so that the initiation and propagation stages are distinct. The second phase stabilises a growing crack because when the crack encounters the particle it has either to cut through or detour around the zone and the energy demand suddenly increases. Crack propagation will therefore be halted unless there is an increment in the operating stress. The toughness and strength of such multiphase materials is thus higher than that of the single phase brittle matrix.

Dispersion strengthening of a continuous glass matrix has been attributed by Hasselman and Fulrath[2] to the fact that hard crystalline dispersions within the matrix will limit the size of the Griffith flaws thereby raising the stress required to initiate or propagate a crack. They divided the effects of dispersions on the size of flaws distributed throughout the bulk or surface of the glass into two regions. In the first, the average distance between particles is greater than the flaw size, a condition which is obtainable with suitable volume fractions and particle sizes of the second phase.

In this region, the size of an average flaw will be reduced according to the equation

$$a = a_o (1 - \phi) \qquad (1)$$

where a and a_o are the flaw sizes in the composite and glass

matrix respectively and ϕ = volume fraction of dispersed phase.

Substituting this equation into the Griffith relation[3] for the macroscopic strength S_o of a flat glass plate containing an elliptical flaw viz.

$$S_o = \left(\frac{4\gamma E}{\pi a}\right)^{\frac{1}{2}} \qquad (2)$$

γ = surface energy or energy associated with the formation of unit area of the surface formed by fracture; E = Elastic Modulus of the system and a = twice the major axis of the ellipse, i.e. the flaw size.

Substituting for 'a' from (1) into (2) and rearranging gives

$$S = S_o (1 - \phi)^{-\frac{1}{2}} \qquad (3)$$

At higher volume fractions or smaller particle sizes, the flaws as given by (2) will be larger than the average distance between particles which means that the flaw size is now governed by the mean free path between the particles. This is region II. An expression for the mean free path 'λ' between spherical particles of uniform radius R distributed statistically through a matrix takes the form

$$\lambda = \frac{4R}{3} \frac{(1 - \phi)}{\phi} \qquad (4)$$

and a substitution for 'a' in equation (1) gives

$$S = \left[\frac{3\gamma E \phi}{\pi R(1-\phi)}\right]^{\frac{1}{2}} \qquad (5)$$

A plot between strength and reciprocal square root of mean free path should therefore be practically horizontal at high values of mean free path and should show a change in slope at the point where mean free path equals the original flaw size. Thereafter as the mean free path decreases further, the plot should follow a straight line through the origin.

Lange[4] postulated a different model to account for dispersion strengthening of glass. His model is based on the fact that a crack front possesses a line energy and tends to bow out between the second phase dispersion while still remaining pinned at all positions where it encounters the dispersion. Thus, during the initial stage of crack propagation, both new fracture surface and the length of the crack front is increased due to its change in shape between pinning positions and the fractional increase in crack front per unit crack extension will depend on the particle spacing. Catastrophic failure occurs when the crack front just breaks away from its pinning positions and the fracture energy depends not only on the amount of energy required to form new surface area but also on the spacing between the dispersed second phase. This is represented in the equation

$$G_c = 2\left(\gamma_o + \frac{T}{\lambda}\right) \qquad (6)$$

G_c = amount of energy required to extend a crack by a unit length, γ_o = surface energy of the material/unit area, T = line energy per unit length of crack front and λ equals

distance between second phase dispersions.

The strength of a material $S \propto \sqrt{G_c}$ (Irwin 1958) (7)

Thus the strength of a composite containing a second phase dispersion is inversely proportional to the square root of the distance between the second phase dispersion.

Dispersion strengthening may also be looked at in the light of elastic moduli, Thermal Expansion Coefficients and Thermo-Mechanical stresses.

Load sharing occurs in a dispersion of a higher modulus second phase in a lower modulus glassy matrix. If the components in the system share the applied load in proportion to their elastic moduli, the strain in all components in unidirectional tension will be the same or in other words the matrix and the second phase deform to the same extent. Then

$$\varepsilon_p = \varepsilon_g = \varepsilon_T$$

and

$$\sigma_p/E_p = \sigma_g/E_g = \sigma_T/E_T, \text{ giving by rearrangement:}$$

$$\sigma_{f_T} = \left(\frac{E_T}{E_g}\right) \sigma_{f_g} \qquad (8)$$

where subscripts p, g and T refer to the second phase, the glassy matrix and the composite system respectively. Subscript f refers to conditions at fracture. This mechanism depends on an effective stress transfer to the dispersed

phase; which requires that the bonding between the dispersed phase and the matrix should be very strong.

Borom[5] put forward the theory that thermomechanical mismatch between the second phase and the glass matrix gives rise to a state of variable compressive stress throughout the matrix, which would oppose crack propagation. The development of a variable compressive stress in the glassy matrix can be visualized by considering the stresses for the case of a single particle of a high expansion coefficient material cooled from a high-temperature zero-stress state in a lower expansion coefficient matrix. The particle is in a state of hydrostatic tension and the matrix experiences at the interface, hoop compressive stresses and radial tensile stresses which decrease as the distance from the interface increases. The boundary conditions for the stress distribution in the above concentric sphere case require that the radial tensile stresses decrease to zero at a free surface but the hoop compressive stresses do not. In a low-expansion matrix containing a random dispersion of high-expansion spheres, the radial tensile component need not decrease to zero between particles but, due to interaction with the higher and more gently decaying hoop compressive stress from an orthogonally positioned pair of particles, the radial tensile component can be reduced or even reversed in sign. Such an interaction would thus create compressive stresses in the glass matrix.

The shape of the second phase particles would also affect the strength of the composite. Spherically shaped particles have the lowest stress concentrating effect, whereas adversely shaped particles with sharply pointed dimensions could act as very effective stress concentrators.

The net effect of the second phase particles is thus a combination of a variety of factors such as Elastic Moduli, Thermal Expansion Coefficients, shape size and volume fractions of the dispersed phase, original flaw size in the glass matrix, interfacial bonding and the existence of residual or localized stresses. The maximum strength attainable by particle reinforcement is generally only 2-3 times that of the unreinforced matrix.

1.3 Glasses Containing Bismuth and Silver

Silver has been grown[6] by subjecting a glass of composition 71.5 SiO_2, 23.5 Na_2O, 4 Al_2O_3, 1 ZnO, 0.02 CeO_2 (photosensitive nucleating agent) and 0.002 Ag (all weight percents) to irradiation with UV light and then to a controlled heat treatment to get silver particles of about 160 Å size which are spherical in shape.

Keshavaram[7] has studied some mechanical properties of glasses containing silver incorporated due to the addition of Ag_2SO_4 in the original glass batch. Glasses in the

system SiO_2-B_2O_3-Sb_2O_3-K_2O-Al_2O_3-As_2O_3 containing 4 and 6 mole Ag_2O were found to exhibit strengths of about two to three times that of the corresponding glass matrices. Transmission electron micrographs of such glasses revealed dark droplets of almost spherical shape distributed statistically in the glassy matrix. Sizes of the particles were measured to lie between 450-1200 Å.

Chakravorty, Vithlani and Mehta[8] have studied the Self Diffusion coefficients of sodium for glasses in the system Na_2O-B_2O_3-Bi_2O_3-SiO_2 and have also studied their D.C. resistivities in the same range of temperature. The glasses were found to have a microstructure consisting of a distribution of droplets of an electronically dense phase in the glassy matrix. From correlation factor studies, they concluded that the droplet phase does not consist solely of Bismuth, but also contains some Alkali ions.

Electrical and switching properties of various other glasses containing Bi_2O_3 in the systems Na_2O-Bi_2O_3-B_2O_3[9], Na_2O-CaO-SiO_2-Bi_2O_3[10] and PbO-Bi_2O_3-B_2O_3[11] have been studied, and in all cases similar microstructures have been observed.

Bismuth and silver can be incorporated fairly easily (even though silver is rather prone to coagulation) into a variety of glass matrices, giving rise to glass-crystal-

composite systems. Volume fractions and particle sizes of the dispersed phase can be varied by preparing glasses containing different amounts of Ag_2O or Bi_2O_3 and/or by controlling the melt conditions.

1.4 Glass Fibres

The theoretical strength of glass is 10^6 psi, but strengths achieved in practice are known to be less than a hundredth of this value. This is because the strength of glass depends almost entirely on the condition of the surface and particularly on the presence of stress-concentrating features of both a microscopic and a macroscopic nature. These could be holes, notches, steps or changes of section, inclusions etc. For glass, the apparent ratio of strength of fine glass fibres to that of bulk glass is about 50:1. Griffiths in 1920 suggested that the surface of bulk glass contained innumerable small flaws of average depth 5μ. which acted as stress concentrators. In fibres, such deep flaws are not possible and the possibility of encountering them would decrease as the diameter of the fibre decreases. The surface area of a fibre is also very much less than that of bulk glass and consequently the density of flaws is also correspondingly much less. Again, during the drawing process, pores and gas bubbles get elongated into capillaries along the central line of the fibre (leaving the surface free) and their stress concentrating effect is reduced.

In fibres subject to damage by abrasion, the 'size' effect is due entirely to the fact that flaw density increases with increasing surface area. This fact was established conclusively in 1960 by Thomas,[12] who showed that an unabraded or 'virgin' fibre did not show any appreciable change in strength over a wide range of diameters.

Fibres drawn from silver containing glasses were shown by Keshavaram to exhibit a slightly higher strength than the fibres of the corresponding base glasses.

The major application of glass fibres is in composites. The most extensively used fibres are that of 'E' glass and have a virgin Tensile Strength of 5×10^5 psi and a Modulus of Elasticity of about 10.95 mpsi.

Chapter 2

OBJECTIVES OF STUDY

(1) To incorporate Bismuth and Silver dispersoids into glass systems SiO_2-Al_2O_3-B_2O_3-K_2O and SiO_2-Na_2O-CaO-MgO-As_2O_3 respectively.

(2) To draw fibres from all the metal containing and base glass compositions.

(3) Measurement of Rupture Modulus and Young's Modulus in bending for all the bulk glasses.

(4) Study of Tensile strength and Young's Modulus of fibres drawn from all the compositions.

(5) DTA studies to observe the effect of metal additives on the glass Transition Temperature of the base glass.

(6) Transmission Electron Microscope studies to determine the microstructure of all the glasses and the glass fibres and to correlate measured mechanical properties with observed microstructure.

(7) Optical Microscope studies on crystallized glasses and glass fibres to observe shapes, sizes and volume fractions of the crystalline phase.

(8) X-ray diffraction studies on crystallized bulk glasses and glass fibres to identify the crystalline phase.

(9) Fracture surface replica studies to compare the fracture of the metal-containing glasses with that of the base glasses and to study the interaction of the crack front with the dispersed phase.

Chapter 3

EXPERIMENTAL

3.1 Preparation of Glass

Nine glass compositions in all were studied and are listed in Table 3.1A. Reagent grade chemicals were used in their preparation. K_2O, Na_2O and CaO were added as their carbonates, Ag_2O was added as Ag_2SO_4 and B_2O_3 was taken in the form of H_3BO_3. Requisite quantities of batch powders were weighed out in an analytical balance transferred to a mortar and mixed thoroughly with the aid of Acetone.

In each case the batch was melted in alumina crucibles. An electrically heated 'globar' furnace with a maximum attainable temperature of 1450°C was employed for the melting of the Bismuth containing glasses and an Alumina lined gas fixed furnace capable of withstanding temperatures up to about 1700°C was used to melt the silver containing glasses as well as the corresponding base glass compositions. An oxygen-Indane gas mixture was used as fuel in the gas fired furnace whereas the globar furnace melting was carried out under ordinary atmospheric conditions. In both cases, the heating rate was kept fairly slow uptil 1800°C, partly to avoid cracking of the crucibles due to thermal shock and partly because gases

like CO_2, SO_2 and H_2O are given out in this range of temperature. Glass melts were stirred from time to time with an alumina rod, partly to remove bubbles and partly to judge when the casting consisting was reached. Achievement of bubble free glass was found rather difficult in the case of the Bismuth glasses, as they tend to corrode the crucible if kept at high temperatures for fairly long periods of time. It was also found to be very difficult to prevent the coagulation of silver during the melting of the silver containing glasses. In all cases, the glasses were cast onto Aluminium molds to slabs of dimension 20 cm x 4 cm x 1 cm and then annealed slowly from a suitable annealing temperature (Table 3.1b) up to room temperature.

3.2 Conversion of Bulk Glass to Glass Fibre

Fibres were drawn from all the nine glass compositions in a resistance heated globar furnace.with a maximum attainable temperature of 1550°C. The rates of heating and cooling were kept to within 150°C/hour. The shape and dimensions of the single hole high Alumina Bushing employed for fibre drawing are shown in Fig. 3.2. The diameter of a fibre of a given composition depends on various factors such as Bushing temperature, Bushing-tip temperature, Head of glass in the bushing, fibre winding speed, diameter of the nozzle of the bushing, Bushing design etc. The shape and size of

the bushing used was the same in all cases and so also the nozzle diameter. The bushing was filled with glass up to 3/4 of its total height in the case of the Bismuth glass series whereas only a quarter filled bushing was used for the silver glasses. Fibre drawing temperatures and winding speeds were so manipulated as to get fairly fine fibres in all cases. Furnace temperatures during drawing ranged from 960°C to 1340°C. Fibre diameters are in the range 5 μm-11μm except in the case of Glass 6 for which the range is 8-15 μm. Winding speeds varied from 2666.3 - 2912.4 ft/min. Fibre drawing parameters are listed in Table 3.1B.

3.3 Ultimate Tensile Strength and Young's Modulus of Fibres

In the case of the Bismuth glasses, the untouched filaments or 'virgin' fibres between the bushing and the winding drum were mounted for testing during the drawing process itself. A few 'off the drum' fibres were also tested to see whether there was any appreciable change in strength between the two. In the case of the silver glasses, only 'off the drum' fibres were tested.

Fairly stiff, smooth rectangular bits of paper of width 1.5 cm, thickness 0.5 mm and lengths of about 6.0 cm more than the test gage length of fibres were used as fibre mounts. An oval slot of about 1.2 cm semi minor axis

and a length exactly equal to the test gage length of fibres and parallel to the length of the mount was cut in the centre of each mount. The fibres were then mounted in a line through the centre of each slot and parallel to the length of the slot. Quick fix was used at the mouths of the oval slot to hold the fibre firmly to the mount. The extra lengths of fibre extending for about 3 cm beyond the slot on either side were fixed to the ends of the mounts by using cellotape. These extra ends were used for diameter measurements in cases where the bits of fibre remaining within the gage length after breaking were too small to be of any use. The mounts were stored by suspending them vertically from a round circular stand which just fitted into a dessicator. Since fibres could usually be tested only a day or so after mounting, this ensured that in the meantime the fibres were protected from attack by moisture and dust particles and also from further abrasion.

The Instron was used to break the fibres in tension. The load cell used had a range 0-50 gms with a least count of 0.1 gm. A uniform chart speed of 2 cm/min was used throughout. Two cross head speeds were tried out, one of 0.02 cm/min and the other of 0.05 cm/min. Gage lengths tested were 2.0 cm and 5.0 cm respectively.

The Instron was first calibrated and then the fibre mount was suspended freely from the upper grip of the machine and adjustment was made for the weight of the mount. The

fibre mount was then firmly grippeo between the two grips of the Instron ano the loao was then aojusteo to a suitable reference zero. The sioes of the mount were then cut carefully, leaving the fibre intact so that when the cross heao was maoe to move, the fibre took up the entire loao. Fibres were pulleo to breaking ano the breaking loaos were reao off oirectly from the Instron chart. Strains were obtaineo by use of the following equation:

$$\text{Strain} = \frac{\text{Cross Heao Speeo x Time Taken for breaking}}{\text{Original gage length of the fibre}} =$$

$$\frac{\text{Cross Head Speed x Total Distance Covered by Chart Upto Point of Breaking}}{\text{Chart speed x Original gage length of fibre}} \qquad (9)$$

The oiameter of the fibres were measureo after breaking. Two different instruments were trieo out for this purpose -- A reflected light optical microscope ano a horizontal 'Sheffielo' Accution. Fibre oiameters were measureo at a magnification of 750X in the optical microscope using a calibrateo eyepiece capable of reaoing up to 0.1967 µm. Since fibre oiameters were measureo in air ano not in a meoium of suitably contrasting refractive inoex, oiffraction banos were obtaineo on either sioe of the fibre. These banos hao to be incluoeo in the oiameter of the fibre as it was impossible to oistinguish where the fibre enoeo ano the oiffraction bano began.

A Sheffield horizontal Accutron was also used to measure fibre diameters. The Accutron was first calibrated by using standard slip gages and then the pointer on the scale was adjusted to zero with the tips of the horizontal measuring device just touching each other. The fibre was then introduced between the two tips and their resulting separation was read off directly on the graduated scale to accuracy of 0.00001" or 0.2540 μm. For fibres fatter than about 10.2 μm, the scale was switched to the next higher one which could read diameters up to 20.3 μm with a least count of 0.508 μm.

Between 12-20 fibres were tested of each composition and the ultimate Tensile strength (UTS) was calculated in each case. The Young's modulus was obtained by dividing the ultimate Tensile Strength of each fibre by the strain as obtained from equation (9). Results are presented in the Tabular form and also in the form of Histograms.

3.4 Rupture Modulus and Young's Modulus in Bending of Bulk Glass

The rectangular slabs of glass of dimensions 20 cm x 4 cm x 1 cm were sliced (parallel to the width of 4.0 cm) into slices of width about 1.0 cm using a Diamond tipped wheel. These rectangular slices were then ground down to dimensions of about 4.0 cm x 0.5 cm x 0.5 cm using in

succession SiC of mesh sizes 100 and 240. After the dimensions were thus reduced, rough polishing was carried out with SiC of mesh sizes 400, 600 and 800 in that order. Ultimately Al_2O_3 powder of 0.3 μm size was used to impart an optical finish to the glass surfaces.

CT-3 strain gages (Rohits Co. India) of resistance 122 ohms and gage factor 1.96 were then affixed (one to each glass slab) to a surface of the polished slab using SR-4 strain gage cement. After fixing, a 1.5 Kg weight was kept firmly pressed onto the strain gages for at least 24 hours to ensure a strong bonding. Long strain gage wires were then soldered to the strain gages. The samples were then broken by 3-point bending in a jig of the type shown in Fig. 3.4. The modulus of rupture of the rectangular beams for centre loading was then calculated using the expression

$$\sigma_f = \frac{3}{2} \frac{P_f L}{bd^2} \qquad (10)$$

where P_f = breaking load or force, L = span or distance between the two outer (knife) edges of the jig, b = width and d = thickness of the bar. The stress at any load P can also be obtained from the above expression.

For determining the Young's Modulus in bending, the strain gage attached to the sample was connected in a quarter bridge circuit and strains were read off at load intervals of 2.5 Kg (or less) in the load range from zero load to breaking load in a Budd P350-A Model Strain Indicator.

Stresses were calculated at every 2.5 Kg (or less) load interval and were then plotted against the corresponding strains as read off on the strain indicator. The slope of the plot gives the Young's Modulus in Bending in each case. An average of about four specimens of each composition were tested and the mean values of the Ultimate Tensile Stress (UTS) and the Young's Modulus in Bending E_b were calculated for each composition.

3.5 Microstructure of Glasses and Glass Fibres by Transmission Electron Microscopy

To prepare samples for TEM studies from Bulk glass, the surface of a slice of glass was cleaned thoroughly with Acetone and then scratched with a fine tipped diamond scratcher. Very small wedge shaped particles were thus obtained and a few of these were transferred onto a 200 mesh copper grid coated with a carbon layer about 100-200 Å thick. The thin edge of the wedge shaped particles is about 100 Å thick and was found to be transparent to the electron beam. The sample containing grid was then coated with another layer of carbon of about the same thickness. The carbon films provided a mechanical support to the glass particles and prevented them from falling off the grid into the EM column. They also served to conduct heat away from the glass particles which are very poor conductors of heat.

The grid containing glass particles sandwitched between two layers of carbon was then studied by TEM.

For fibre studies, a bunch of glass fibres was powdered in an agate mortar to 325 mesh size and a pinch of fibre powder was added to about 10 cc of distilled water in a clean test tube. The test tube was subjected to ultrasonic shaking for about 2 minutes to disperse the powder. It was then left undisturbed for 5-10 minutes to allow the heavier particles if any to settle down. A drop of the milky top solution was pipetted onto a carbon coated grid and was allowed to dry. Another carbon layer was then coated onto the powder just as in the bulk glass sample. This method of preparing fibre samples gave a uniform dispersion of fine particles throughout the grid.

Microstructural details were photographed in the TEM and SAD patterns were also recorded to study the crystalline phase.

Photographs of microstructure were used to measure particle sizes and volume fractions of the dispersed second phase.

3.6 Preparation of Fracture Surface Replicas for TEM Studies

A two-stage replica technique was adopted for studying the fracture surfaces of the metal containing and the base

glasses. The fractured surface of the specimen was cleaned thoroughly using El Acetone. A square of cellulose Acetate based replicating tape cut to dimensions slightly bigger than those of the fracture surface was dipped carefully into El grade Acetone such that only one surface touched the Acetone. The sticky side of the replicating tape was then pressed down carefully and firmly onto the fracture surface. After about fifteen minutes the edges of the tape sticking out beyond the fracture surface were trimmed and the entire section of tape was lifted carefully off the fracture surface with the aid of a strip of cellotape. The strip of cellotape with the fracture replica facing upwards was fastened firmly onto a thoroughly cleansed glass slide. A layer of Gold about 50 Å thick (just sufficient to impact a faint bluish tinge) was then evaporated onto the glass slide at an angle of about 5-10. Immediately afterwards the slide was coated with a 150-200 Å thick carbon layer. The coated square of replicating tape was then cut out and lifted away from the cellotape. The square was then quartered and each of the quarters were transferred to a dish containing El grade Acetone. After about half an hour the plastic dissolved and the carbon coated gold film floated on the surface. These films were then fished out and transferred to fresh El grade Acetone in another dish. After another half hour when no plastic was left adhering to the film,

it was lifted out on a 200 mesh copper grid, dried for a few minutes and then studied under the TEM. A 60 KV beam potential was used for all samples as it was found to give a good contrast.

3.7 X-Ray Diffraction Studies of Crystallised Glasses and Crystallised Glass Fibres

Some of the glasses and glass fibres were suspected to be crystallized and then X-ray diffraction patterns were studied in order to identify the crystalline phase present. Each of the crystallized glasses and glass fibres were powdered separately in an agate mortar to a fine powder of particle size smaller than 325 mesh. This powder was mounted on a perspex mount in the case of glasses 7 and 6 respectively and on a clean glass slide in the case of glass 5 and glass fibres 5 and 7. The samples were scanned in the diffractometer from 20° to about 80°, using CuK_{α} radiation of wavelength 1.54062 $\mathring{A}$. Two different c.p.s. were used, one of 100 and one of 500. Angles at which well defined peaks occurred were noted down in each case and the corresponding 'd' values were calculated from the Bragg equation

$$2d \sin \theta = n\lambda$$

n = an integer, here taken as unity

λ = Wavelength of X-ray radiation

θ = Bragg Angle

d = interplanar spacing.

The 'd' values and the relative intensities of observed peaks were then compared with standard data from the A.S.T.M. tables in order to identify the crystalline phase.

3.8 Microstructural Studies by Optical Microscopy

Crystallised glasses and glass fibres were studied under a reflected light optical microscope. The glass fibres were focussed at a magnification of 750X when the crystalline phase showed up as bright streaks along the length of the fibre. Photographs were taken at a camera magnification of 1/3rd the microscope magnification with exposure times of 2, 3 and 5 secs respectively. Optimum contrast was obtained with the 5 sec exposure.

For crystallised bulk glass studies, the glass surfaces were polished down to 0.3 μm surface finish and then etched for a suitable length of time in a 5% HF solution for a suitable contrast. Photographs were taken with exposure times of 2, 3 and 5 secs respectively at a microscope magnification of 300x. Camera magnification was 100x.

Wherever possible, the volume percent of the crystalline phase was computed from the photographs by using the point counting technique. A transparent graph sheet was pinned to the photograph and the no. of intersection points of the graph paper which coincided with the crystalline phase were noted.

The total number of intersection points in that area of the graph paper were also noted. The percent volume of crystallization was then obtained from the expression,

$$\text{Percent volume crystallization} = \frac{n}{N} \times 100$$

where n = number of intersection points in the selected area of graph paper which coincide with the crystalline phase.

N = Total no. of intersection points in the selected area of graph paper.

3.9 Differential Thermal Analysis (DTA), Thermogravimetry (TG) and Derivative Thermogravimetry (DTG)

DTA measures the changes in heat content as a function of difference in temperature existing between the sample under investigation and a thermally inert material taken as a reference compound, the two being heated at a fixed rate, simultaneously. TG measures the changes in weight of the sample under investigation as it is heated at a predetermined rate. The DTG technique consists of measuring the rate of weight loss of the sample as it is heated at a specified rate. The DTA, TG and DTG curves for all the nine glasses have been recorded in a 'Mom Derivatograph'.

Samples were prepared for DTA, TG and DTG by crushing the glasses to particles of a size between -14 to +20 mesh, a size range which has been reported in literature as being

large enough to avoid surface crystallization. The glass particles were then mixed with fine Al_2O_3 powder in the ratio of 7:3 by volume to preventing their getting sintered during the run. The glass samples were run at a heating rate of $10^{o}C$/min in the temperature range from room temperature to $1000^{o}C$. In most cases, a high sensitivity of 1/5 had to be used in DTA to clearly distinguish the Glass Transition Temperature represented by the first dip in the curve.

Chapter 4

RESULTS

4.1 Differential Thermal Analysis of Glasses 1 to 9

The glass transition temperatures for glasses 1 to 9 as indicated by the first dip in the DTA curve are shown in Figs. 4.1A and 4.1B and are tabulated in the table 4.1.

The introduction of Bi_2O_3 or Ag_2O into the glass batch is generally seen to lower the glass transition temperature. The lowering is more in the silver containing glasses than in the Bismuth containing ones.

4.2 Ultimate Tensile Strengths and Young's Modulii of Glass Fibres

The Tensile strengths and Young's Modulii of 12-27 fibres of 2.0 cm gage length in each of the nine glass compositions are recorded in the Tables 4.201 to 4.209. They are also plotted in the form of Histograms in Fig. 4.21 to 4.29. The diameters of the fibres have been measured using the Accutron.

Table 4.210 shows the Ultimate Tensile Strength and Young's Modulus values for fibres of Glass 9 using values of diametered measured by the Optical Microscope. Optical Microscopic data gave a Young's Modulus of 6.3 mpsi as

against the value of 10.02 mpsi obtained for the same fibres using Accutron measured diameters.

It was observed that the strengths of fairly fine and relatively fat Bismuth containing glass fibres of the same composition differed very little from one another. Again 'off' the drum metal containing glass fibres showed the same strengths as the untouched fibres of the same glass composition with the same diameter. In order to verify whether this effect was due to the presence of the metal or not, 5.0 cm gage lengths of fibres of glasses 7 and 9 were tested under identical conditions and the Tensile Strengths and Young's Moduli so obtained are tabulated in Tables 4.211 and 4.212 respectively.

The decrease in the average strength of the 5.0 cm gage lengths fibres of Glass 9 as compared to that of the 2.0 cm gage length fibres of the same composition, tested in the same way, is 36.56%.

The corresponding decrease in the strength of fibres of Glass 7 is seen to be only 19.1%.

4.3 Rupture Modulus and Young's Modulus in Bending of Bulk Glasses

The Rupture Moduli and Young's Moduli in Bending of bulk glasses, 1, 2, 4, 5, 6, 7, 8 and 9 are tabulated in Tables 4.31 and 4.32. Glass 3 had a very high level of

porosity and therefore values obtained for this glass are not tabulated.

Rupture Modulii and Young's Modulii of the Bismuth containing glasses are higher than those of the corresponding base glass. In the silver series, the Rupture Modulii of the metal containing glasses are higher than that of the base glass, but the Young's Modulii do not show any appreciable change.

The values of E_b quoted in the Tables 4.31 and 4.32 are calibrated ones. Calibration has been done with respect to A and C glasses of known E_b values which were broken under exactly identical conditions. Care was taken to keep the same level of strain in the A and C glasses as in the experimental glass compositions.

Fig. 4.31 has been included to show how E_b has been obtained from the stress values as calculated from the Instron chart and sample dimensions and the strain values as obtained from the strain indicator. It also gives some idea of the level of strain in the sample for a given applied load.

4.4 X-Ray Diffraction Analysis of Glasses and Glass Fibres

Bulk Glasses 7 and 6 were found to give 4-5 peaks in the X-ray Diffraction pattern. The angles corresponding to the peaks and the relative heights of the peaks were

used to calculate d_{hkl} and I/I_1 values for these glasses. The values are tabulated in the Table 4.41. A.S.T.M. tables for silver and calcium magnesium silicate are shown in the Table 4.67. The d_{hkl} and I/I_1 values for these bulk glasses are seen to compare very favourably with those for silver. Some of the d_{hkl} values are also seen to be similar to those for calcium Magnesium Silicate; although here the correspondence is not as good as in the case of Silver.

The X-ray Diffraction of fibres of glasses 5, 6 and 7 were studied but only those of glass 7 gave peaks. I/I_1 and d_{hkl} values for these peaks are also shown in the Table 4.41. Values of d_{hkl} are in fairly close agreement with those for silver.

X-ray Diffraction patterns for glasses 6 and 7 and glass fibres 7 are shown in figures 4.41, 4.42 and 4.43 respectively.

4.5 Microstructure by Optical Microscopy

Glasses 5, 6 and 7 and glass fibres of glasses 5, 6 and 7 were studied under the optical microscope using reflected light. The crystalline phase in glasses 6 and 7 showed up as small, fairly regular shaped particles, at a microscope magnification of 300x. Photographs were taken after subjecting the glass surfaces to a suitable etch

treatment, but still showed a very poor contrast. The crystalline phase in the glass 5 showed up only very vaguely in the microscope and was not photographed.

The percent volume fraction of the crystallized phase in glass 6 was computed from the photograph 4.51 and is about 47.8. The average particle size is about 22 μm. The contrast in photograph 4.52 for glass 7 is too poor to make any reliable measurements but the volume fractions and particle sizes of the dispersed phase when seen directly under the microscope appear to be very close to those for glass 6.

The crystalline phase in fibres of glasses 5, 6 and 7 shows up as bright streaks parallel to the fibre axis (photographs 4.53 to 4.55). It is not possible to estimate the volume fraction of the crystalline phase from these photographs, because at a particular focus of the microscope only a few streaks are visible in a given length of fibre. On slightly altering the focus without moving the fibre, the streaks already present fade away and others come into view.

4.6 Microstructure of Glasses and Glass Fibres by TEM Studies

The microstructure in the Bismuth containing glasses and glass fibres, consists of spherically shaped, electronically dense droplets distributed in the glassy matrix.

The volume fractions as calculated from the micrographs 4.601 to 4.607 are tabulated in the table 4.61 and range from about 26 percent to 42 percent. The average size of the dispersed spheres ranges from 97Å to 313 Å. In the silver containing glasses and glass fibres, spherically shaped particles were not observed in all cases. Generally, in this series of glasses, patchy regions were observed. Typical microstructures in silver glasses and glass fibres are shown in photographs 4.608 to 4.613.

S.A.D. photographs 4.615 to 4.619 were taken to identify the crystalline phases present in the glasses and glass fibres. The phase is Bismuth in the case of the Bismuth glasses and glass fibres and Silver and Calcium Magnesium Silicate in the case of silver glasses and glass fibres (Tables 4.62 to 4.67).

S.A.D. photographs were usually obtainable directly from certain patchy regions. The spherical regions generally gave only very feeble spots on the screen, but on subjecting these regions to electron beam bombardment in the EM, for a fairly long period of time, coagulation occurred to give patchy regions which showed intense diffraction spots.

4.7 Fracture Surface Replicas

Fracture surface replicas of the metal containing and base glass compositions are shown in photographs 4.701 to 4.710.

Photographs 4.701 to 4.704 show the increased fracture surface roughness of metal containing glasses as compared to those of the base glasses as seen in photographs 4.705 to 4.708.

Replicas of some of the crystalline glasses in the silver series show fracture steps formed by the interaction of the crack front with the dispersed phase. This is seen in photographs 4.709 and 4.710 . Such steps were not observed in the base glass replicas.

Chapter 5

DISCUSSION

5.1 DTA Curves:

In general, the DTA curves reveal that the glass transition temperature of the base glass is lowered when Ag_2O or Bi_2O_3 is added to it. This is probably because these oxides act as network modifiers and render the glass network less rigid; thereby altering the viscosity of the glass. This change is reflected in the lowering of T_g and also in the fact that the metal containing glasses are found to be more fluid at any given temperature above the liquidus temperature, than the corresponding base glass.

The lowering of T_g is seen to be more for the silver containing glasses than for the Bismuth based glasses.

5.2 Ultimate Tensile Strength and Young's Modulus of Fibres

The Tensile Strengths and Young's Modulii of Bismuth containing glass fibres are seen to be higher than those of the corresponding base glass. The base glass in this series is a low modulus glass, having a modulus of only 5.3 mpsi. The modulus of the dispersed phase is probably higher than this value, which would account for the increase in Young's Modulus of the base glass when Bi_2O_3 is added to it.

The Tensile Strengths of the fibres of glasses 1,2,3,4 and 5 are respectively about (1.0, 1.5, 1.2, 1.9 and 0.8)x10^5 psi Their Young's Modulii are respectively 6.4, 8.0, 6.0, 9.7 and 5.3 mpsi. When these values of σ and E are substituted into the equation (8); values of σ_{f_T} obtained in each case are slightly less than the actual strengths observed. This implies that there is a slight strengthening over and above that expected merely due to modulus enhancement in each case. The increase is probably attributable to flaw size limitation and/or to strengthening due to induced thermo-mechanical compressive stresses created during casting.

In the silver series, the Young's Modulus of the base glass fibres is obtained as $\sim$ 10 mpsi; whereas that of silver (hand drawn) is reported to be 11.24 mpsi. No appreciable modulus enhancement is therefore expected, and observations tally with this fact. The tensile strengths of fibres in this series are lower than those of the corresponding base glass. Optical microscopic evidence shows the crystalline phase in such fibres to be in the form of sharp streaks along the fibre axis and strength decrease could be because of stress concentrating effects associated with such streaks.

In all cases, Accutron measured fibre diameters give values of strengths and Modulii which are reasonably close to

literature values for the kind of compositions studied, keeping in mind the fact that none of the fibres were coated with a sizing agent. Optical microscopic measurements of fibre diameters (in air) give rise to a large error in the UTS and E values. This is because of the fact that diffraction bands are included in the measured diameters. In all cases, values of UTS and E as obtained by using the optical microscope are about 1.4 - 2.0 times lower than those obtained from Accutron diameters; for the range of fibre diameters used here.

The percentage decrease in the strength of fibres of glass 9 when a 5.0 cm gage length is used instead of 2.0 cm gage length is about 36.6 percent as against 19 percent for fibres of glass 7. This implies that the effect of flaw density in metal containing glass fibres is not as significant as it is for the non-metal containing base glass fibres.

5.3 Rupture Modulus and Young's Modulus in Bending for Bulk Glass:

The Rupture Modulii and Young's Modulii in bending for the Bismuth containing glasses are higher than the corresponding values for the base glass. Here again, strength increase is attributable to modulus enhancement and to flaw size limitation and/or thermomechanical stresses.

Young's Modulii in bending of glasses in the silver series do not show any appreciable increase over that for the base glass, as is expected. In this case the increase in Rupture Modulus over that of the base glass is not due to modulus enhancement, but can be attributed to flaw size limitation. Fracture surface replicas for glasses 6 and 7 bear out this fact.

The Young's Modulii in 3-pt. bending have been obtained from stress-strain values and not from the expression (11)

$$E_b = \frac{PL^3}{4bd^3y} \qquad (11)$$

(P,L,b,and d have the same meaning as in equation (10) and y is the deflection of the sample corresponding to a given load P).
used by Hing and McMillan[13] in a similar experiment. E_b values when calculated using the above expression were found to be an order of magnitude lower than the expected values. This is probably due to the fact that the jig also takes up some strain and the deflection y when calculated from factors like Cross-Head speed, chart speed and distance moved by chart from zero load to the breaking load; is not the actual deflection of the sample. Values of y are thus overestimated giving very low E_b values.

Strain gages were therefore used on the samples to measure the maximum strain in the sample (i.e. strain gages are positioned on the glass surface at a point just below the middle bar of the 3-pt. bending apparatus), and E_b was calculated from the stress-strain curve. This method proved much better but because the strain gage cement used was a little old, slightly high E_b values were obtained and the results had to be calibrated with respect to samples of 'A' and 'C' glasses with the same level of strain.

5.4 X-Ray Diffraction Analysis:

Values of d_{hkl} and I/I_1 for bulk glasses 6 and 7 are in very close agreement with those for silver. In the case of fibres of glass 7, d_{hkl} values match well, but the I/I_1 values do not.

Some of the d_{hkl} values for calcium magnesium silicate and Akermanite also come fairly close to those obtained from the glass samples. The ASTM data for calcium magnesium silicate (and Akermanite) have been obtained using Co K_α radiation whereas Cu K_α radiation was used for the glass samples. It is, therefore, possible that calcium magnesium silicate is also present in these glasses. The supposition is further borne out by the fact that this phase is known to commonly occur in $CaO-MgO-SiO_2$ based glasses and that silver is known to act as a nucleating agent for the growth of various

The fact that only Glass 7 fibres gave diffraction peaks is probably because only 50-60 percent of fibres of glasses 5 and 6 were seen to contain crystalline streaks, whereas in glass 7 every fibre showed the streaks. In spite of the fact that it has the maximum number of streaks, fibres of glass 7 still show the highest strength values among the three silver containing glass fibres and this is explainable on the basis of the fact that the streaks in glass 7 fibres are longer and more continuous throughout the length of the fibre.

5.5 Optical Microscopy:

Optical microscopic evidence show bulk glasses 6 and 7 and fibres of glasses 5, 6 and 7 to be crystallized. The average particle size in glasses 6 and 7 is about 20 μm and the percent volume of crystallization is roughly 48. Particles are not quite spherical and are also quite large in size, which accounts for the relatively low Rupture Modulii observed here as compared to values reported for various glass ceramics. Rupture Modulii are however a little higher than that of the base glass.

The relatively high volume fractions obtained here can be explained on the basis of the fact that the crystalline phase is not silver alone but also includes calcium magnesium silicate.

In the glass fibres, the crystalline phase is observed as longish streaks because it is getting extruded along the fibre axis during the drawing process.

5.6 TEM Studies for Characterization of the Microstructure of Glasses and Glass Fibres:

The micro-structure in Bismuth containing glasses and glass fibres, as revealed by TEM consists of a distribution of dark spheres in the glassy matrix. These spheres act as barriers to crack propagation and marginally increase the length of the crack front, thereby raising the stress required to propagate the crack. The slight increase in strength over and above that due to modulus enhancement alone could be explained by this model.

The relatively high volume fractions observed in some cases are explainable on the basis of the work of Chakravorty, Vithlani and Mehta who established that the dark spherical regions in Bismuth glasses contain some Alkali ions in addition to Bismuth. The spherical phase in such cases is thus rich in Bismuth but does not consist solely of Bismuth.

S.A.D. photographs of Bismuth containing glasses and fibres were analysed. Some of the d_{hkl} values obtained are in fairly close agreement with the corresponding d_{hkl} values for Bismuth. Analysis of one such typical SAD pattern is included in the tables.

The mean free paths for crack propagation in Bismuth glasses and glass fibres were calculated from the particle sizes and volume fractions of the dispersed spherical phase. For both bulk glasses and glass fibres, the strength is seen to increase when the mean free path decreases, (Table 5.61). A plot of $\sqrt{1/\lambda}$ versus UTS for Bismuth containing fibres is shown in the Fig. 5.61. Two straight lines can be drawn as shown; in accordance with Hasselman and Fulrath's theory. The plot is not very reliable as strength values for fibres have a fairly wide scatter and their average value has been used in the plot. Again, only four data points are there and many more are actually required to draw a reliable plot of this kind. An idea of the order of surface energy can be obtained however. Using the expression, $\nu = \pi(\text{slope})^2/E$ and a value of E = 5.3 mpsi, the surface energy for uncoated Bismuth containing fibres is obtained to be 2676.5 Ergs/cm^2.

The trend of increasing strength values with decreasing mean free path was also observed in the Bismuth containing bulk glasses. In this series, strengths are in the order: Glass 1 > Glass 2) > Glass 4 > Glass 8 and mean free paths are in the inverse order. The amounts of Bi_2O_3 added to glass batches 1,2 and 4 during the glass melting are respectively 3,5 and 10 mole percent. The actual percent volume fractions of spheres in these glasses are however,

about 42, 34 and 25 respectively. The amount of Bismuth in the glass is therefore, dependant not on the starting composition of the glass alone, but also on other factors such as the casting temperature, and time for which the glass melt was kept at different temperatures.

The Young's Modulii of Bismuth fibres follow the sequence: $E_{Glass\ 4} > E_{Glass\ 2} > E_{Glass\ 1}$. The volume fractions as calculated from TEM photographs are in the sequence $\phi_{Glass\ 2} > \phi_{Glass\ 4} > \phi_{Glass\ 1} > \phi_{Glass\ 3}$. The modulus of glass 4 fibres is higher than that for fibres of glass 2, even though the volume fraction of spheres in glass 4 fibres is a little lower than that for glass 2 fibres. This could be attributed to the fact that there is a large amount of inter connected dispersed phase in Glass 4 fibres.

For bulk Bismuth glasses, Modulii are in the sequence $E_{glass\ 4} > E_{glass\ 1} > E_{glass\ 2}$, and volume fractions are in the order $\phi_{glass\ 1} > \phi_{glass\ 2} > \phi_{glass\ 4}$. Glass 4 is seen to have both large isolated spheres and very fine interconnected particles. Volume fractions have been calculated for the large spheres but the modulus value would seem to be better explained had the interconnected phase been considered.

In the silver glass series, the above kind of analysis is not possible as in some cases, volume fractions are not estimatable from the photographs. Particle shapes are also seen to be spherical in some TEM photographs but irregular in others and the expression for mean free path used here is valid for a uniform distribution of spherical particles. Fibres in this series generally showed patchy microstructure in TEM and no idea of the volume fraction could be obtained from these.

5.7 Fracture Surface Replicas:

In the ideal Griffith system, the condition for fracture is reached when the increase in surface energy resulting from a small extension of the crack is balanced by the release of elastic energy in the body surrounding the crack; and the elastic system under stress passes from the unbroken to the broken state by a process involving a continuous decrease in the potential free energy.

For any single fracture crack, following the attainment of the criterion of fracture, the release of elastic energy must then be in excess of that represented by the surface energy of the advancing crack. This energy must be absorbed in some manner, for example, by some augmentation of the surface area of the crack. This characteristic is found in different degrees in various types of fracture. Surface

augmentation in some cases takes the form of an increased surface roughness. This roughness is very pronounced in the metal containing glasses as compared to that in the base glasses as is seen in the photographs 4.701 to 4.708.

Another characteristic feature of the interaction of a crack front with dispersed obstacles are the fracture 'steps' at the rear of the obstacles. These are seen in photographs 4.709 and4.710. These steps have been explained by Lange as arising from the fact that the crack front is pinned down by the obstacles and at the same time it tries to break away by bowing out from between the pinning positions. When the crack front just breaks away, its arms meet at the rear of the obstacle, leaving these steps.

No such steps are observed in replicas of the non metal containing or base glasses.

Glass No.	Glass composition in mole percent									
	SiO_2	B_2O_3	Al_2O_3	K_2O	Bi_2O_3	Na_2O	CaO	MgO	Ag_2O	As_2O_3
1	55	30	6	6	3					
2	55	29	6	5	5					
3	55	27	6	5	7					
4	55	24	6	5	10					
5	72					13	9	4	1	1
6	72					13	8.5	4	1.5	1
7	72					13	8	4	2	1
8	55	33	6	6						
9	72					13	10	4		1

TABLE 3.1A

Glass	Casting Temperature (°C)	Annealing Temperature (°C)	Temperature at top of Bushing (°C)	Temperature at Bushing Tip (°C)	Fibre Winding Speed (ft/min)	Diameter Range of Fibres (μm)
1	1380	450	1120	910	2871.4	7.020-10.429
2	1420	450	1050	810	2871.4	5.334- 9.847
3	1300	400	960	763	2871.4	6.622-11.184
4	1280	400	980	750	2871.4	5.668- 8.038
5	1550	500	1300	1095	2871.4	7.264-10.560
6	1560	500	1340	1080	2666.3	8.382-14.896
7	1600	500	1260	1052	2871.4	7.238- 9.883
8	1680	500	1330	1066	2871.4	8.850-10.371
9	1650	500	1340	1060	2912.4	7.020- 8.897

Table 3.1B. Glass Melting and Fibre Drawing Parameters.

Sl. No.	Glass	T_g
1	1	470°C
2	2	470°C
3	3	500°C
4	4	477.5°C
5	5	550°C
6	6	570°C
7	7	590°C
8	8	497°C
9	9	618°C

Table 4.1. Glass Transition Temperatures of Glasses 1 to 9.

GLASS 1 FIBRES

Cross Head Speed = 0.02 cm/min
Chart speed = 2 cm/min
Gage length = 2.0 cm

S.No.	Breaking Load (gms)	Chart distance (cm)	Dia. (μm)	$U_1 S \times 10^{-8}$ N/M^2	$U_1 S \times 10^{-5}$ psi	Strain x 10^2	$D \times 10^{-10}$ N/M^2	E mpsi
l_1	2.95	2.9	8.155	5.537	0.803	1.45	3.816	5.537
l_2	4.35	3.8	8.452	7.603	1.103	1.9	4.001	5.806
l_3	1.75	1.75	7.677	3.707	0.538	0.875	4.236	6.147
l_4	4.1	3.9	7.088	10.187	1.478	1.95	5.224	7.580
l_5	2.9	2.8	8.299	5.256	0.763	1.4	3.754	5.443
l_6	5.075	2.85	10.429	5.825	0.845	1.425	4.088	5.932
l_7	4.4	2.1 (1.9cm gage)	9.837	5.677	0.824	1.105	5.135	7.455
l_8	5.2	4.1	8.077	9.950	1.444	2.05	4.854	7.043
l_9	2.7	2.1	8.521	4.642	0.674	1.05	4.421	6.415
l_{10}	6.7	5.2	8.957	10.427	1.513	2.75	3.791	5.501
l_{11}	5.25	4.4	8.232	9.673	1.403	2.2	4.397	6.380
l_{12}	2.15	2.8	7.020	5.446	0.790	1.4	3.890	5.646
l_{13}	3.05	2.4	8.159	5.720	0.830	1.2	4.767	6.917
l_{14}	4.5	3.925	7.324	10.473	1.520	1.963	5.335	7.741
l_{15}	4.275	3.8	7.905	8.541	1.239	1.9	4.495	6.523
l_{16}	1.775	1.8	7.602	3.835	0.556	0.9	4.261	6.182
l_{17}	5.0	4.2	7.786	10.296	1.494	2.1	4.903	7.114
					Average 1.048			Average 6.433

Table A.201

GLASS 2 FIBRES

Cross Head Speed = 0.02 cm/min
Chart speed = 2 cm/min
Gage length = 2.0 cm

S.No.	Breaking Load (gms)	Chart distance (cm)	Dia. (μm)	UTSx10^{-8} N/M^2	UTSx10^{-5} psi	Strain x 10^2	Ex10^{-10} N/M^2	E mpsi
2_1	7.2	3.4	8.946	11.232	1.630	1.7	6.607	9.587
2_2	5.1	2.75	8.732	8.351	1.212	1.375	6.073	8.813
2_3	7.7	3.7	9.847	9.913	1.438	1.85	5.358	7.775
2_4	5.2	2.6	9.187	7.691	1.116	1.3	5.916	8.584
2_5	4.25	2.0	9.139	6.352	0.922	1.0	6.352	9.217
2_6	3.6	3.65	6.400	10.973	1.592	1.825	6.013	8.725
2_7	6.25	3.55	9.347	8.930	1.296	1.775	5.031	7.300
2_8	5.4	3.75	7.935	10.706	1.553	1.875	5.710	8.285
2_9	3.25	3.1	6.742	8.925	1.295	1.55	5.758	8.355
2_{10}	4.3	2.95	8.642	7.188	1.043	1.475	4.873	7.071
2_{11}	5.2	2.95	9.297	7.510	1.090	1.475	5.092	7.388
2_{12}	1.75	2.15	5.525	7.157	1.038	1.075	6.658	9.66
2_{13}	3.55	3.85 (1.8 cm gage)	5.842	12.99	1.885	2.14	6.07	8.81
2_{14}	2.8	3.7	6.541	8.17	1.185	1.85	4.42	6.41
2_{15}	6.5	4.5	8.255	11.91	1.73	2.25	5.293	7.68
2_{16}	2.1	3.0	6.096	7.655	1.02	1.5	4.70	6.80
2_{17}	8.9	6.6	8.601	17.36	2.519	3.3	5.26	7.63
2_{18}	6.5	4.25	8.380	11.55	1.68	2.125	5.44	7.89

...Contd.

GLASS 2 FIBRES (...Contd.)

S.No.	Breaking Load (gms)	Chart distance (cm)	Dia. (μm)	UTSx10^{-8} N/M^2	UTSx10^{-5} psi	Strain x 10^2	Ex10^{-10} N/M^2	E mpsi
2_{19}	2.05	3.15	5.715	7.836	1.137	1.575	4.975	7.22
2_{20}	4.6	6.15	5.715	17.58	2.55	3.075	5.72	8.295
2_{21}	4.4	6.4	6.35	13.62	1.977	3.2	4.26	6.176
2_{22}	2.2	2.7	5.967	7.71	1.12	1.35	5.71	8.29
2_{23}	3.0	5.1	5.334	13.16	1.91	2.55	5.16	7.488
2_{24}	3.65	5.2	5.715	13.95	2.02	2.6	5.37	7.79
					Average 1.498			Average 7.969

Table 4.202

GLASS 3 FIBRES

Cross Head Speed = 0.02 cm/min
Chart speed = 2 cm/min
Gage length = 2.0 cm

S.No.	Breaking Load (gms)	Chart distance (cm)	Dia. (μm)	UTSx10^{-8} N/M^2	UTSx10^{-5} psi	Strain x 10^2	Ex10^{-10} N/M^2	E mpsi
3_1	3.1	3.15	7.004	7.889	1.145	1.575	5.009	7.268
3_2	5.7	4.2	9.060	7.756	1.125	2.1	3.693	5.359
3_3	8.35	3.95	11.184	8.334	1.209	1.975	4.220	6.123
3_4	9.5	4.75	10.770	10.225	1.484	2.375	4.305	6.247
3_5	5.4	3.85	8.726	8.854	1.285	1.925	4.560	6.674
3_6	4.5	4.75	7.566	9.813	1.424	2.375	4.132	5.995
3_7	2.8	3.95	7.499	6.216	0.902	1.975	3.148	4.567
3_8	5.275	4.25	8.927	8.263	1.199	2.125	3.888	5.642
3_9	3.15	3.25	7.840	6.398	0.928	1.625	3.937	5.713
3_{10}	2.35	1.85 (1.7cm gage)	7.215	5.635	0.818	1.088	5.179	7.515
3_{11}	5.35	5.0	8.098	10.184	1.478	2.5	4.073	5.911
3_{12}	4.1	4.1	7.925	8.151	1.183	2.05	3.976	5.769
3_{13}	4.15	3.5	8.475	7.214	1.047	1.75	4.122	5.981
3_{14}	4.6	3.9	7.806	9.425	1.368	1.95	4.834	7.015
3_{15}	3.3	3.65	8.089	6.296	0.914	1.825	3.450	5.006
3_{16}	2.85	4.25	7.481	6.357	0.922	2.125	2.992	4.341
3_{17}	3.1	2.7	7.911	6.183	0.897	1.35	4.580	6.646
3_{18}	2.8	2.85	7.696	5.902	0.856	1.425	4.142	6.010

...Conta.

GLASS 3 FIBRES (...Conta.)

S.No.	Breaking Load (gms)	Chart distance (cm)	Dia. (μm)	UTSx10^{-8} N/M^2	UTSx10^{-5} psi	Strain x10^2	Ex10^{-10} N/M^2	E mpsi
3_{19}	3.9	4.4	7.942	7.718	1.199	2.2	3.508	5.09
3_{20}	3.35	3.3	7.323	7.798	1.132	1.65	4.726	6.858
3_{21}	3.65	4.2	7.470	8.165	1.185	2.1	3.888	5.642
3_{22}	7.0	5.05	9.056	10.656	1.546	2.525	4.220	6.123
3_{23}	4.175	3.0	9.236	6.110	0.887	1.5	4.073	5.911
3_{24}	6.25	4.5	10.097	7.959	1.155	2.25	3.537	5.133
3_{25}	5.45	5.2	7.511	12.060	1.750	2.6	4.639	6.731
3_{26}	4.45	4.3	7.984	8.716	1.265	2.15	4.054	5.882
3_{27}	4.425	4.55	6.622	12.598	1.828	2.275	5.535	8.032
					Average 1.190			Average 6.044

Table 4.20b

GLASS 4 FIBRES

Cross Head Speed = 0.02 cm/min
Chart speed = 2 cm/min
Gage length = 2.0 cm

S.No.	Breaking Load (gms)	Chart distance (cm)	Dia. (μm)	UTSx10^{-8} N/M^2	UTSx10^{-5} psi	Strain x 10^2	Ex10^{-10} N/M^2	E mpsi
4_1	3.4	4.05	6.499	10.048	1.458	2.025	4.962	7.20
4_2	3.825	3.5	6.016	13.192	1.914	1.75	7.538	10.938
4_3	3.95	4.0	5.668	15.350	2.227	2.0	7.675	11.136
4_4	4.85	2.85	7.833	9.868	1.432	1.425	6.925	10.048
4_5	5.125	3.75	7.206	12.320	1.788	1.875	6.571	9.534
4_6	4.35	4.1	7.277	10.256	1.488	2.05	5.003	7.259
47	3.3	3.35	6.570	9.544	1.385	1.675	5.698	8.268
4_8	4.2	2.5 (1.85 cm gage)	8.038	8.116	1.178	1.35	6.012	8.723
4_9	6.05	5.3 (1.8 cm gage)	7.412	13.747	1.995	2.94	4.676	6.785
4_{10}	4.225	3.55	6.018	14.566	2.114	1.775	8.206	11.900
4_{11}	2.675	2.3	6.246	8.560	1.242	1.15	7.443	10.800
4_{12}	5.3	4.45	5.969	18.57	2.695	2.225	8.346	12.110
4_{13}	5.475	4.5	6.923	14.262	2.069	2.25	6.339	9.198
4_{14}	4.25	3.4	6.223	13.70	1.988	1.7	8.059	11.693
					Average 1.784			Average 9.686

Table 4.204

GLASS 5 FIBRES

Cross Head Speed = 0.02 cm/min
Chart speed = 2 cm/min
Gage length = 2.0 cm

S.No.	Breaking Load (gms)	Chart distance (cm)	Dia. (μm)	UTSx10^{-8} N/M^2	UTSx10^{-5} psi	Strain x 10^2	Ex10^{-10} N/M^2	E mpsi
5_1	3.47	2.4	8.278	6.321	0.917	1.2	5.268	7.644
5_2	4.7	3.25	8.661	7.821	1.135	1.625	4.813	6.984
5_3	9.6	5.4	7.865	19.373	2.811	2.7	7.175	10.411
5_4	6.1	2.3	8.484	10.580	1.535	1.15	9.199	13.349
5_5	6.9	4.4	8.233	12.707	1.844	2.2	5.776	8.381
5_6	8.35	4.325	7.747	17.369	2.520	2.163	8.03	11.652
5_7	8.15	3.95	9.056	12.407	1.800	1.975	6.282	9.115
5_8	6.0	3.7	7.827	12.228	1.774	1.85	6.609	9.590
5_9	5.4	2.9	7.204	12.770	1.853	1.45	8.81	12.785
5_{10}	14.5	4.85	10.566	16.214	2.353	2.425	6.686	9.702
5_{11}	4.8	3.0	7.391	10.970	1.592	1.50	7.313	10.612
5_{12}	13.1	5.0	9.589	17.786	2.58	2.5	7.114	10.323
5_{13}	12.45	4.5	10.057	15.057	2.185	2.25	6.692	9.710
					Average 1.915			Average 10.020

Table 4.205

GLASS 6 FIBRES

Cross Head Speed = 0.02 cm/min
Chart speed = 2 cm/min
Gage length = 2.0 cm

S.No.	Breaking Load (gms)	Chart distance (cm)	Dia. (μm)	UTSx10^{-8} N/M^2	UTSx10^{-5} psi	Strain x 10^2	Ex10^{-10} N/M^2	E mpsi
6_1	6.1	3.25	8.573	10.363	1.504	1.625	6.377	9.255
6_2	28.25	5.35	14.896	15.894	2.306	2.675	5.942	8.622
6_3	7.375	3.5	8.653	12.296	1.784	1.75	7.026	10.195
6_4	8.95	3.5	9.209	13.176	1.912	1.75	7.529	10.925
6_5	17.8	3.9	13.589	12.024	1.746	1.95	6.17	8.955
6_6	10.75	2.45	12.836	8.146	1.182	1.225	6.650	9.648
6_7	12.95	2.8	12.758	9.933	1.441	1.4	7.095	10.295
6_8	9.75	2.85	11.278	9.570	1.389	1.425	6.716	9.745
6_9	10.3	2.1	13.449	7.109	1.032	1.05	6.77	9.82
6_{10}	6.5	2.625	8.954	10.121	1.469	1.313	7.708	11.185
6_{11}	8.45	3.0	9.652	11.323	1.643	1.5	7.549	10.953
6_{12}	13.15	2.65	14.224	8.114	1.177	1.325	6.124	8.886
6_{13}	13.3	2.0	14.732	7.650	1.11	1.00	7.65	11.10
6_{14}	8.1	3.85	8.382	14.393	2.088	1.925	7.477	10.849
6_{15}	12.55	2.8	13.411	8.711	1.264	1.4	6.222	9.028
6_{16}	14.3	2.9	12.840	10.828	1.571	1.45	7.468	10.835
					Average 1.539			Average 10.02

Table 4.206

GLASS 7 FIBRES

Cross Head Speed = 0.02 cm/min
Chart speed = 2 cm/min
Gage length = 2.0 cm

S.No.	Breaking load (gms)	Chart distance (cm)	Dia. (μm)	UTSx10^{-8} N/M^2	UTSx10^{-5} psi	Strain x 10^2	Ex10^{-10} N/M^2	E mpsi
7_1	11.25	4.45	9.767	14.723	2.136	2.225	6.617	9.601
7_2	9.45	3.65	9.546	12.946	1.878	1.825	7.093	10.293
7_3	11.35	4.5	9.549	15.54	2.255	2.25	6.907	10.022
7_4	4.725	2.2	8.639	7.903	1.147	1.10	7.185	10.425
7_5	8.25	4.0	8.015	16.032	2.326	2.0	8.016	11.631
7_6	5.375	3.0	7.62	11.556	1.677	1.5	7.704	11.18
7_7	6.0	3.25	7.874	12.081	1.753	1.625	7.434	10.787
7_8	7.825	3.4	8.306	14.16	2.055	8.867	8.329	12.085
7_9	6.85	4.0	7.493	15.23	2.21	2.0	7.615	11.049
7_{10}	6.525	2.55	8.853	10.394	1.508	1.275	8.152	11.829
7_{11}	9.1	5.25	8.192	16.928	2.456	2.625	6.449	9.357
7_{12}	8.05	4.45	7.811	16.472	2.39	2.225	7.403	10.742
7_{13}	5.0	3.3	7.238	11.915	1.729	1.65	7.221	10.478
7_{14}	6.1	3.05	8.171	11.405	1.655	1.525	7.479	10.852
7_{15}	8.0	2.7	9.729	10.552	1.531	1.35	7.817	11.342
7_{16}	11.9	4.05	9.883	15.209	2.207	2.025	7.511	10.898
					Average 1.933			Average 10.786

Table 4.207

GLASS 8 FIBRES

Cross Head Speed = 0.02 cm/min
Chart speed = 2 cm/min
Gage length = 2.0 cm

S.No.	Breaking Load (gms)	Chart distance (cm)	Dia. (μm)	UTSx10^{-8} N/M^2	UTSx10^{-5} psi	Strain x 10^2	D x 10^{-10} N/M^2	E mpsi
8_1	4.0	3.25	9.325	5.743	0.833	1.625	3.534	5.128
8_2	2.95	2.3	9.774	3.855	0.559	1.15	3.353	4.865
8_3	5.97	4.2	9.102	8.997	1.305	2.1	4.284	6.217
8_4	4.7	3.2	9.468	6.546	0.950	1.6	4.091	5.936
8_5	2.45	2.3	9.362	3.489	0.506	1.15	3.034	4.403
8_6	4.3	3.1	9.495	5.954	0.864	1.55	3.841	5.574
8_7	4.975	3.25	9.845	6.408	0.930	1.625	3.944	5.722
8_8	4.2	3.9	9.576	5.718	0.830	1.95	2.932	4.254
8_9	3.8	3.05	10.106	4.645	0.674	1.525	3.046	4.419
8_{10}	5.5	3.2	9.955	6.928	1.005	1.6	4.330	6.285
8_{11}	3.225	2.7	9.384	4.572	0.663	1.35	3.387	4.914
8_{12}	6.2	4.15	9.014	9.527	1.382	2.075	4.591	6.66
8_{13}	3.25	2.85	8.850	5.182	0.752	1.425	3.637	5.277
8_{14}	5.25	4.45	10.371	6.094	0.842	2.225	2.739	3.974
8_{15}	3.5	2.5	9.308	5.043	0.732	1.25	4.034	5.854
8_{16}	3.25	2.3	9.881	4.156	0.603	1.15	3.614	5.244
8_{17}	3.15	2.6	9.664	4.211	0.611	1.3	3.239	4.699
					Average 0.826			Average 5.260

Table 4.208

GLASS 9 FIBRES

Cross Head Speed = 0.02 cm/min
Chart speed = 2 cm/min
Gage length = 2.0 cm.

S.No.	Breaking Load (gms)	Chart distance (cm)	Dia. (μm)	UTSx10^{-8} N/M^2	UTSx10^{-5} psi	Strain x 10^2	E x 10^{-10} N/M^2	E mpsi
9_1	13.1	6.3	8.586	22.184	3.219	3.15	7.043	10.219
9_2	9.85	5.35	8.435	17.304	2.511	2.675	6.469	9.386
9_3	8.0	4.05	8.692	13.219	1.918	2.025	6.528	9.472
9_4	7.1	3.5	7.874	14.296	2.074	1.75	8.169	11.855
9_5	6.5	4.1	8.052	12.516	1.816	2.05	6.105	8.859
9_6	10.85	5.5	8.306	19.63	2.85	2.75	7.138	10.358
9_7	10.25	7.15	7.671	21.740	3.155	3.575	6.083	8.826
9_8	9.85	5.3	8.259	18.028	2.616	2.65	6.841	9.926
9_9	8.525	6.35	7.906	17.027	2.471	3.175	5.363	7.782
9_{10}	8.1	4.2	8.697	12.776	1.854	2.1	6.084	8.828
9_{11}	13.5	7.1	8.509	23.277	3.378	3.55	6.557	9.514
9_{12}	8.2	5.0	7.959	16.160	2.345	2.5	6.464	9.379
9_{13}	8.775	4.8	7.741	18.282	2.653	2.4	7.618	11.053
9_{14}	8.675	4.2	7.62	18.652	2.706	2.1	8.882	12.888
9_{15}	10.25	4.85	7.811	20.973	3.043	2.425	8.649	12.549
				Average	2.574		Average	10.060

Table 4.209

GLASS 9 FIBRES

Cross Head Speed = 0.02 cm/min
Chart speed = 2 cm/min
Gage length = 2.0 cm
Diameters measured by Optical Microscope

S.No.	Breaking Load (gms)	Chart distance (cm)	Dia.(μm)	UTSx10^{-8} N/M^2	UTSx10^{-5} psi	Strain x 10^2	Ex10^{-10} N/M^2	E mpsi
9_1	13.10	6.30	10.390	15.149	2.198	3.15	4.810	6.98
9_2	9.85	5.35	10.520	11.110	1.610	2.675	4.150	6.02
9_3	8.00	4.05	10.520	9.024	1.309	2.025	4.460	6.47
9_4	7.10	3.50	10.179	8.550	1.240	1.75	4.886	7.09
9_5	6.50	4.10	9.980	8.150	1.180	2.05	3.980	5.77
9_6	10.85	5.50	10.425	12.460	1.808	2.75	4.530	6.57
9_7	10.25	7.15	9.737	13.497	1.958	3.575	3.780	5.48
9_8	9.85	5.30	11.015	10.13	1.47	2.65	3.820	5.55
9_9	8.525	6.35	9.835	11.000	1.597	3.175	3.460	5.03
9_{10}	8.10	4.20	10.769	8.72	1.265	2.1	4.150	6.03
9_{11}	13.50	7.10	10.425	15.507	2.25	3.55	4.368	6.34
9_{12}	8.20	5.00	10.520	9.250	1.340	2.5	3.700	5.37
9_{13}	8.775	4.80	9.245	12.482	1.860	2.4	5.200	7.55
9_{14}	8.675	4.20	10.294	10.220	1.483	2.1	4.870	7.06
9_{15}	10.250	4.85	10.327	11.999	1.74	2.425	4.950	7.18
					Average 1.621			Average 6.299

Table 4.210

GLASS 7 FIBRES

Cross Head Speed = 0.05 cm/min
Chart speed = 2 cm/min
gage length = 5.0 cm

S.No.	Breaking Load (gms)	Chart distance (cm)	Dia. (μm)	UTSx10^{-8} N/M^2	UTSx10^{-5} psi	Strain x 10^2	Ex10^{-10} N/M^2	E mpsi
7_1	4.37	2.1	8.169	8.170	1.186	1.05	7.781	11.291
7_2	7.007	2.85	8.870	11.114	1.613	1.425	7.799	11.316
7_3	7.154	3.3	8.170	13.373	1.940	1.65	8.105	11.760
7_4	6.958	2.3	9.920	8.822	1.280	1.15	7.671	11.131
7_5	5.782	2.9	7.937	11.454	1.662	1.45	7.899	11.462
7_6	8.379	2.7	9.959	10.541	1.529	1.35	7.808	11.329
7_7	5.488	2.8	8.287	9.973	1.447	1.4	7.123	10.336
7_8	6.370	3.3	8.014	12.376	1.796	1.65	7.501	10.884
7_9	6.958	3.8	7.975	13.651	1.981	1.90	7.185	10.425
7_{10}	5.096	2.35	8.753	8.300	1.204	1.175	7.064	10.250
					Average 1.564			Average 11.02

Table 4.211

GLASS 9 FIBRES

Chart speed = 2 cm/min
Gage length = 5.0 cm

S.No.	Breaking load (gms)	Chart distance (cm)	Cross-Head Speed (cm/min)	Dia. (μm)	UTS x10^{-8} N/M^2	UTS x10^{-5} psi	Strain x10^2	E x10^{-10} N/M^2	E mpsi
9_1	4.3	4.8	0.02	8.939	6.714	0.974	0.96	6.994	10.148
9_2	10.143	15.2	0.02	8.370	18.060	2.622	3.04	5.943	8.623
9_3	8.775	4.2	0.05	8.126	16.580	2.406	2.1	7.895	11.456
9_4	6.075	2.65	0.05	8.370	10.821	1.570	1.375	7.870	11.419
9_5	12.495	3.05	0.05	9.895	10.975	1.593	1.525	7.197	10.443
9_6	6.125	3.55	0.05	8.208	11.345	1.646	1.775	6.392	9.274
9_7	3.528	1.5	0.05	8.756	5.768	0.837	0.75	7.691	11.160
9_8	5.802	2.85	0.05	8.289	10.536	1.529	1.425	7.394	10.728
9_9	5.488	2.7	0.05	8.370	9.776	1.418	1.35	7.241	10.507
9_{10}	5.096	2.35	0.05	8.736	8.332	1.209	1.175	7.091	10.289
9_{11}	9.30	4.25	0.05	8.825	14.901	2.162	2.125	7.012	10.175
						Average 1.633			Average 10.384

Table 4.212

Chart speed = 2 cm/min
Cross Head speed = 0.02 cm/min
Load cell used = 0.50 Kg

Glass (sample)	L cms	b cms	d cms	Breaking Load (Kg)	Rupture Modulus x 10^{-8} N/M^2	$E_b \times 10^{-10}$ N/M^2	E_b mpsi	Average Rupture Modulus x 10^{-8} N/M^2	Average E_b in mpsi
1(i)	1.5	0.440	0.408	24.25	0.730	5.079	7.369		
1(ii)	1.5	0.454	0.330	19.20	0.856	4.920	7.138		
1(iii)	1.5	0.436	0.416	24.80	0.757	5.695	8.263	0.762	7.749
1(iv)	1.5	0.470	0.430	20.25	0.514*	6.612	9.593		
1(v)	1.5	0.436	0.280	10.75	0.703	4.395	6.377		
2(i)	2.0	0.500	0.500	23.75	0.559	5..860	8.503		
2(ii)	2.0	0.450	0.350	10.80	0.576	-	-	0.691	7.533
2(iii)	1.5	0.510	0.338	25.80	0.976	5.349	7.762		
2(iv)	1.5	0.526	0.420	25.00	0.594	4.515	6.552		
2(v)	1.5	0.542	0.486	43.50	0.749	5.041	7.315		
4(i)	1.5	0.470	0.378	19.80	0.650	-	-		
4(ii)	1.5	0.480	0.406	27.60	0.763	7.513	10.901		
4(iii)	1.5	0.506	0.358	15.00	0.510	6.566	9.527	0.614	9.388
4(iv)	1.5	0.538	0.472	31.50	0.580	6.341	9.201		
4(v)	2.5	0.536	0.476	18.75	0.567	5.461	7.924		
8(i)	2.5	0.606	0.534	25.60	0.544	3.719	5.396		
8(ii)	2.5	0.508	0.528	22.15	0.575	4.685	6.798	0.514	5.961
8(iii)	2.5	0.598	0.534	19.60	0.422	3.921	5.690		

Values with asterix against them are not included in the average.

Table 4.31

Chart speed = 2 cm/min
Cross Lead Speed = 0.02 cm/min
Load cell used = 0-50 Kg

Glass (sample)	L cms	b cms	a cms	Breaking Load (Kg)	Rupture Modulus x10^{-8} N/M^2	E_b x10^{-10} N/M^2	E_b mpsi	Average rupture modulus x 10^{-8} N/M^2	Average E_b in mpsi
1	2	3	4	5	6	7	8	9	10
5(i)	1.5	0.436	0.406	25.50	0.782	9.865*	14.314*		
5(ii)	1.5	0.408	0.342	13.10	0.605	5.722	8.274		
5(iii)	1.5	0.454	0.390	26.80	0.586	-	-	0.748	10.03
5(iv)	2.5	0.520	0.508	29.25	0.801	7.563	10.974		
5(v)	2.5	0.562	0.476	28.00	0.808	6.168	8.950		
5(vi)	2.5	0.558	0.464	20.75	0.635	7.020	10.186		
5(vii)	2.5	0.464	0.472	21.00	0.747	8.099	11.752		
6(i)	2.5	0.492	0.462	24.40	0.854	6.830	9.910		
6(ii)	2.5	0.458	0.432	17.90	0.770	7.513	10.901	0.794	10.456
6(iii)	2.5	0.458	0.486	17.25	0.586*	7.178	10.415		
6(iv)	2.5	0.462	0.486	22.50	0.758	7.303	10.596		
7(i)	2.5	0.500	0.420	15.40	0.642	7.137	10.356		
7(ii)	2.5	0.512	0.472	26.50	0.854	6.304	9.147	0.703	9.568
7(iii)	2.5	0.484	0.390	19.50	0.973	6.984	10.134		
7(iv)	2.0	0.476	0.412	18.20	0.662	5.952	8.636		

...Contd.

1	2	3	4	5	6	7	8	9	10
9(i)	1.5	0.460	0.450	26.6	0.630	-	-		
9(ii)	2.5	0.542	0.428	21.25	0.787	6.995	10.150		
9(iii)	2.5	0.450	0.474	19.30	0.702	5.612	8.143	0.700	10.022
9(iv)	2.5	0.550	0.540	33.00	0.756	8.114	11.773		
9(v)	2.5	0.644	0.508	32.70	0.723	-	-		
9(vi)	2.5	0.452	0.480	17.00	0.600	-	-		

Values with asterix against them are not included in the average.

Table 4.52

Glass	Angle 2θ in degrees	d (Å)	I/I_1
7 (Bulk)	38.24	2.35166	100.00
	44.36	2.04038	37.11
	64.56	1.44232	23.71
	77.48	1.23090	27.84
	81.40	1.18124	7.28
6 (Bulk)	38.08	2.3610	100.00
	44.24	2.0460	32.56
	64.48	1.4440	20.93
	77.38	1.2320	27.13
7 (Fibres)	38.08	2.3612	100.00
	44.20	2.0474	70.00
	77.60	1.2293	32.00

Table 4.41

Glass Fibre	Average UTSx10^{-5} (psi)	Average percent volume fraction ϕ of the dispersed phase	Average size R, of the dispersed phase ($\mathring{A}$)	Mean free path for crack propagation, ($\mathring{A}$)	$\sqrt{\frac{1}{\lambda}} \times 10^2$ ($\mathring{A}$)$^{-\frac{1}{2}}$
1	1.048	26.190	313.04	1176.30	2.916
2	1.498	40.278	133.455	263.84	6.156
3	1.190	22.421	127.44	587.958	4.124
4	1.784	38.889	97.149	203.55	7.009
8	0.826				

Bulk Glass	Average Rupture Modulus x10^8 p/in^2	Average percent volume fraction ϕ of the dispersed phase	Average size R, of the dispersed phase ($\mathring{A}$)	Mean free path for crack propagation, ($\mathring{A}$)	$\sqrt{\frac{1}{\lambda}} \times 10^2$ ($\mathring{A}$)$^{-\frac{1}{2}}$
1	0.762	41.666	122.749	229.138	6.606
2	0.691	33.974	107.663	278.98	5.987
4	0.614	25.992	168.766	640.713	3.951
8	0.514				

Table 4.61

Radius of Ring r_n (cms)	r_n^2	r_n^2/r_1^2	$\frac{h_n^2+k_n^2+l_n^2}{h_1^2+k_1^2+l_1^2}$ (t.c.)	h k l	Camera constant λL (Å cm)	a_{hkl}	d_{hkl} (silver)
1.150	1.323	1.000	1.000	111		2.357	2.359
1.325	1.756	1.327	1.333	200		2.045	2.044
1.880	3.534	2.672	2.667	220		1.441	1.445
2.220	4.928	3.725	3.667	311	2.710	1.221	1.231
2.350	5.406	4.085	4.000	222		1.153	1.180
2.950	8.703	6.578	6.333	331		0.919	0.938
3.025	9.151	6.917	6.067	420		0.896	0.914

Table 4.62: SAD analysis of photograph 4.619.

Glass	Distances of spots from centre r_n(cms)	Camera constant (L) Å cm	d_{hkl}(Å)
2 Fibres	1.30	2.9631	1.272
	1.70		1.743
	1.75		1.693
	1.95		1.52
	2.30		1.293
	2.35		1.261
	2.99		0.991
	3.025		0.980

Table 4.63

Glass	Diameter of Rings (cms)	Radius of ring r (cms)	Camera constant (L) Å cm	d_{hkl} (Å)
5 Fibres	2.15	1.075	2.9631	2.76
	2.48	1.24		2.39
	3.30	1.65		1.796
	3.725	1.59		1.59
	3.90	1.80		1.52
	4.35	2.175		1.36

Table 4.64

Glass	Distance of spots from centre r_n (cms)	Camera constant (ρ_L) in Å cm.	d_{hkl} (Å)
	0.675		4.39
	1.075		2.76
	1.20		2.47
6 Fibres	1.24	2.9631	2.39
	1.625		1.82
	1.875		1.58
	2.175		1.36

Table 4.65

A.S.T.M. DATA

Bismuth Bi, Hexagonal					
a (Å)	I/I_1	hkl	a (Å)	I/I_1	hkl
3.95	9	003	1.1843	2	028
3.74	3	011	1.1399	4	119
3.28	100	102	1.1368	4	220
2.39	40	014	1.1179	2	127
2.273	41	110	1.0932	4	306
2.030	8	105	1.0738	5	132
1.976	3	006	1.0561	2	218
1.970	10	113	1.0399	2	1.0.11
1.941	1	201	1.0247	3	314
1.868	23	022	0.9920	1	135
1.639	9	204	0.9854	3	226
1.556	6	017	0.9709	2	402
1.515	2	025	0.9455	2	0.2.11
1.491	13	116	0.9301	4	309
1.387	4	108	0.9276	2	1.2.10
1.330	11	124	0.9178	2	317
1.319	1	009	0.9065	2	1.1.12
1.312	6	300	0.8928	2	322
1.284	2	207			
1.261	2	215			
1.246	1	303			

Table 4.56

A.S.T.M. DATA

Calcium Magnesium Silicate $Ca_2MgSi_2O_7$ (Tetragonal)			Akermanite or Melilite $2CaO \cdot MgO \cdot 2SiO_2$			Silver (f.c.c.) Ag		
d (Å)	I/I_1	hkl	d (Å)	I/I_1	hkl	d (Å)	I/I_1	hkl
4.22	30	101	1.76	80	312	2.359	100	111
3.72	50	111	1.73	50	331	2.044	40	200
3.51	30	210	1.67	20	003	1.445	25	311
3.09	70	201	1.66	20	421	1.231	26	311
2.87	100	211	1.64	50	322	1.1796	12	222
2.51	20	002	1.60	50	113	1.0215	4	400
2.48	70	310	1.54	30	203	0.9375	15	311
2.43	50	221	1.52	30	412	0.9137	12	420
2.39	60	102	1.51	60	213	0.8341	13	422
2.32	60	301	1.49	30	332			
2.28	50	112	1.47	50	511			
2.22	20	311	1.46	20	520			
2.11	20	202	1.44)	60	(422			
2.04	70	212	1.43)		(223			
2.00	30	321	1.41	50	303			
1.96	60	400	1.40	70	521			
1.90	60	410	1.39	50	440			
1.86	30	222	1.39	20	313			
1.85	60	330						
1.78	60	411						

Table 4.67

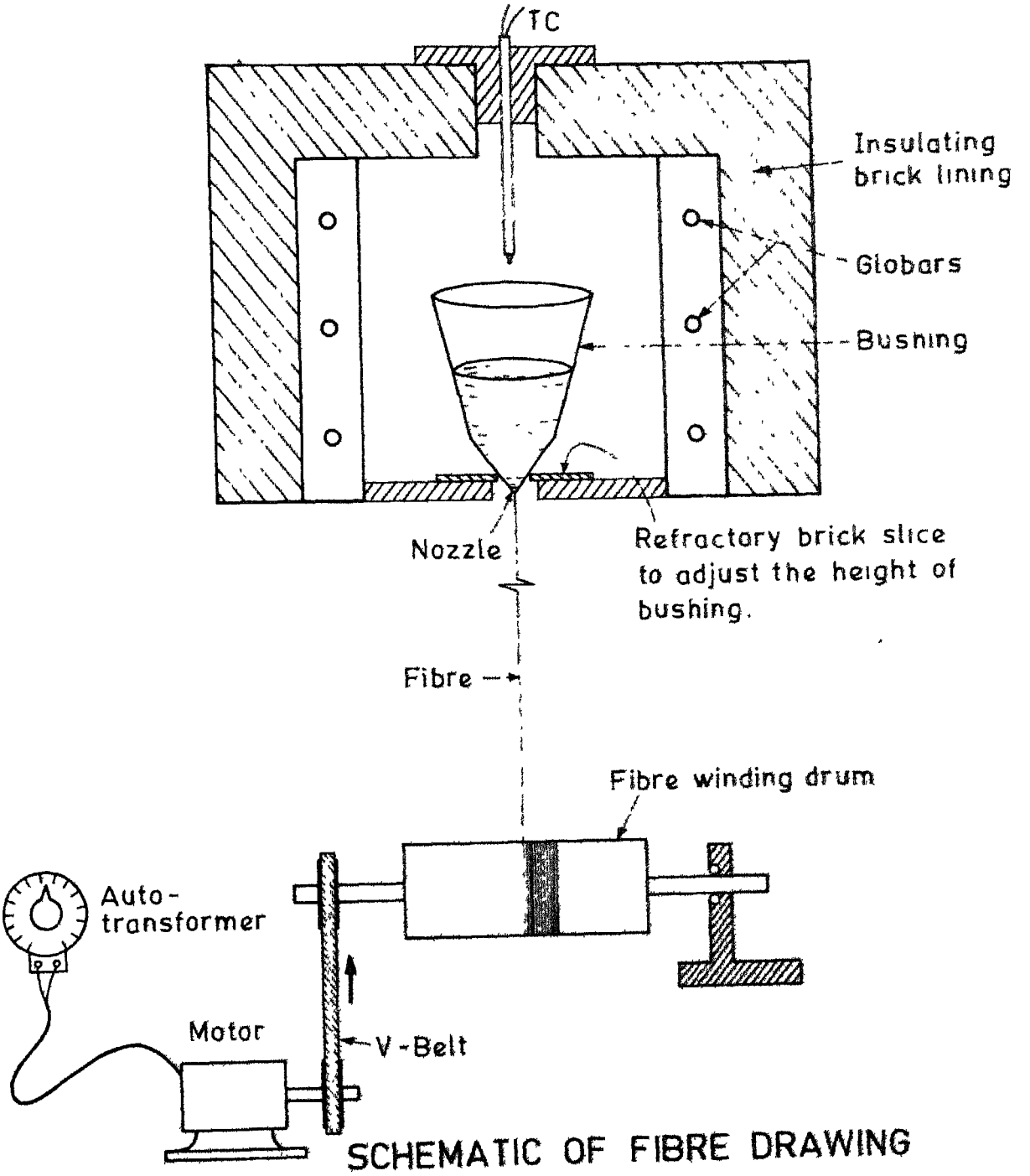

SCHEMATIC OF FIBRE DRAWING ASSEMBLY.

FIG. 3.2

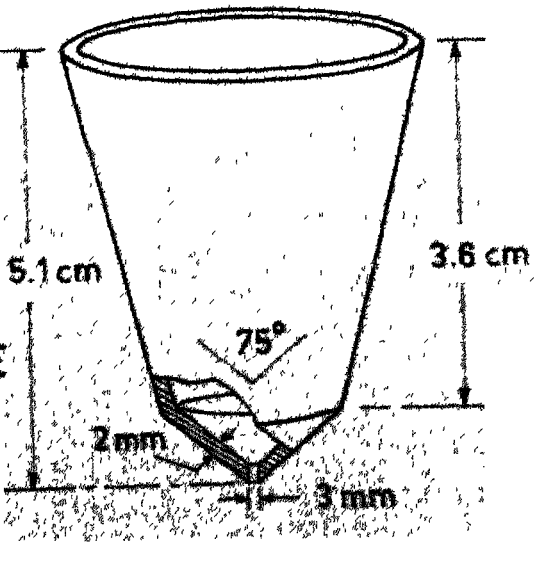

HIGH ALUMINA BUSHING USED FOR DRAWING THE FIBRES.

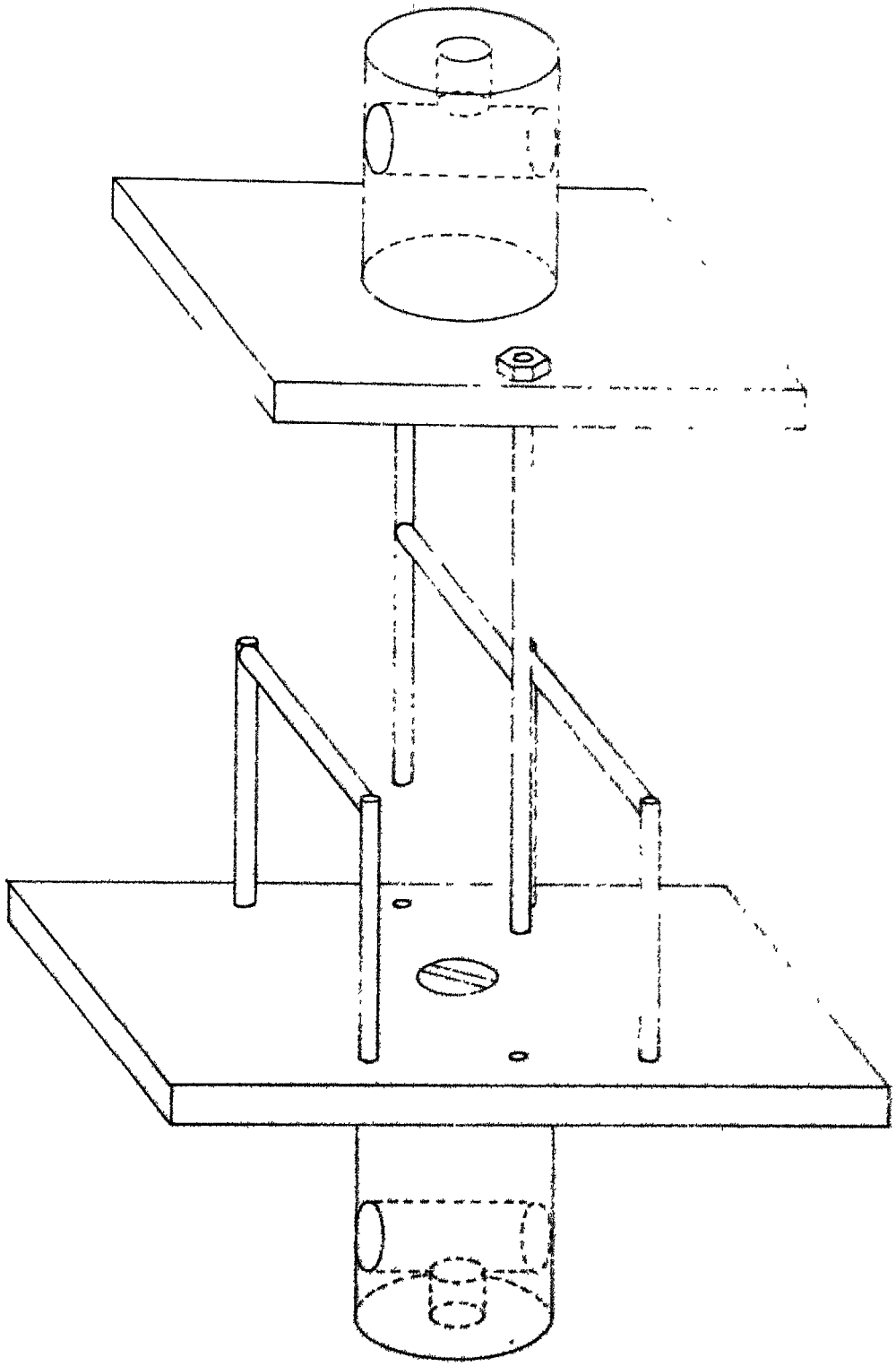

Fig. 3.4 JIG USED FOR DETERMINATION OF RUPTURE MODULUS AND YOUNG'S MODULUS IN BENDING OF BULK GLASSES.

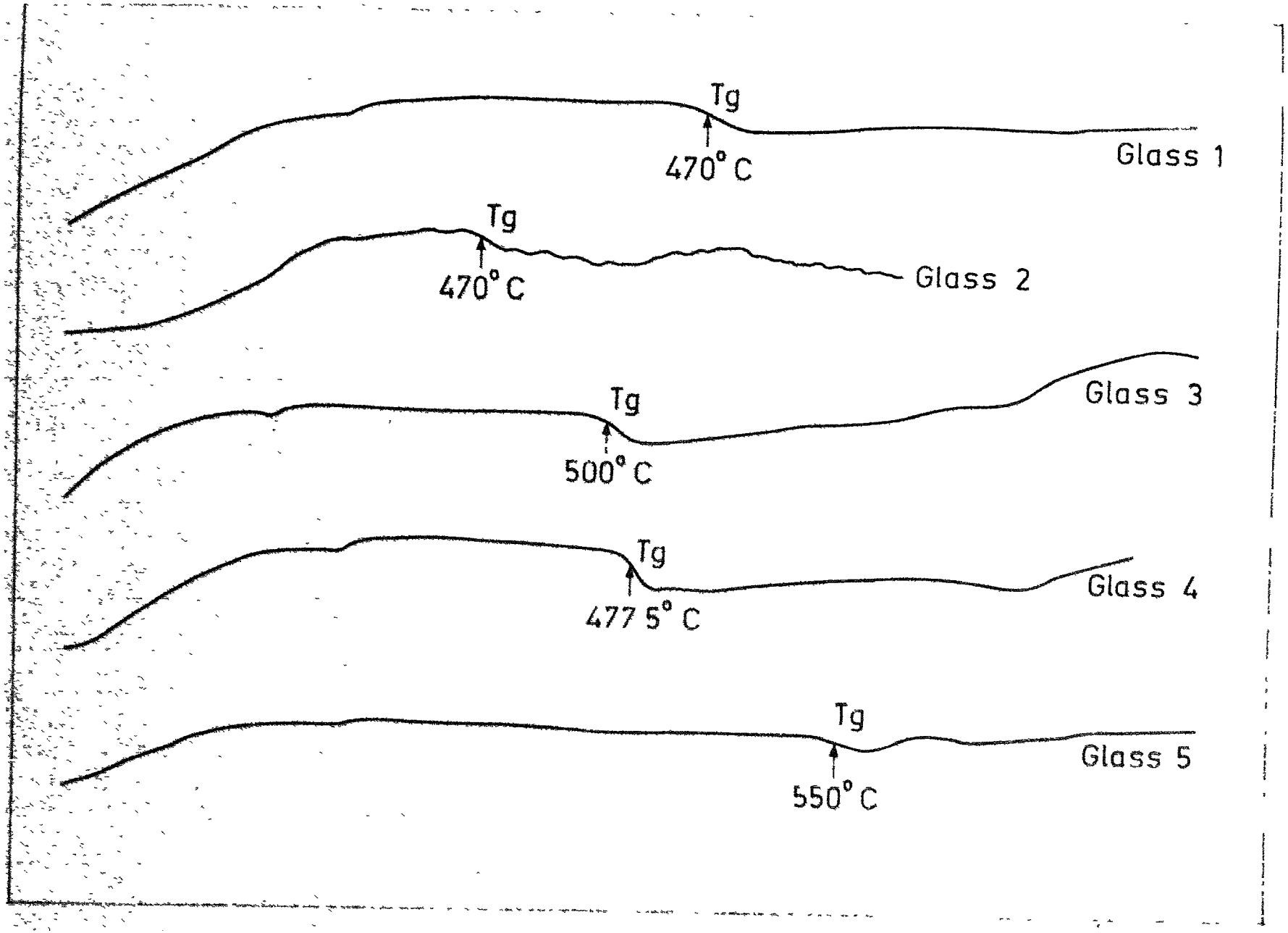
Tg
470° C
Glass 1
Tg
470° C
Glass 2
Tg
500° C
Glass 3
Tg
477 5° C
Glass 4
Tg
550° C
Glass 5

Fig. 4.1a

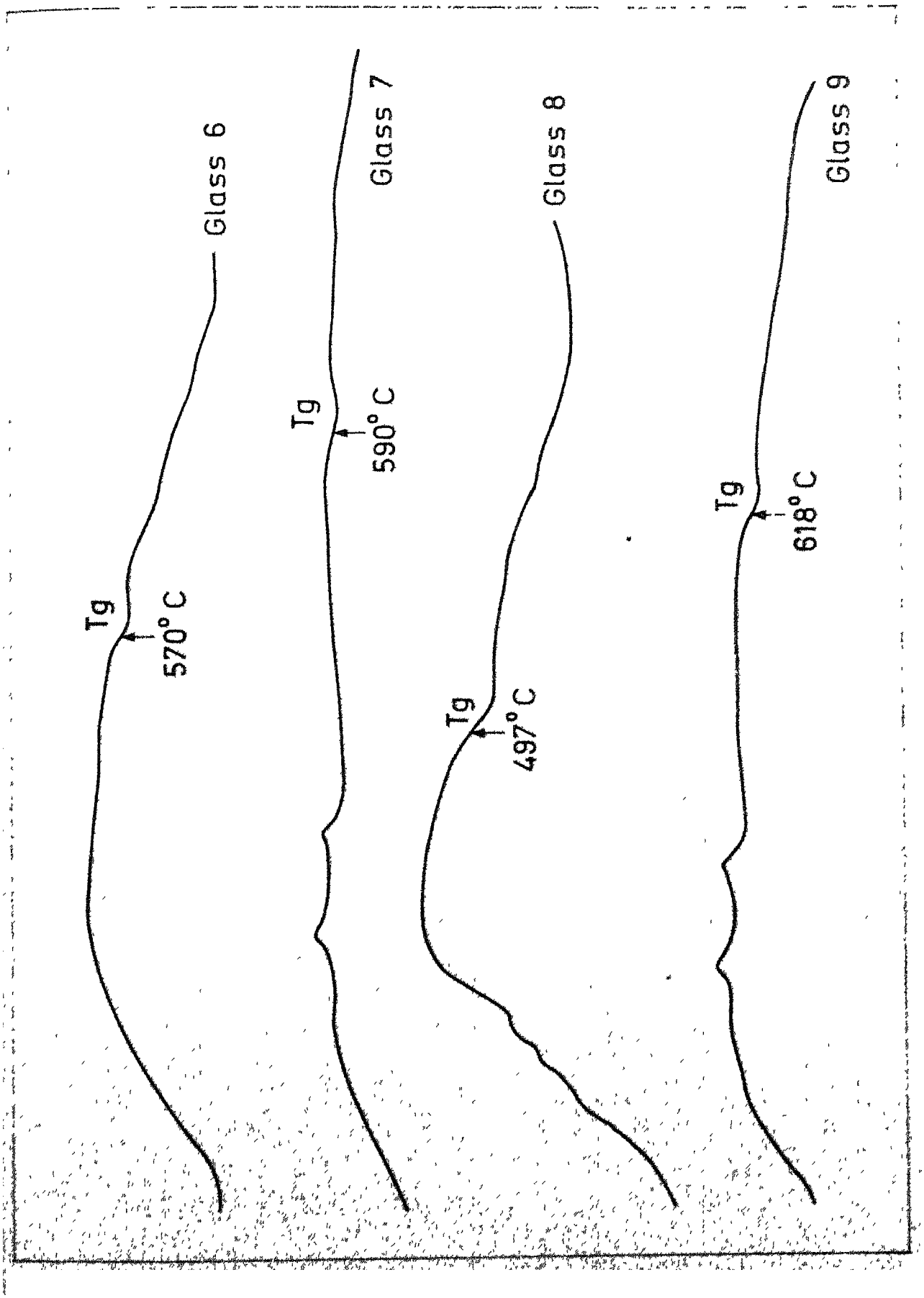

Fig. 4.1b

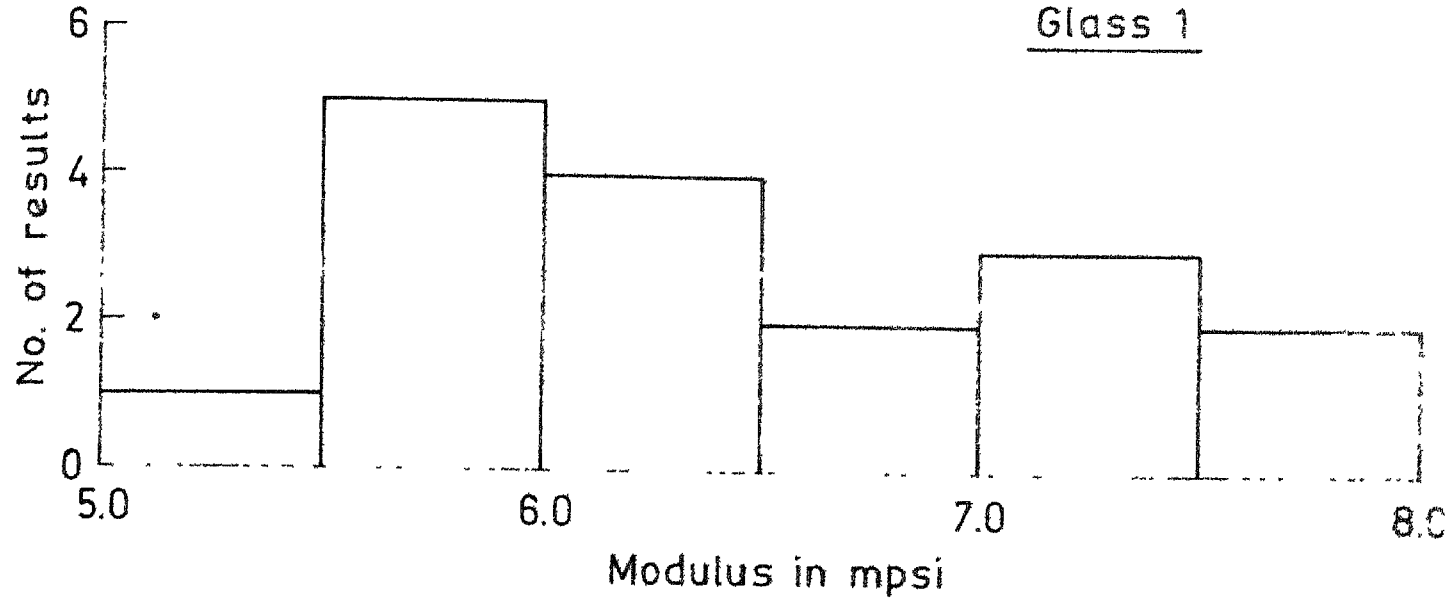
Glass 1
No. of results
0
2
4
6
5.0
6.0
7.0
8.0
Modulus in mpsi

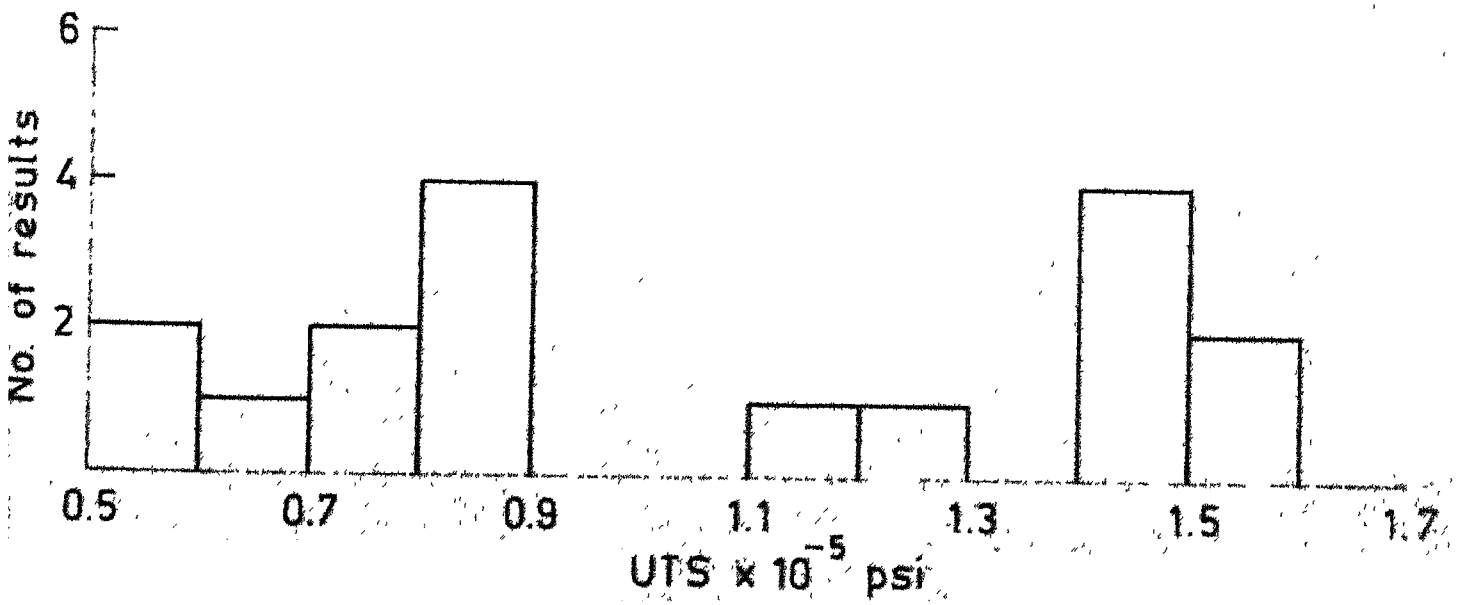
No. of results
0
2
4
6
0.5
0.7
0.9
1.1
1.3
1.5
1.7
UTS x 10⁻⁵ psi

Fig. 4.21

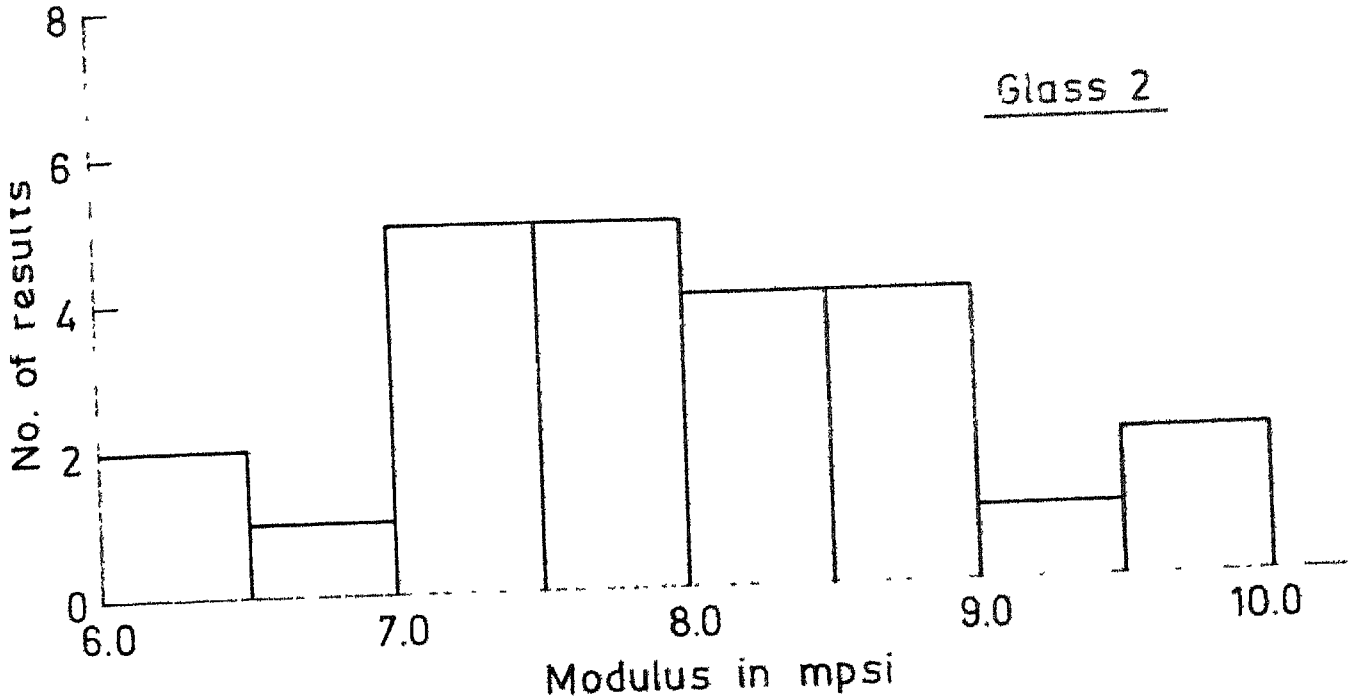
Glass 2
No. of results
0
2
4
6
8
6.0
7.0
8.0
9.0
10.0
Modulus in mpsi

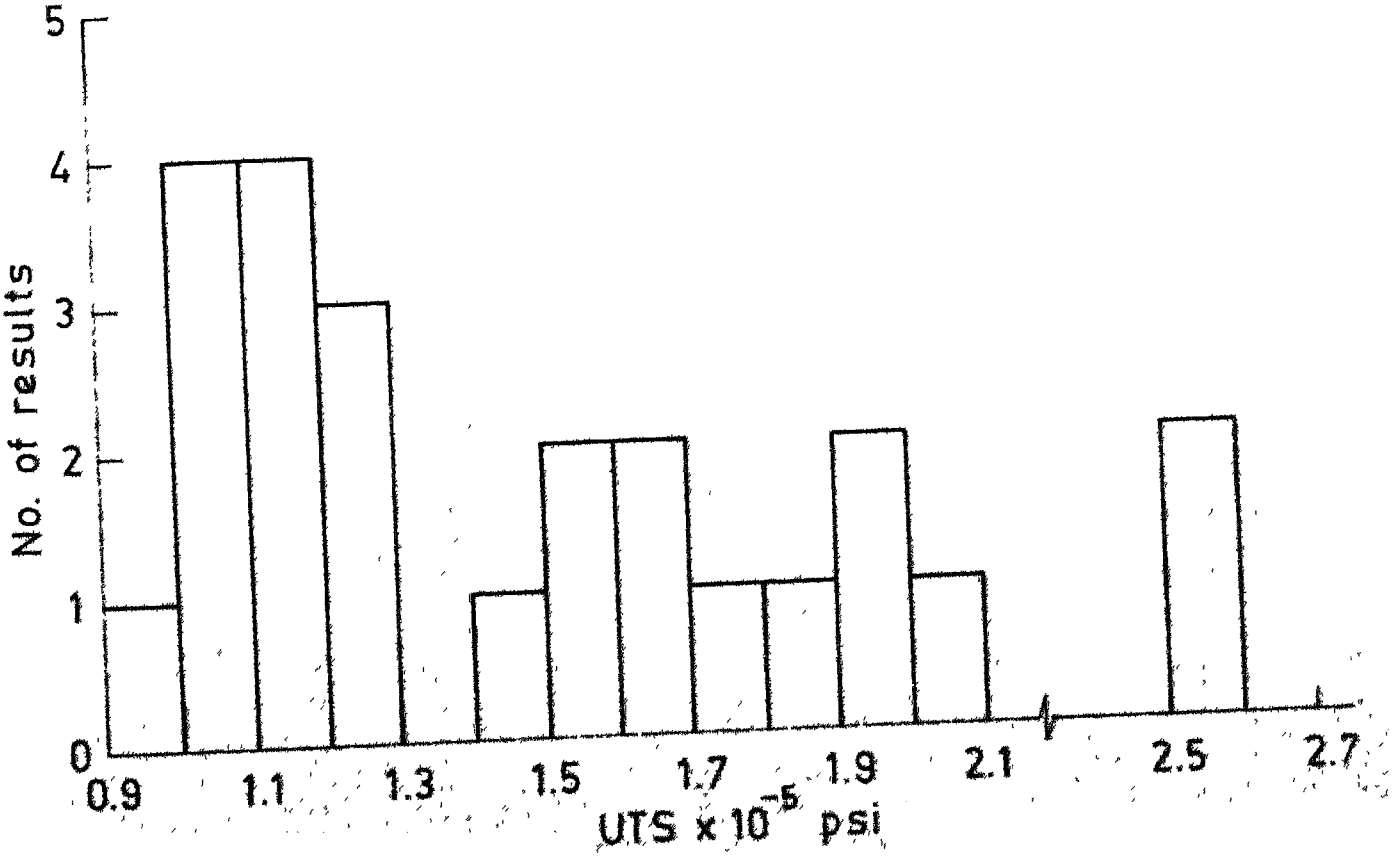
No. of results
0
1
2
3
4
5
0.9
1.1
1.3
1.5
1.7
1.9
2.1
2.5
2.7
UTS x 10⁻⁵ psi

Fig. 4.22

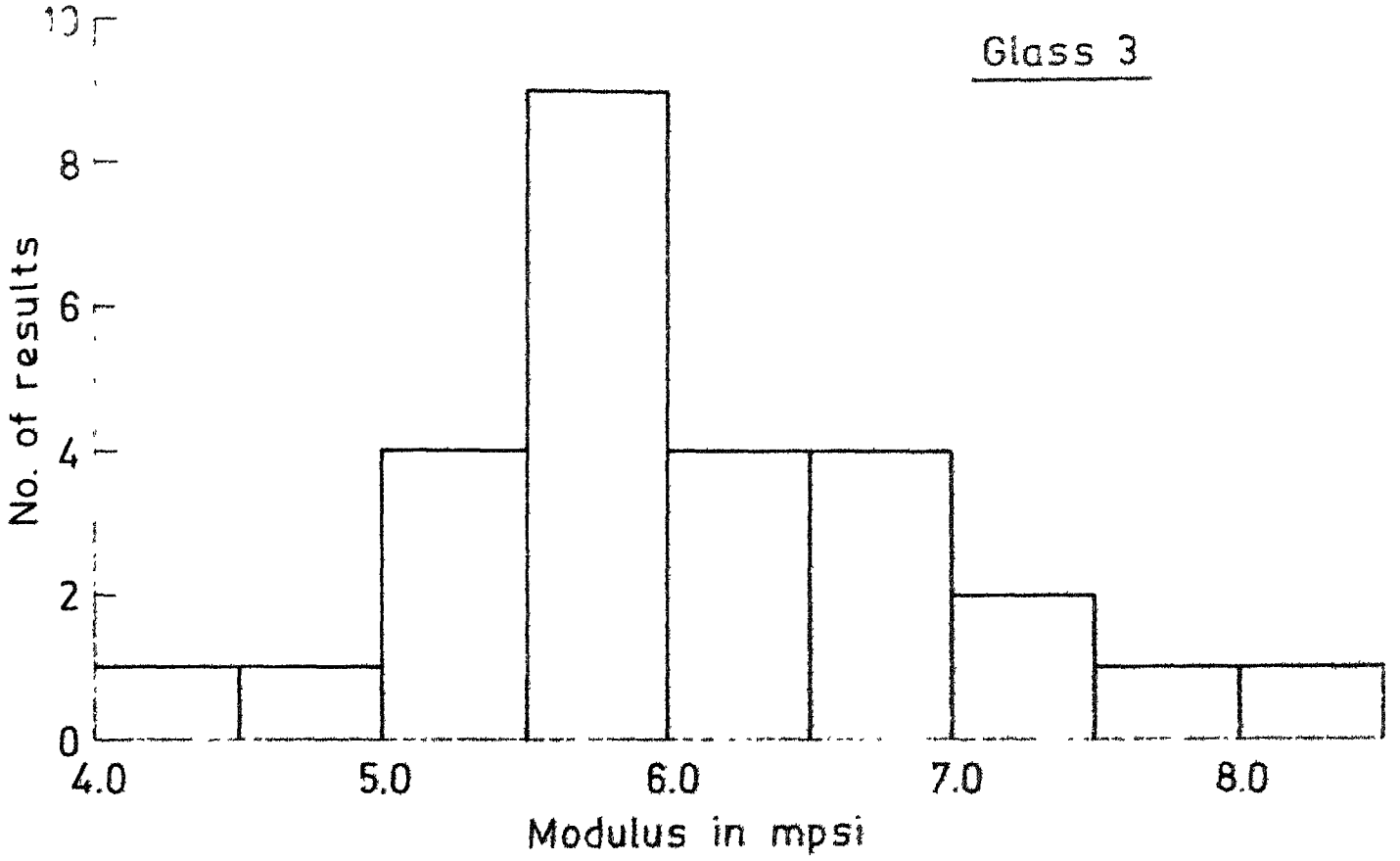
Glass 3
No. of results
0
2
4
6
8
10
4.0
5.0
6.0
7.0
8.0
Modulus in mpsi

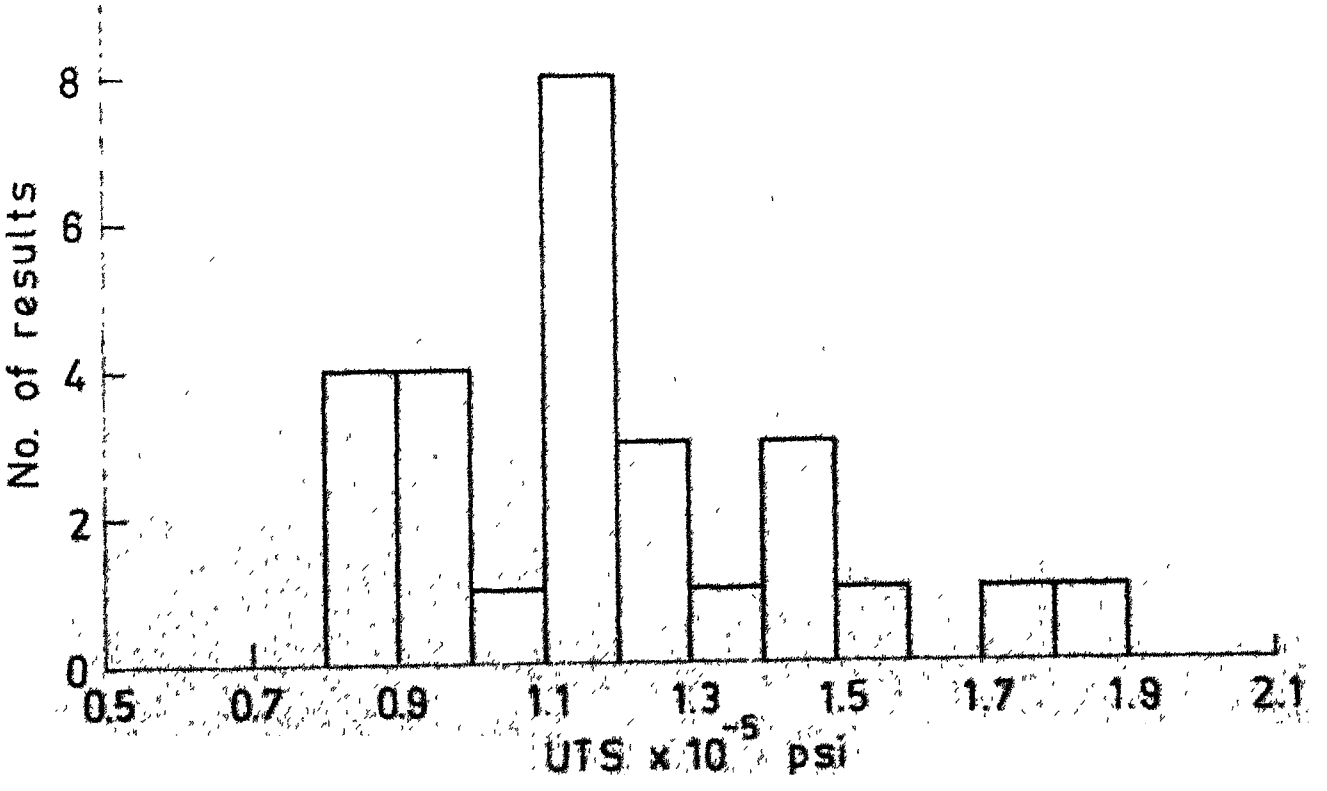
No. of results
0
2
4
6
8
0.5
0.7
0.9
1.1
1.3
1.5
1.7
1.9
2.1
UTS x 10⁻⁵ psi

Fig. 4.23

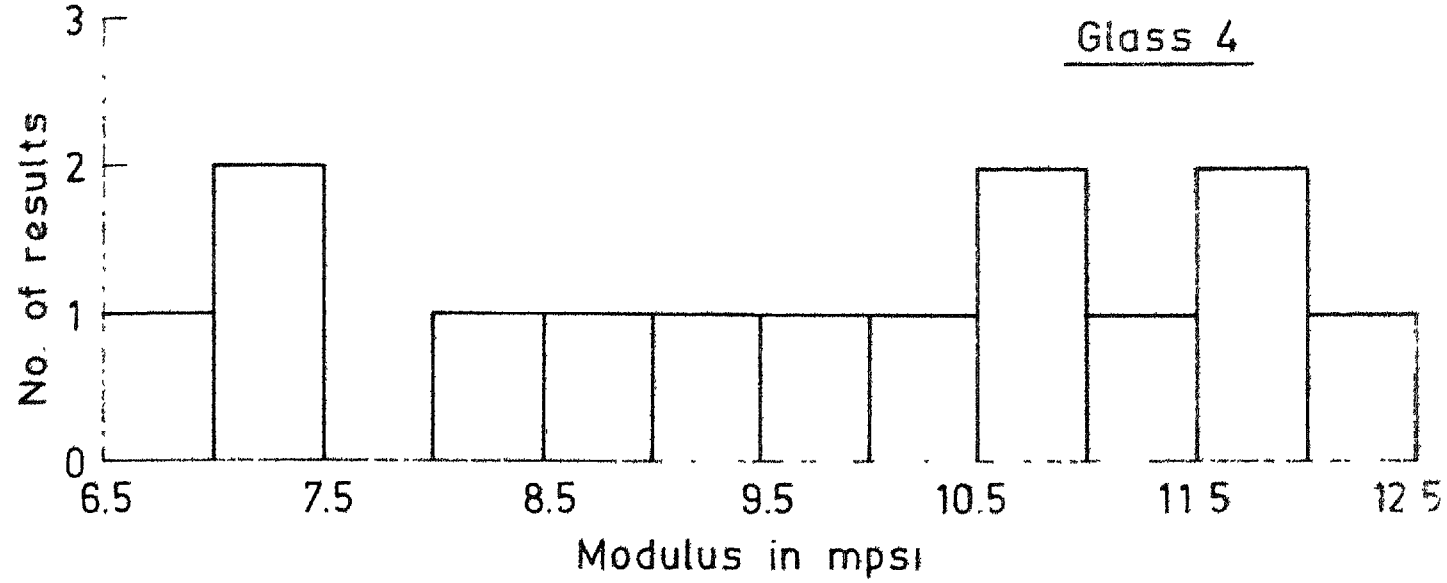
Glass 4
No. of results
0
1
2
3
6.5
7.5
8.5
9.5
10.5
11.5
12.5
Modulus in mpsi

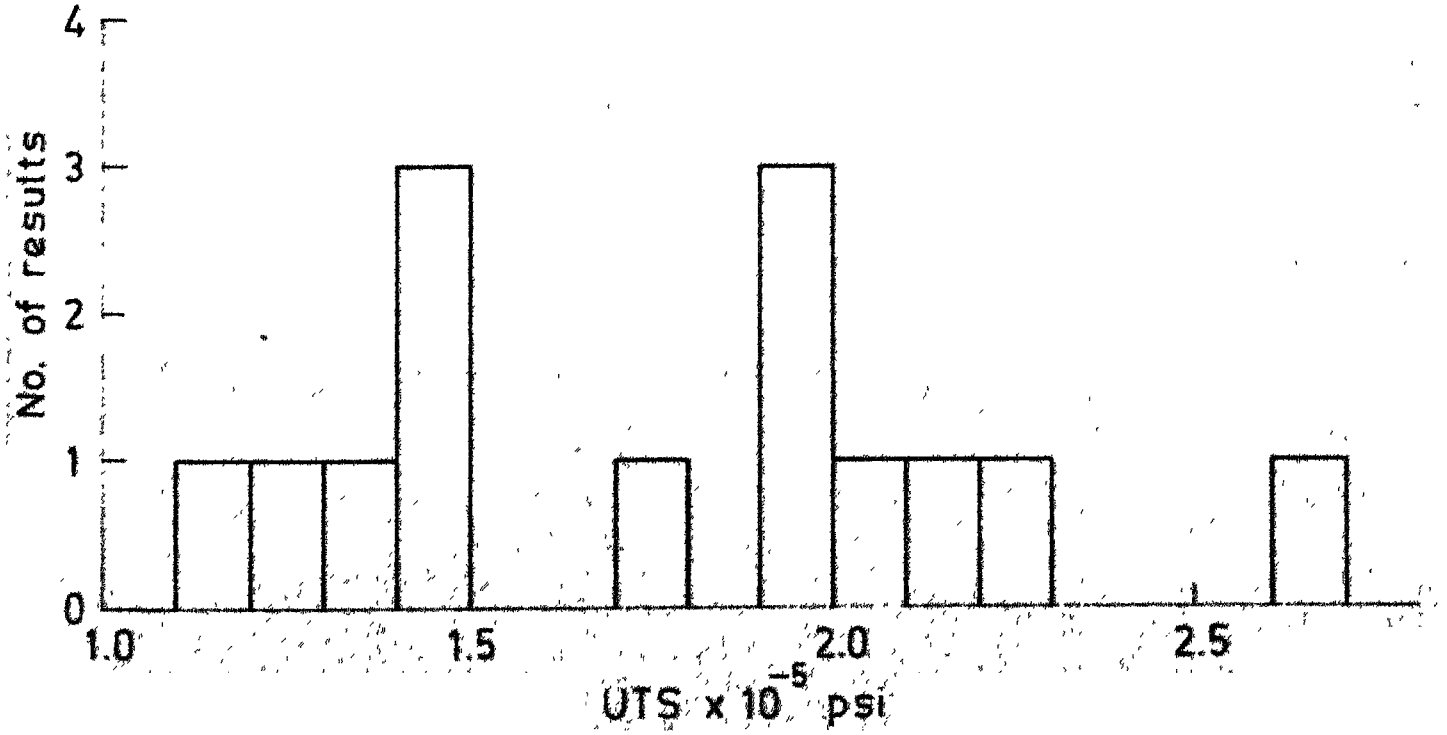
No. of results
0
1
2
3
4
1.0
1.5
2.0
2.5
UTS x 10⁻⁵ psi

Fig. 4.24

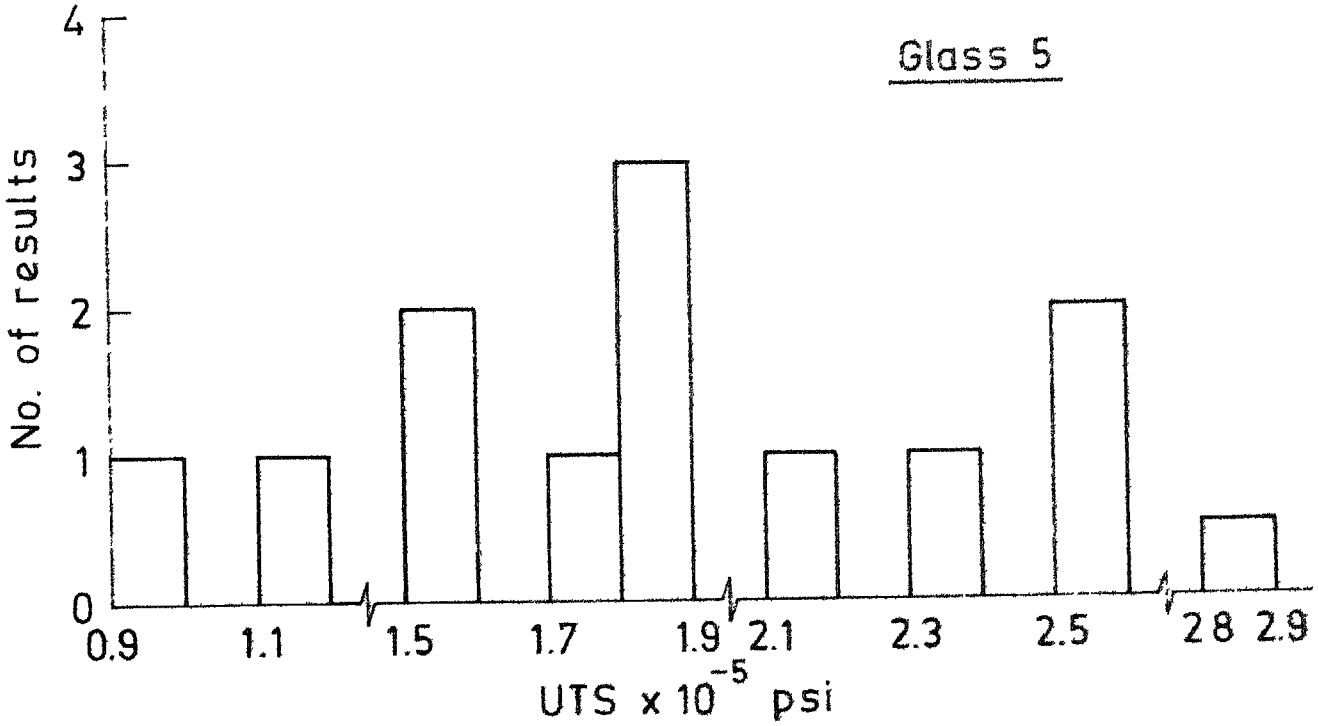
Glass 5
No. of results
0
1
2
3
4
0.9
1.1
1.5
1.7
1.9
2.1
2.3
2.5
2.8
2.9
UTS x 10^-5 psi

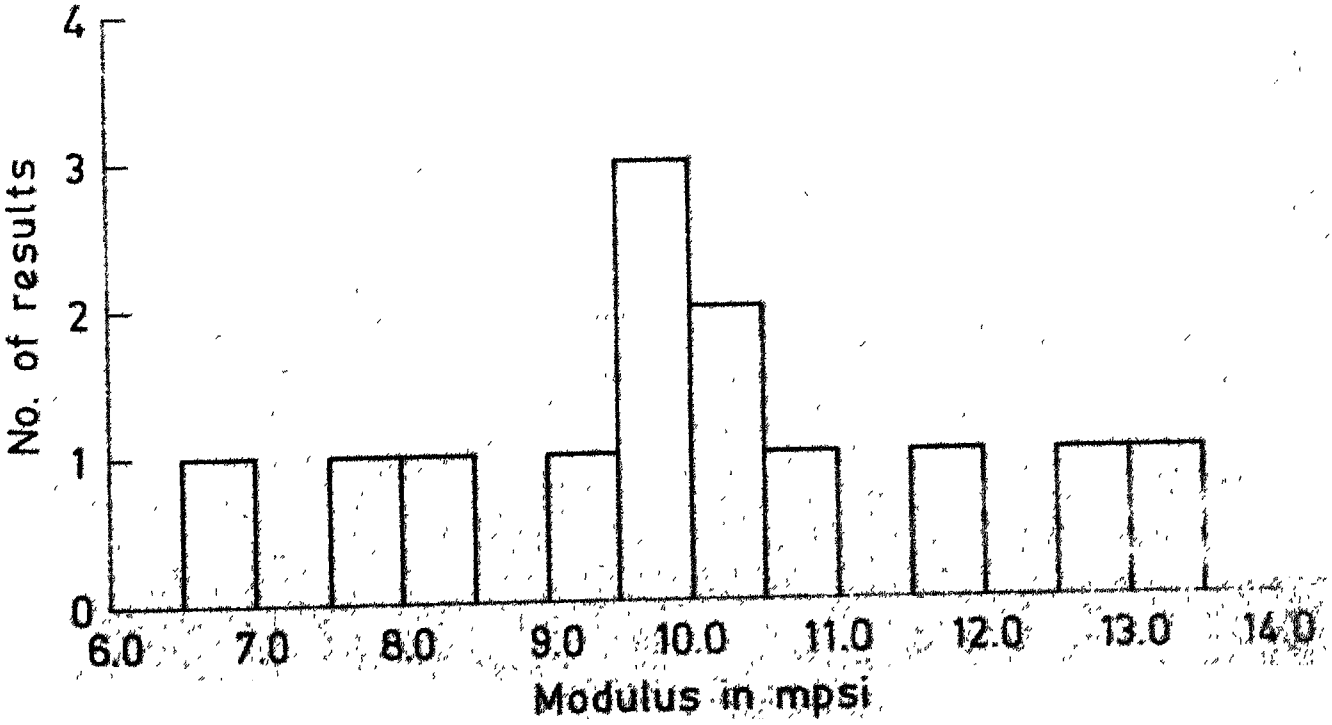
No. of results
0
1
2
3
4
6.0
7.0
8.0
9.0
10.0
11.0
12.0
13.0
14.0
Modulus in mpsi

Fig 4.25

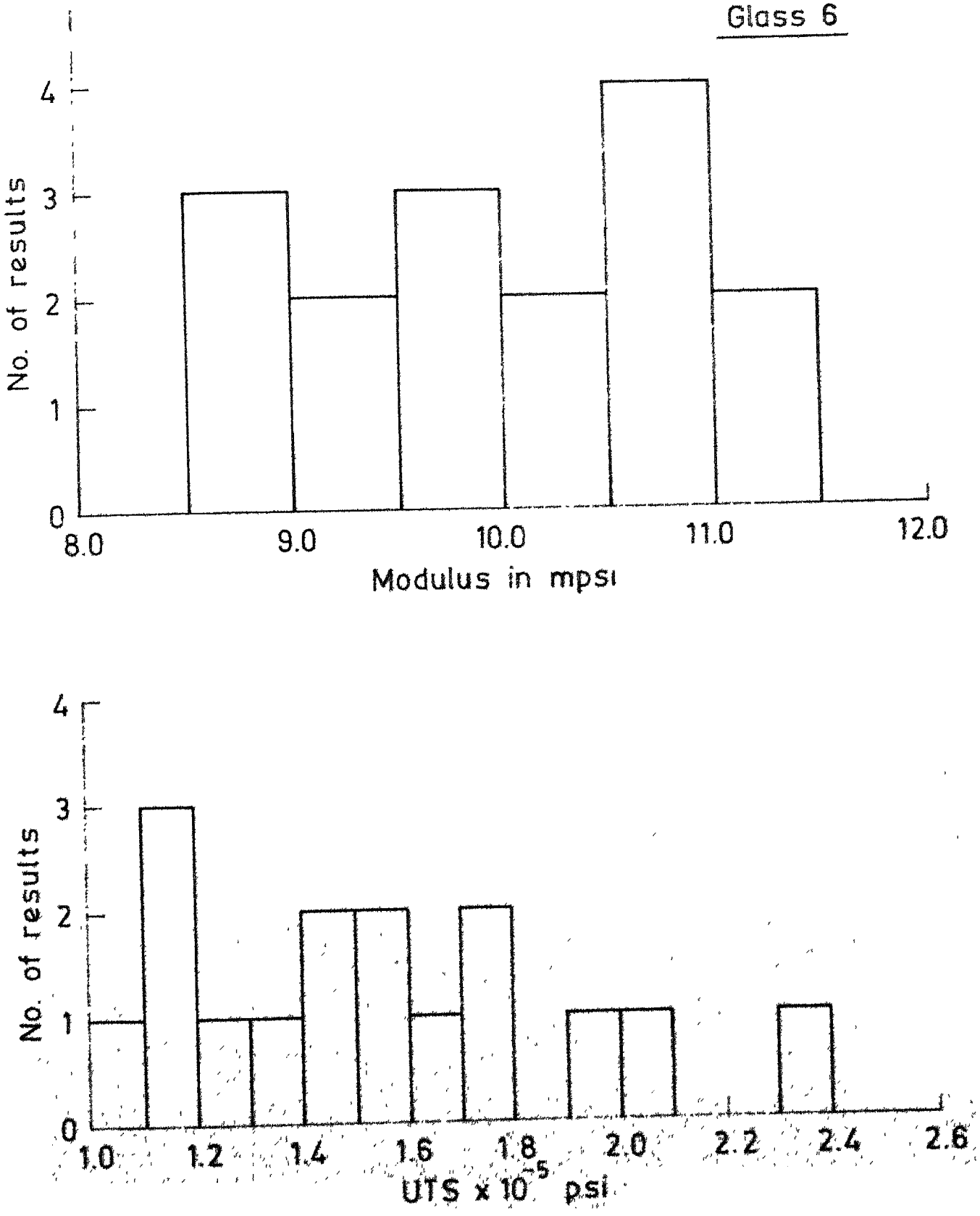
Glass 6
No. of results
0
1
2
3
4
8.0
9.0
10.0
11.0
12.0
Modulus in mpsi
No. of results
0
1
2
3
4
1.0
1.2
1.4
1.6
1.8
2.0
2.2
2.4
2.6
UTS x 10⁻⁵ psi

Fig. 4.26

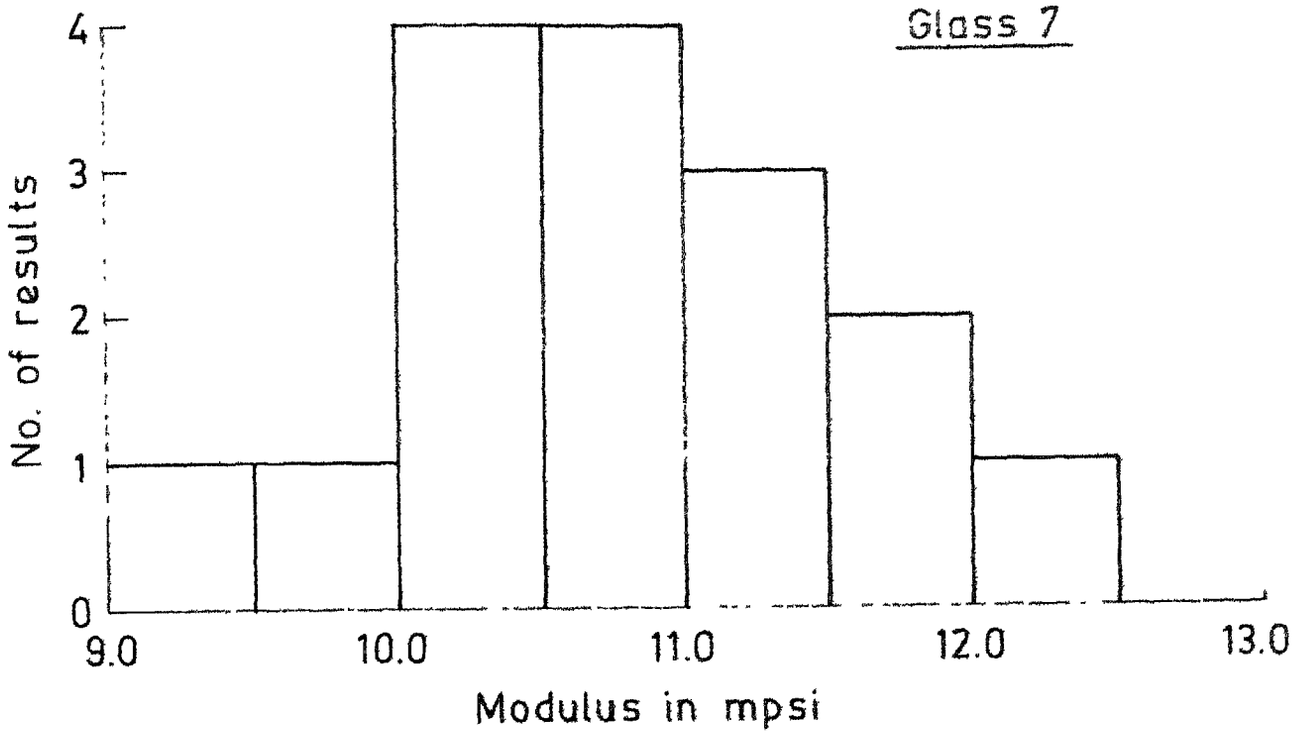
Glass 7
No. of results
0
1
2
3
4
9.0
10.0
11.0
12.0
13.0
Modulus in mpsi

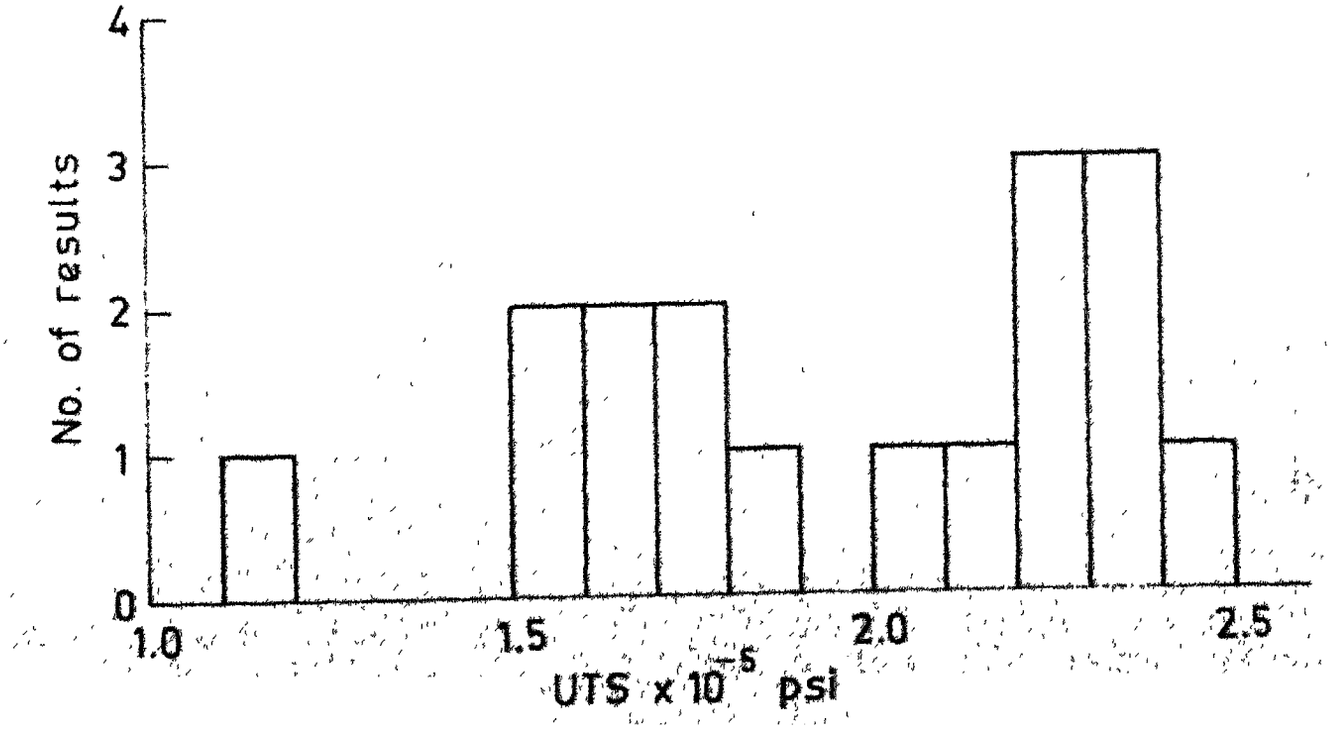
No. of results
0
1
2
3
4
1.0
1.5
2.0
2.5
UTS x 10⁻⁵ psi

Fig. 4.27

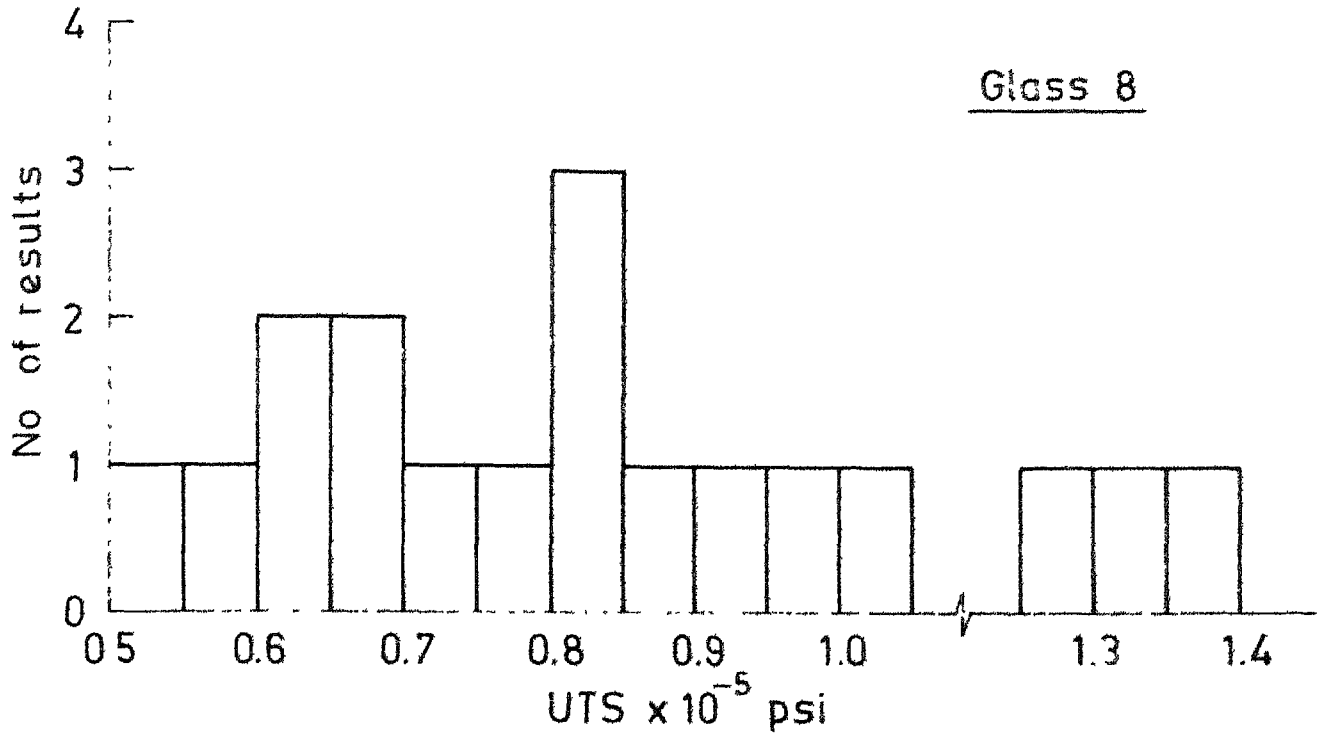
Glass 8
No of results
0
1
2
3
4
0 5
0.6
0.7
0.8
0.9
1.0
1.3
1.4
UTS x 10⁻⁵ psi

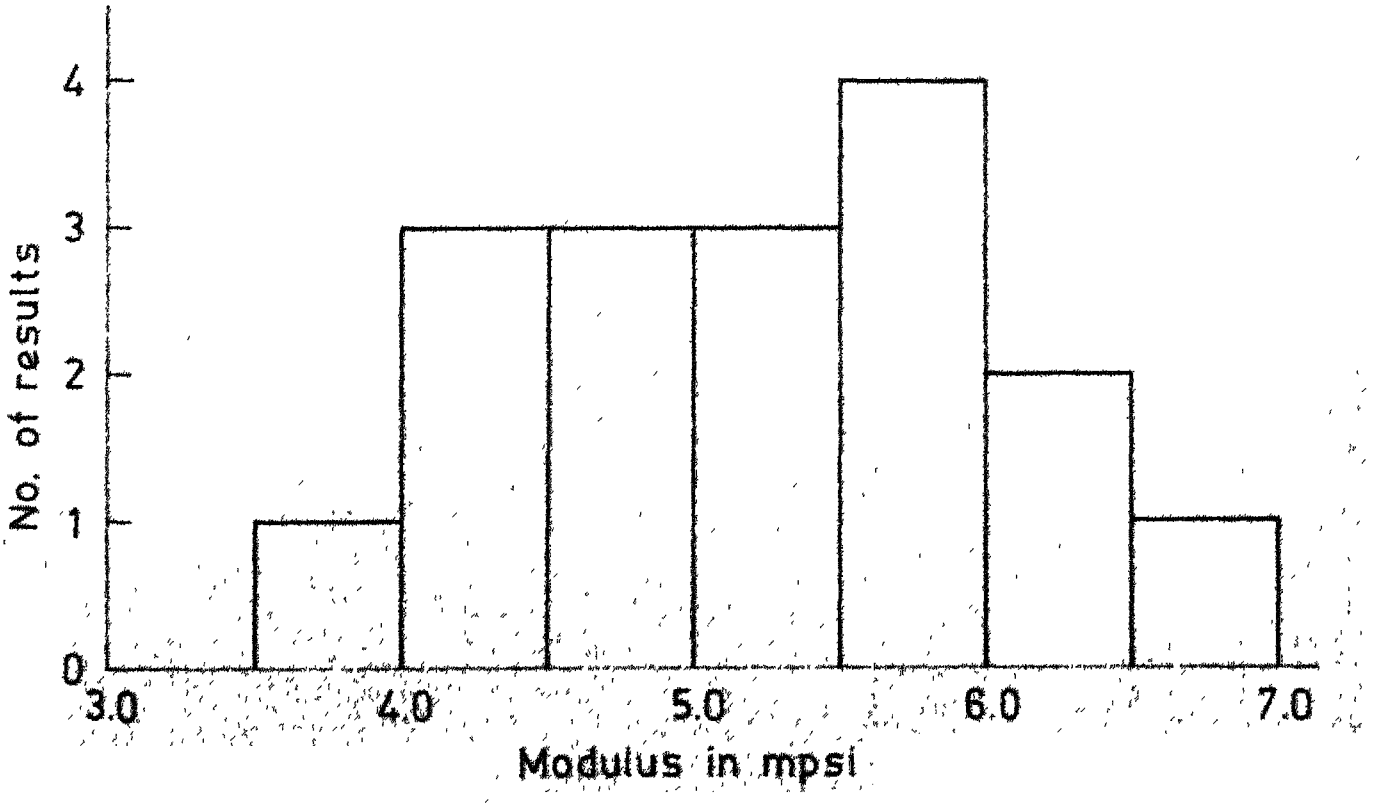
No. of results
0
1
2
3
4
3.0
4.0
5.0
6.0
7.0
Modulus in mpsi

Fig. 4.28

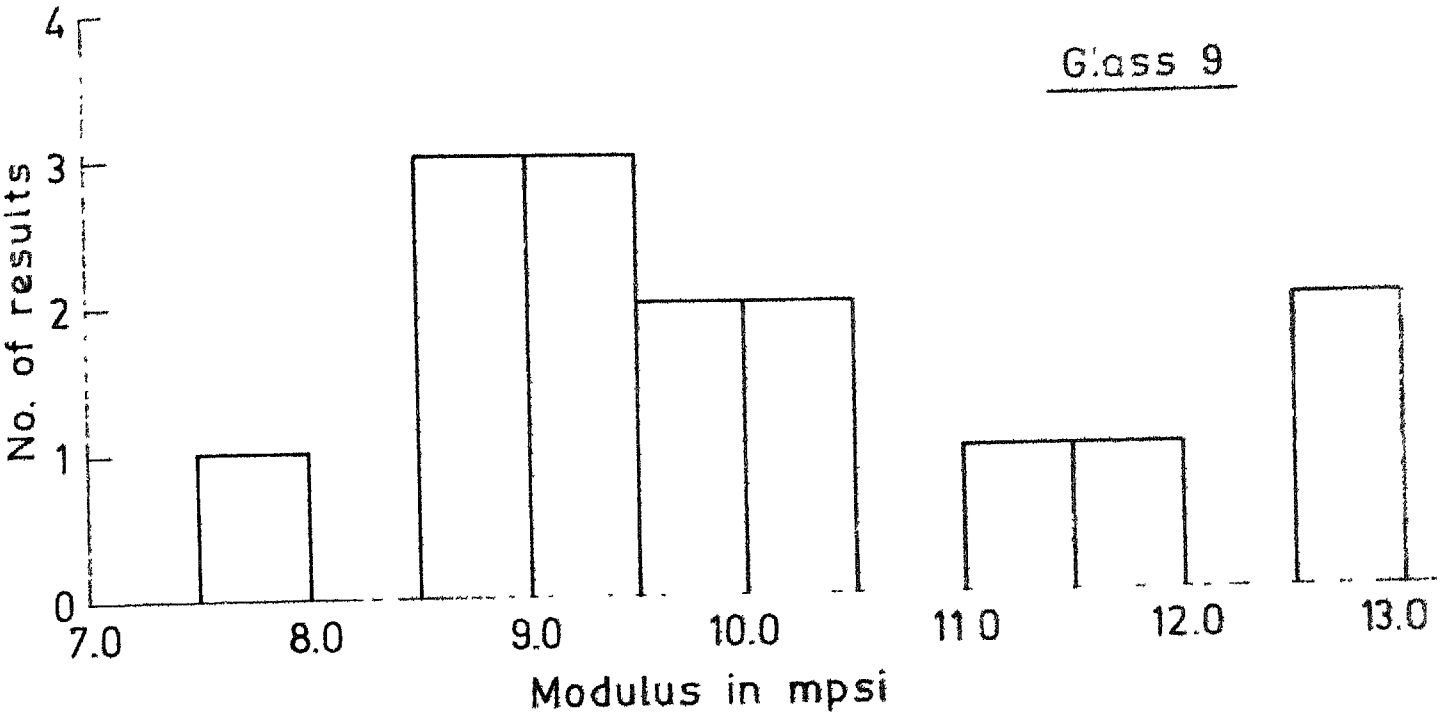
Glass 9
No. of results
0
1
2
3
4
7.0
8.0
9.0
10.0
11.0
12.0
13.0
Modulus in mpsi

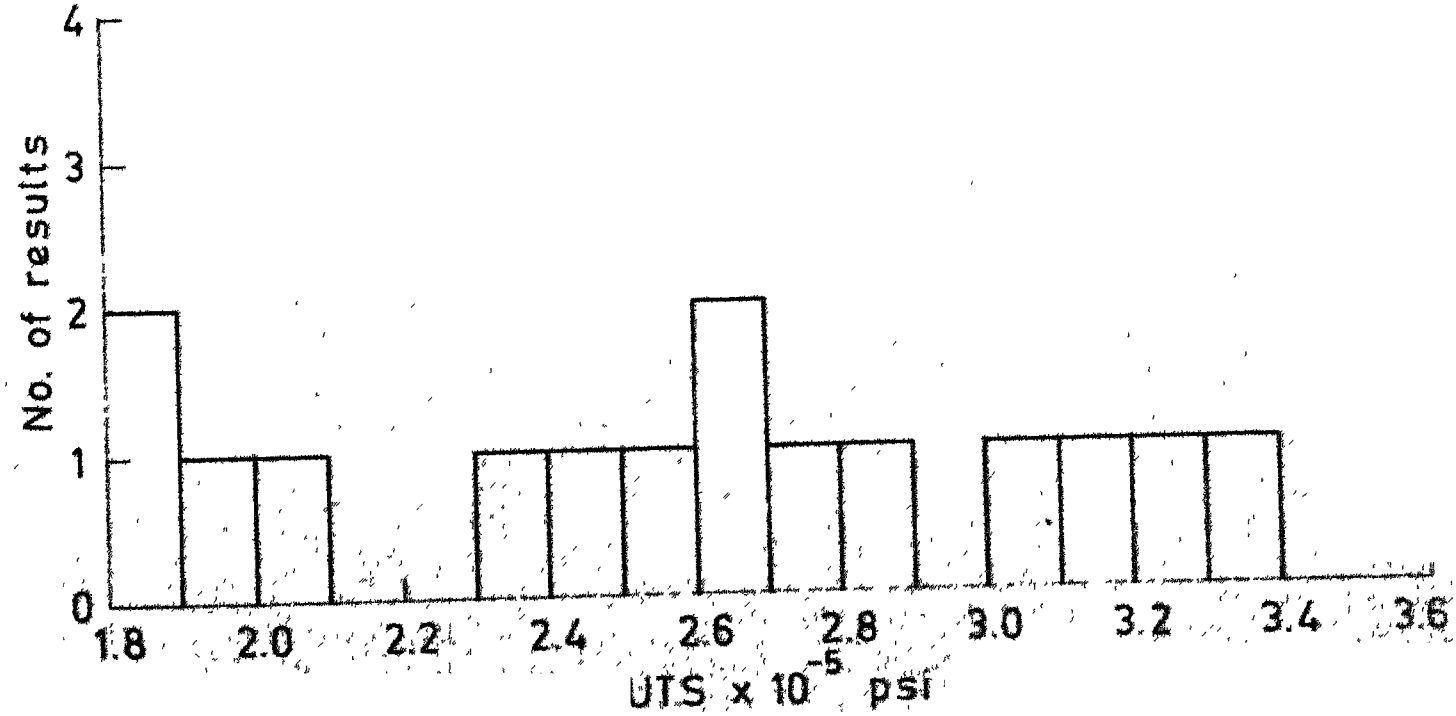
No. of results
0
1
2
3
4
1.8
2.0
2.2
2.4
2.6
2.8
3.0
3.2
3.4
3.6
UTS x 10^-5 psi

Fig. 4.29

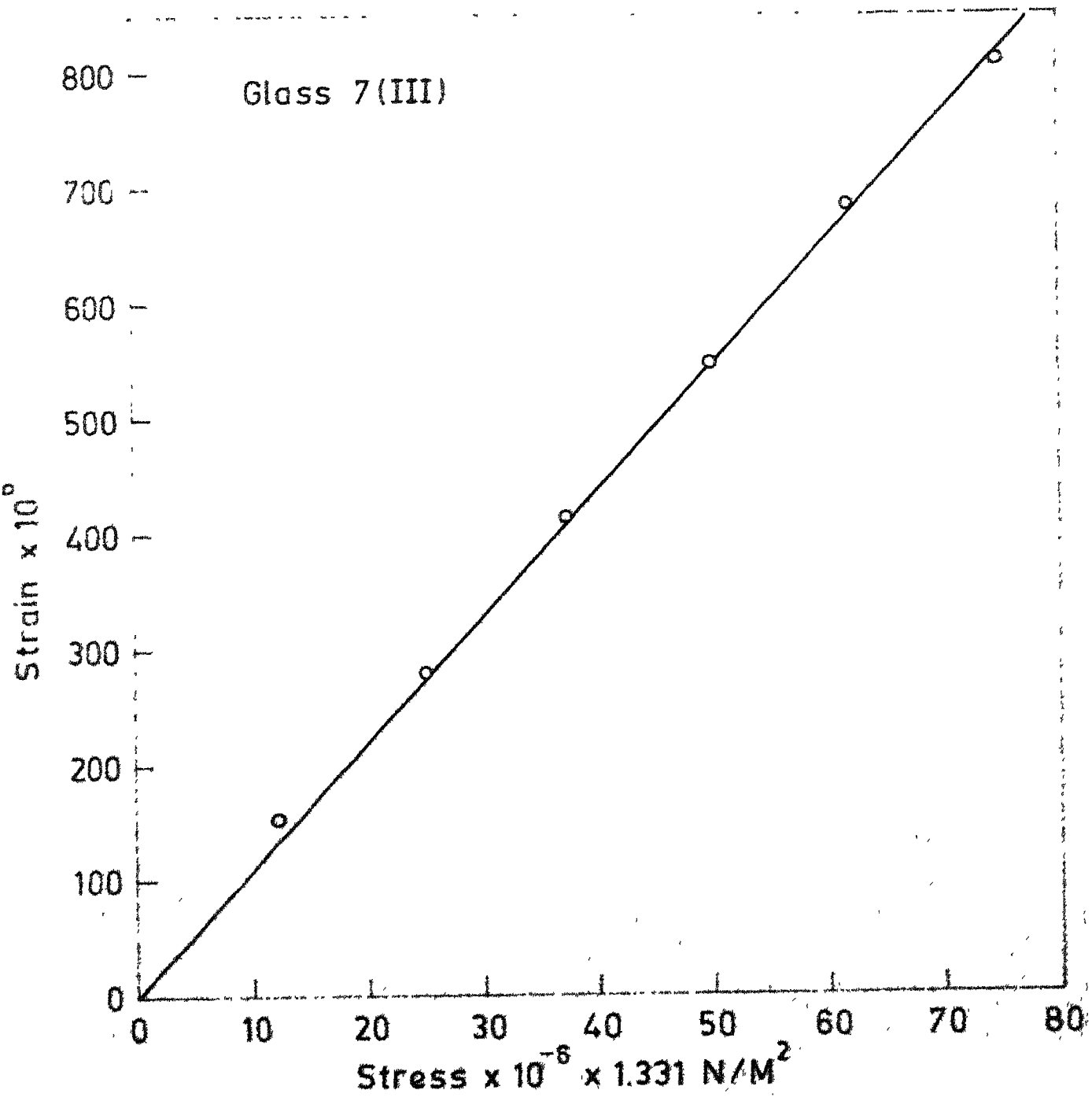
Glass 7(III)
800
700
600
500
400
300
200
100
0
Strain x 10°
0
10
20
30
40
50
60
70
80
Stress x 10⁻⁶ x 1.331 N/M²

Fig. 4.31

CPS = 100

Time constant = 8

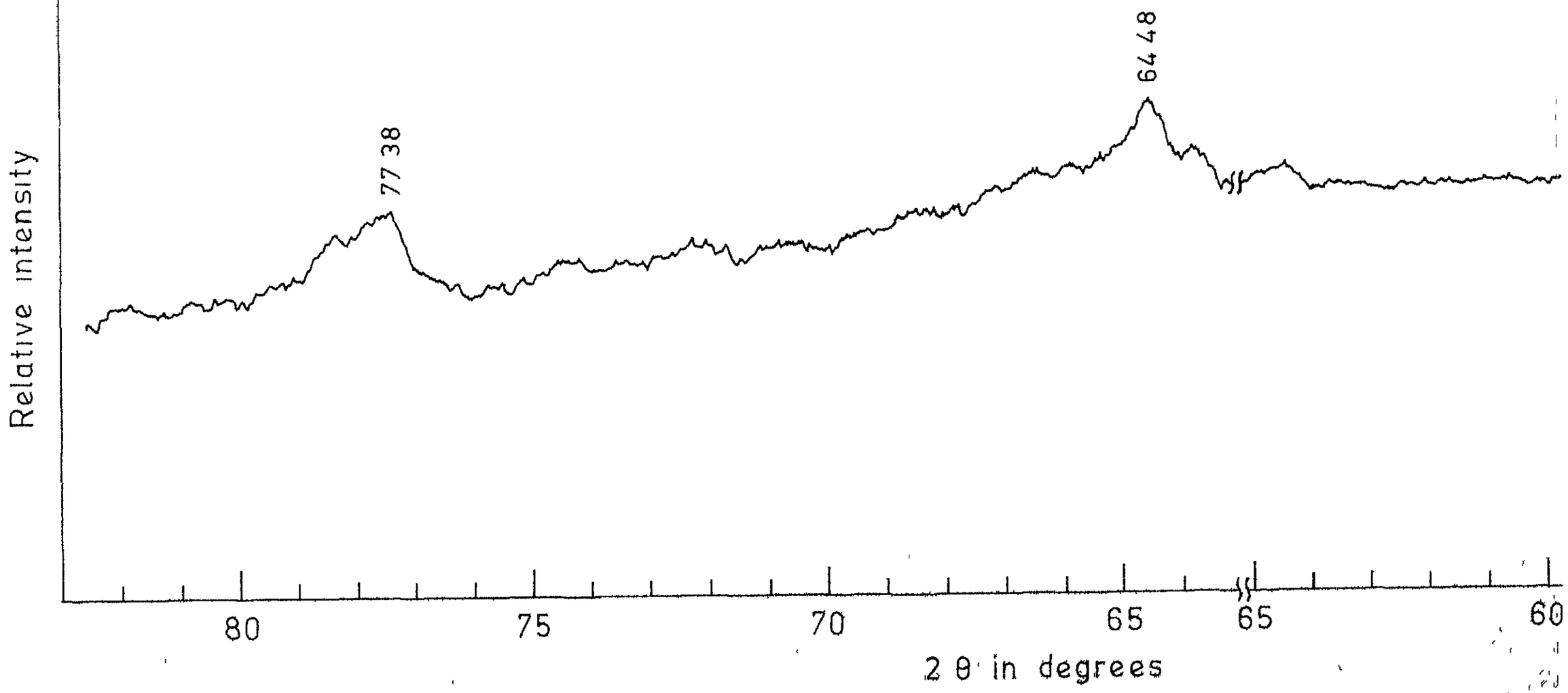

Fig. 4.14

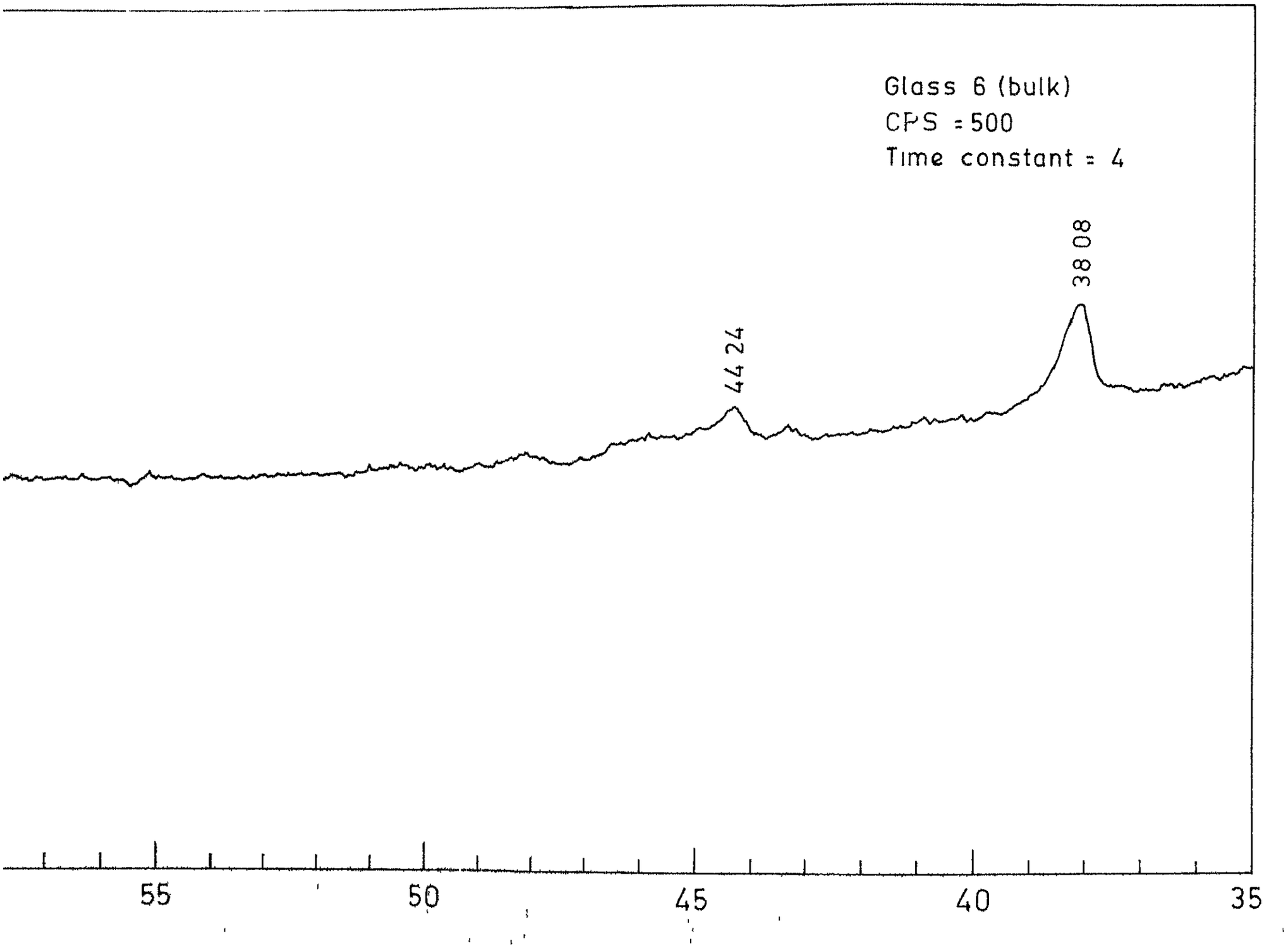
Glass 6 (bulk)
CPS = 500
Time constant = 4
44 24
38 08
55
50
45
40
35

Glass 7 (bulk)
CPS = 100
Time constant = 8

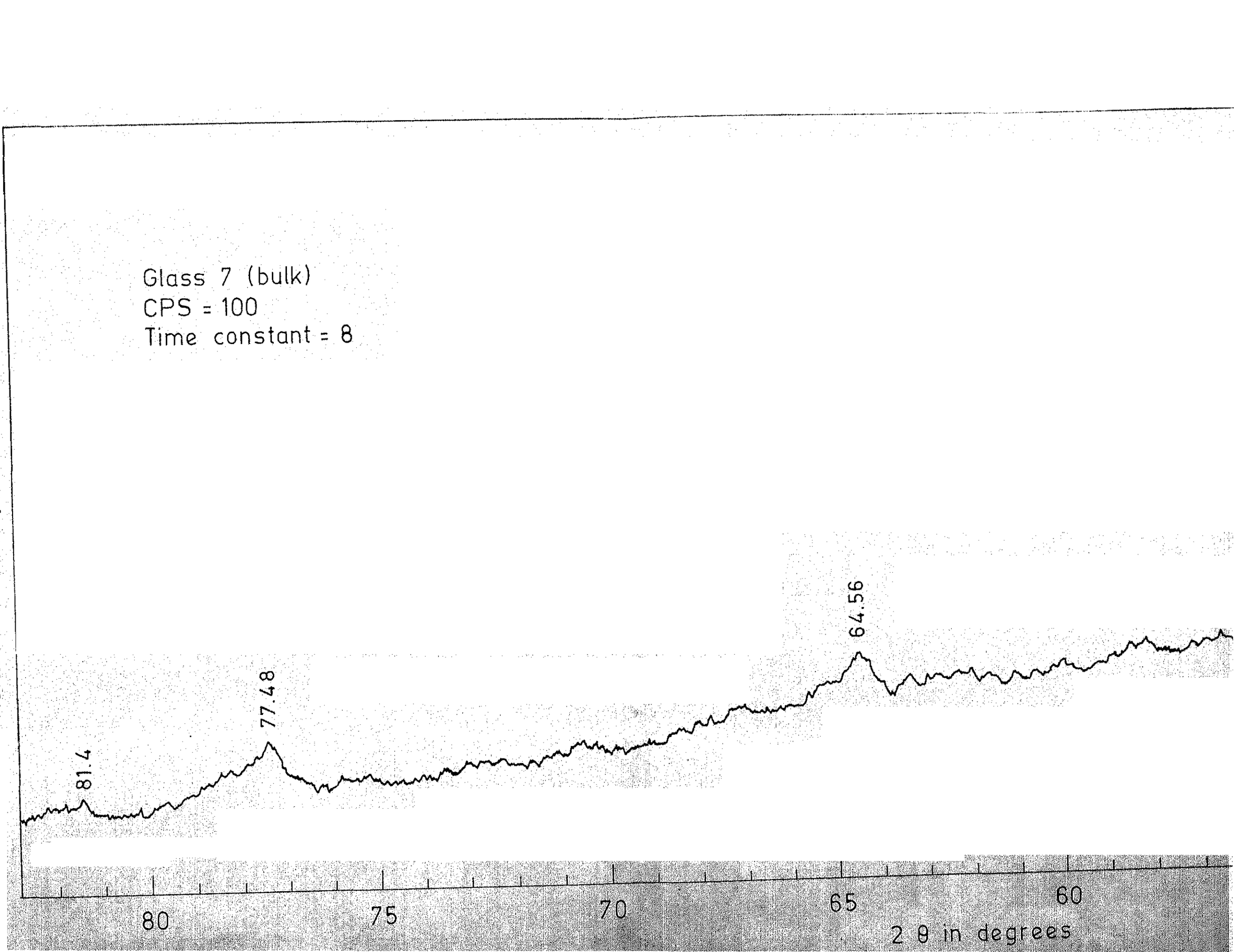

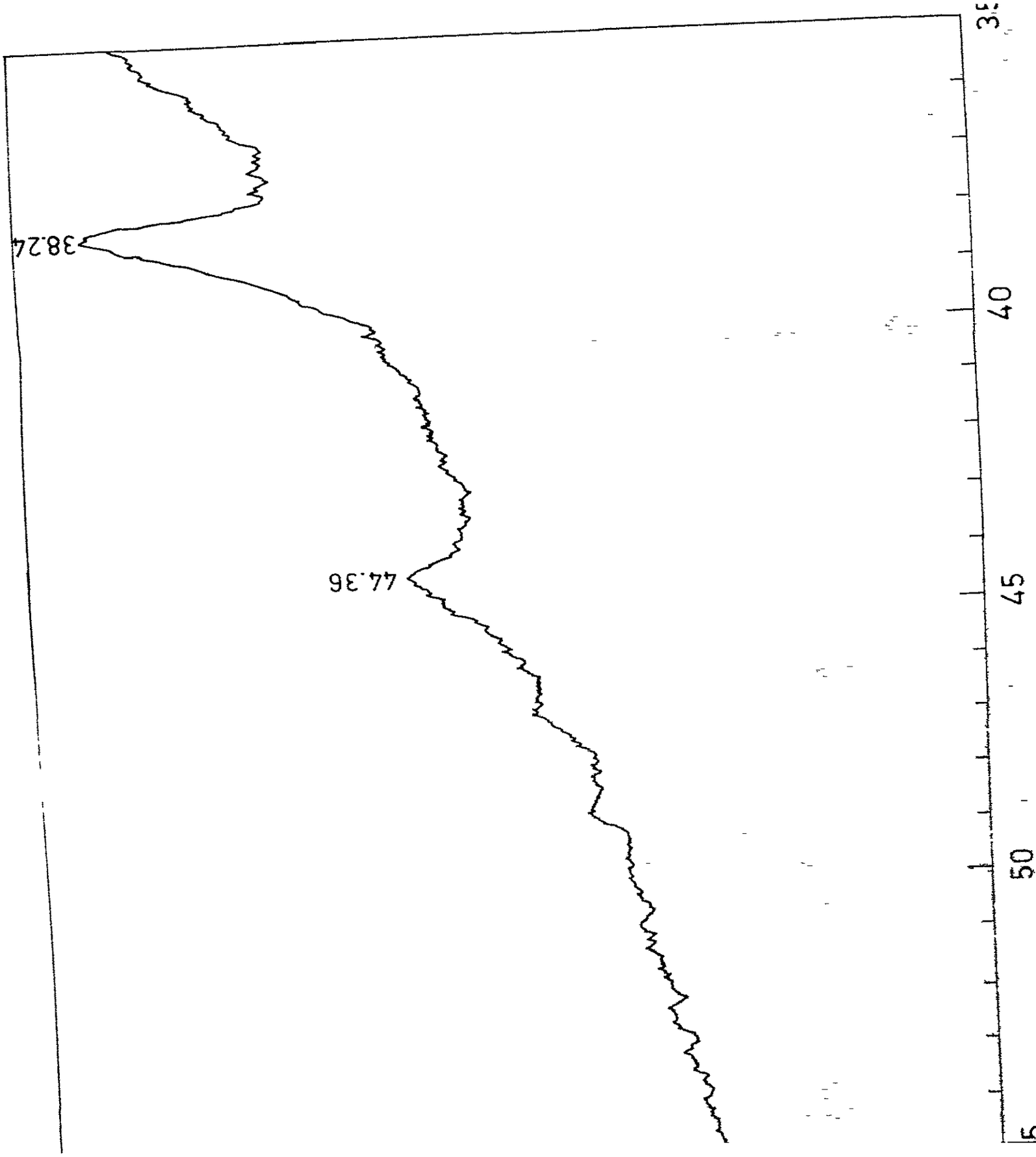
38.24
44.36
35
40
45
50
5

Glass 7 Fibres
CPS = 500
Time constant = 2

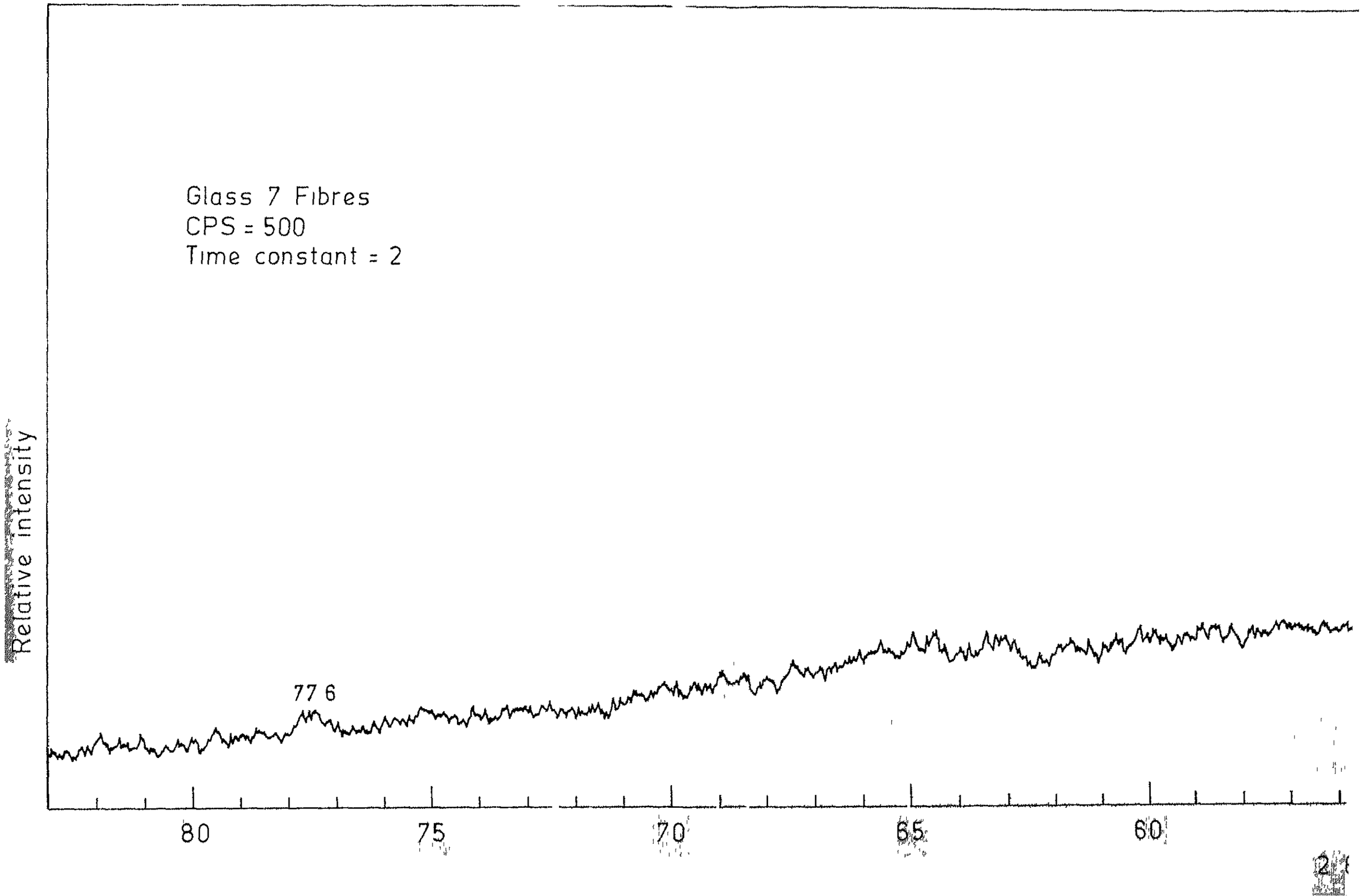

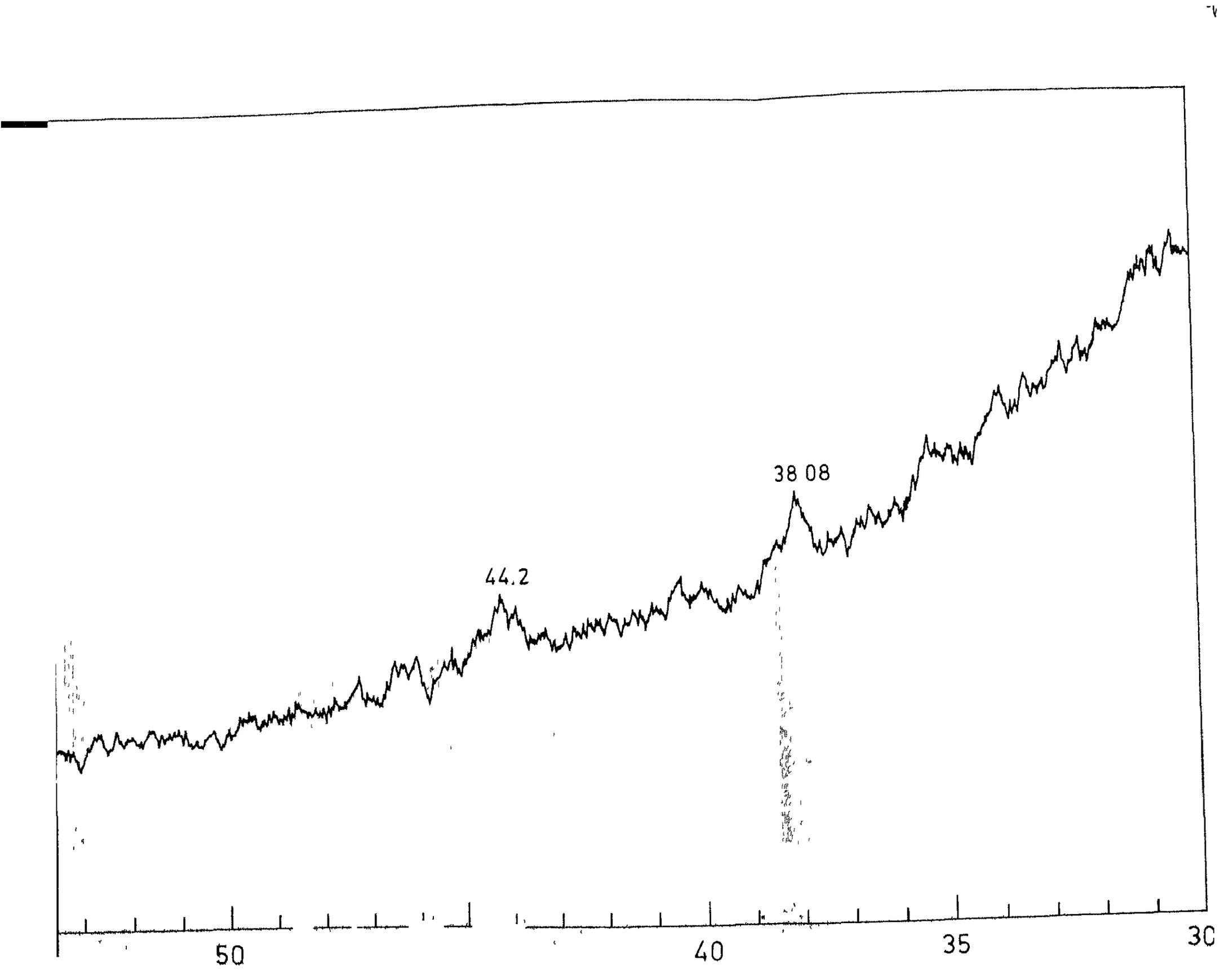
38 08
44.2
50
40
35
30

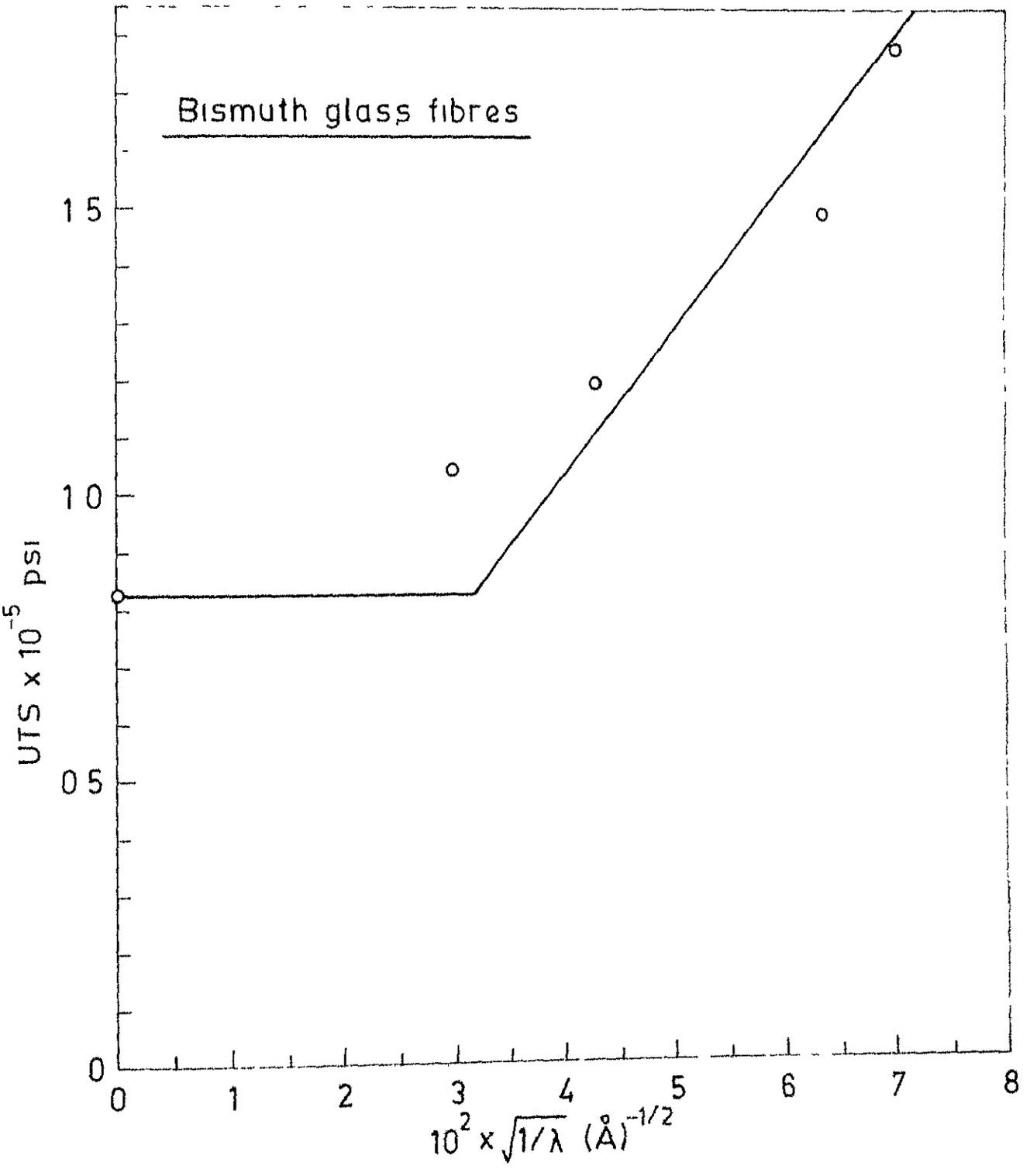
Bismuth glass fibres
UTS x 10^-5 psi
1 5
1 0
0 5
0
0
1
2
3
4
5
6
7
8
10^2 x √(1/λ) (Å)^-1/2

Fig 5.61

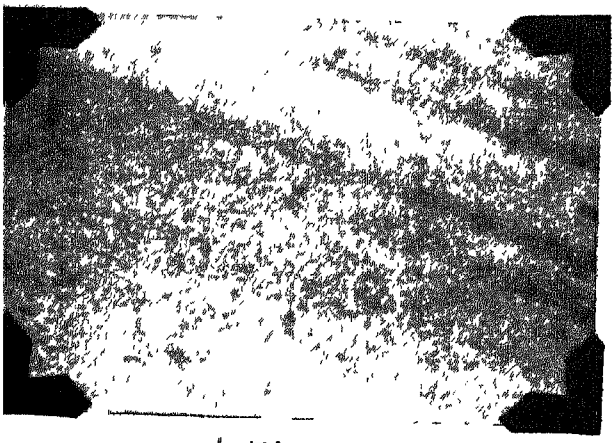

4 51
Magnification = 300 X

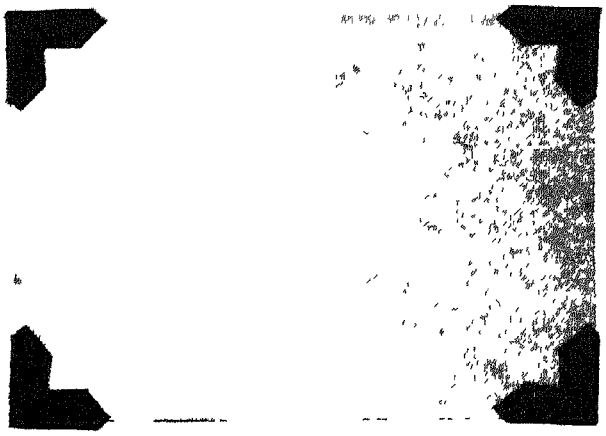

4 52
Magnification = 300 X

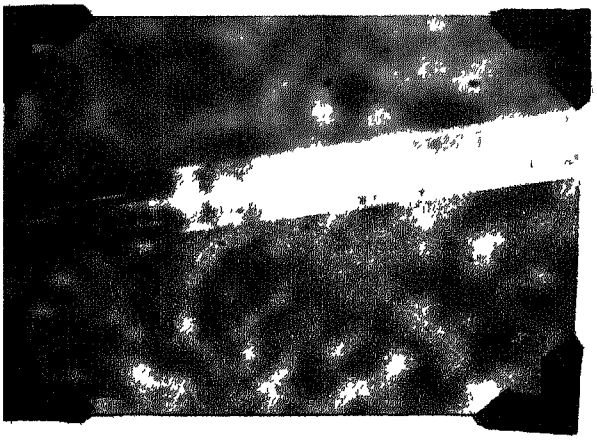

4·53
Magnification = 750 X

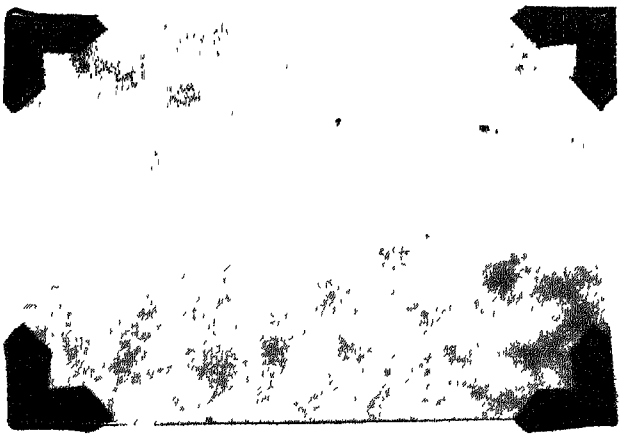

4.54
Magnification = 750 X

4·55
Magnification = 750 X

4.601
Magnification = 104230 X

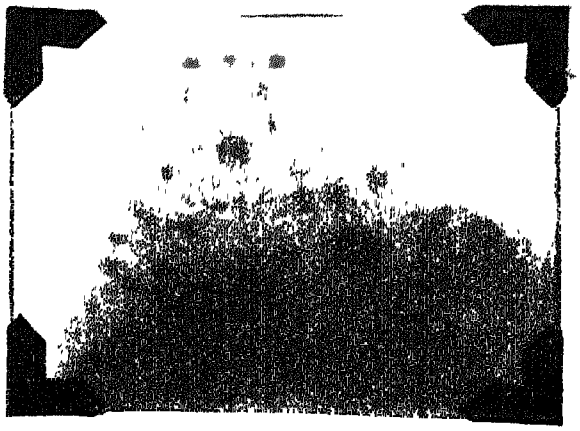

4.602
Magnification = 169041

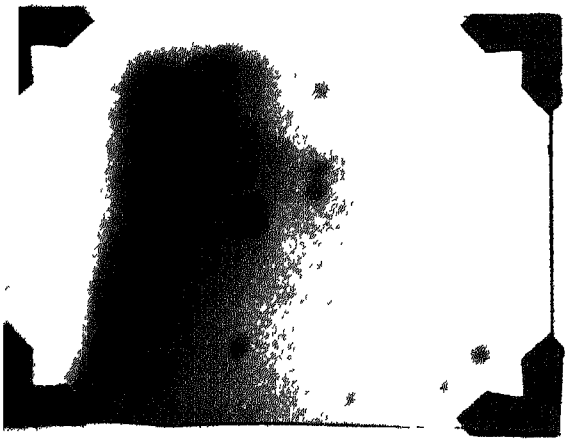

4 603
Magnification = 169484 X

4.604
Magnification = 58404 X

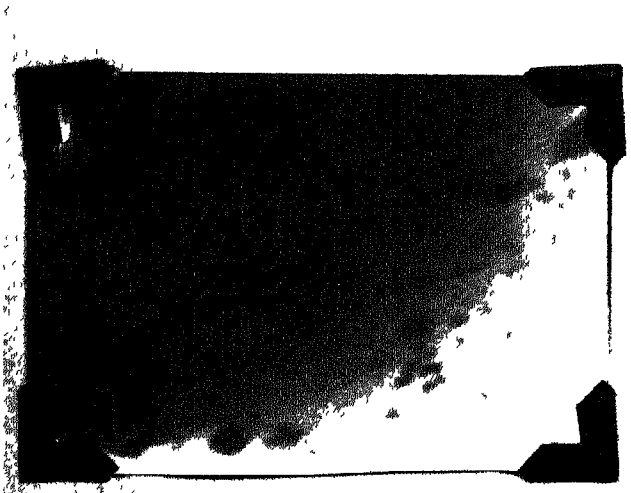

4.605
Magnification = 111133 X

4.606
Magnification = 169484 X

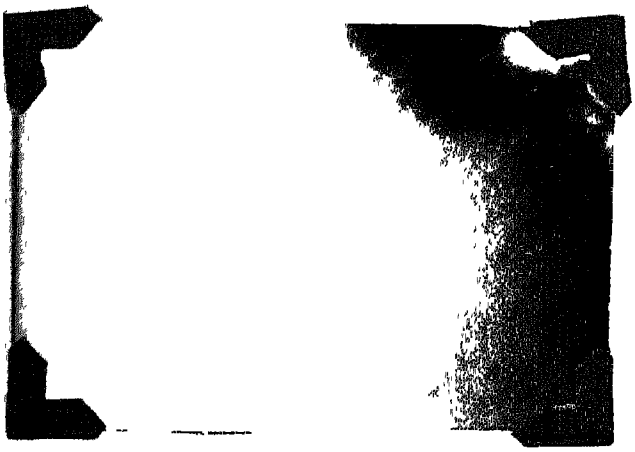

4-607
Magnification = 111133 X

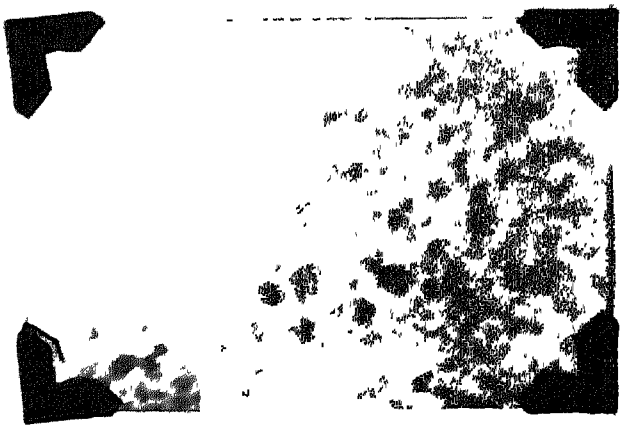

4-608
Magnification = 80779 X

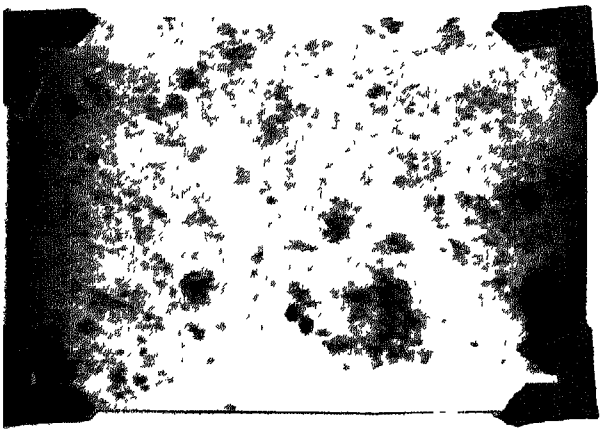

4 609
Magnification = 109752 X

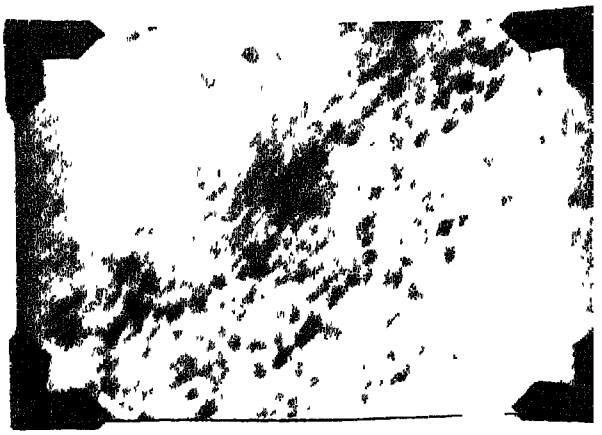

4 610
Magnification = 180637 X
Region of Diffraction 4.619

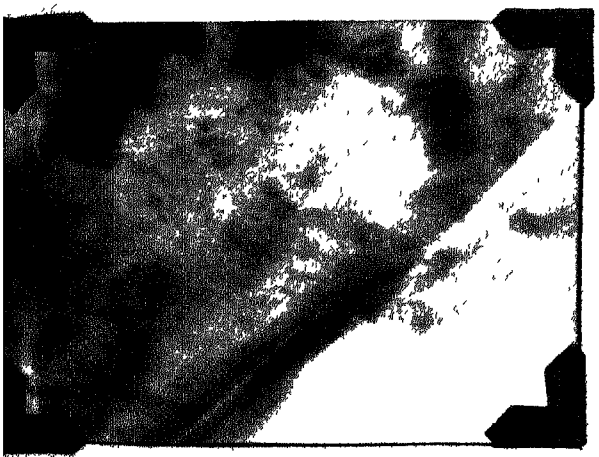

4-611
Magnification = 61582 X
Region of Diffraction 4-616

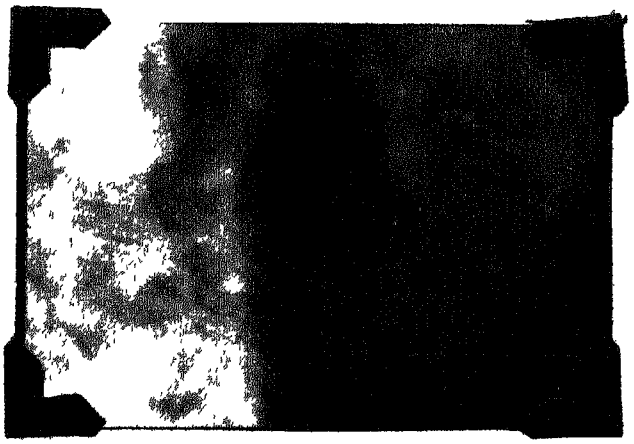

4-612
Magnification = 36584 X
Region of Diffraction 4.61[illegible]

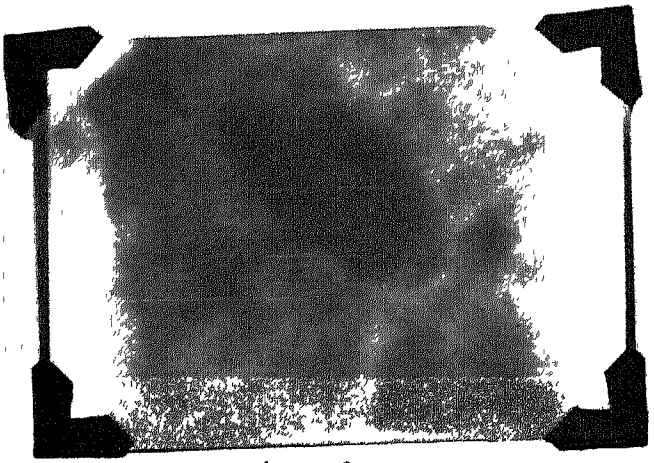

4.613
Magnification = 62690 X

4.614
Magnification = 75329 X
Region of diffraction 4-618

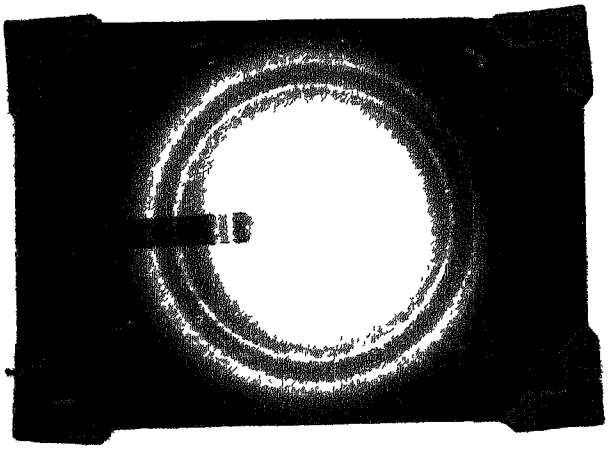

4 617

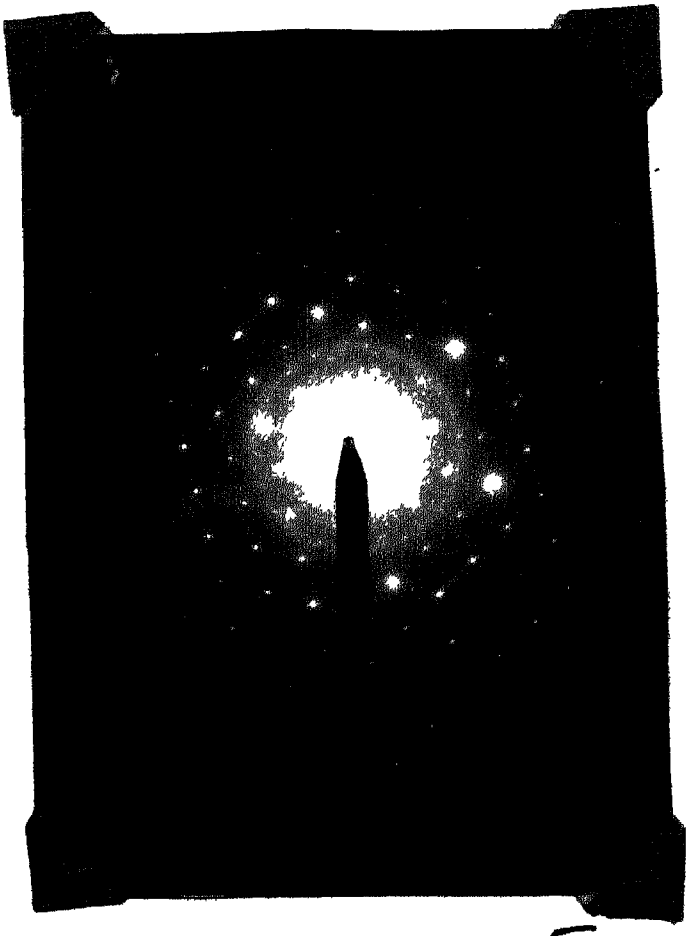

4.615

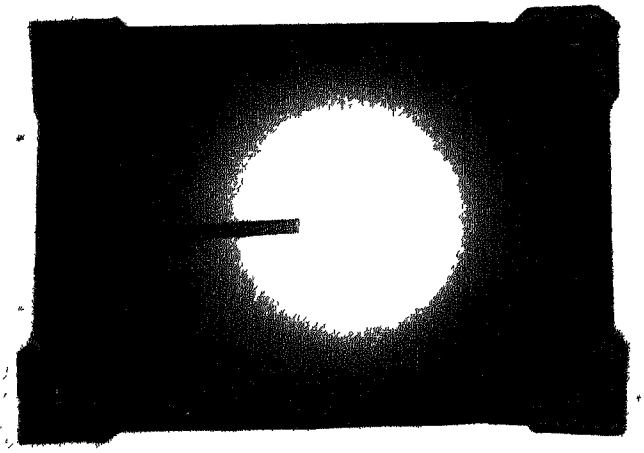

4.618

4 616

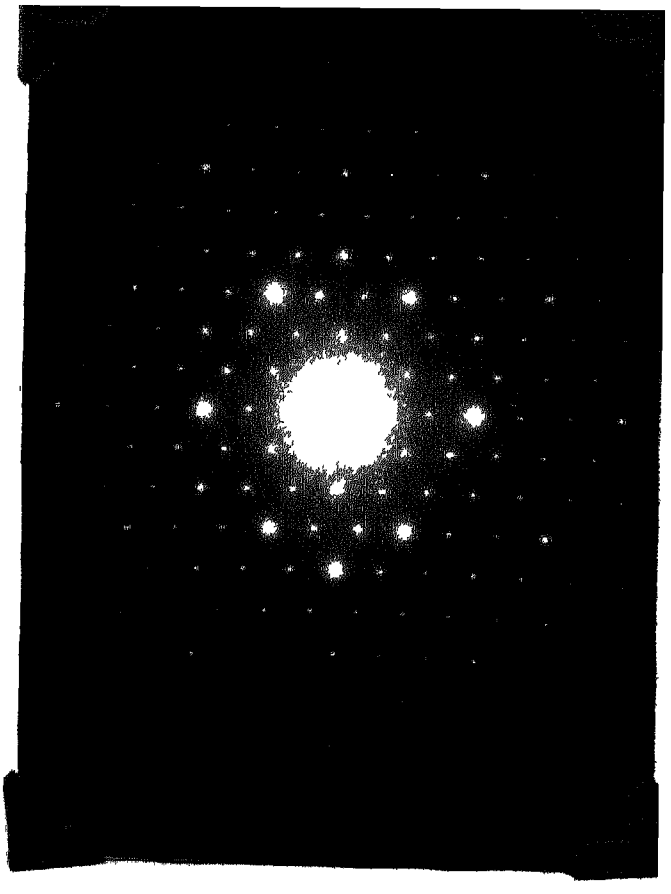

4·614

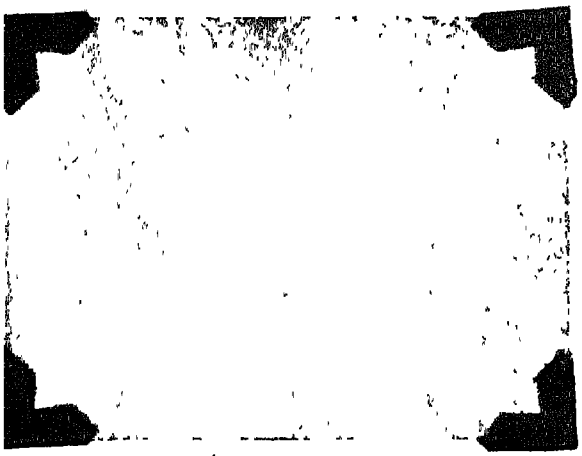

4.701.
Magnification = 5938 X

4.702
Magnification = 7731 X

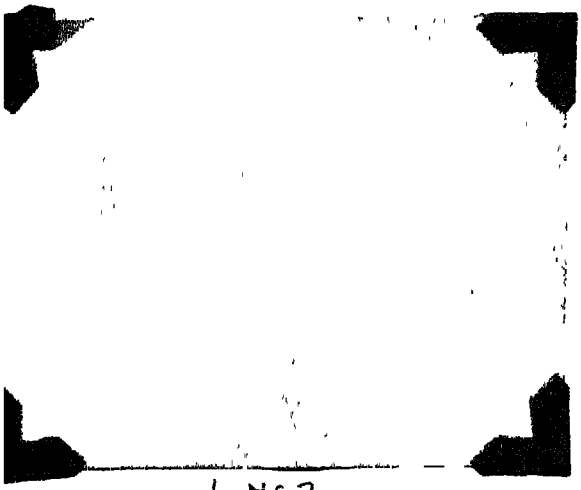

4.703
Magnification = 13901 X

4.704
Magnification = 28319 X

4.705
Magnification = 7533 X

4.706
Magnification = 2236 X

4.707
Magnification = 14623 X

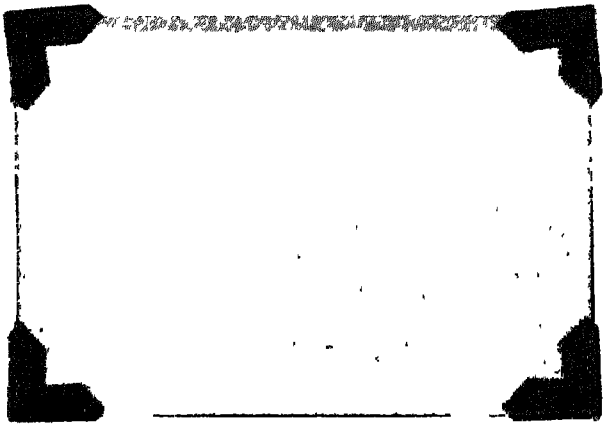

4.708
Magnification = 14442 X

4.710
Magnification = 8028 X

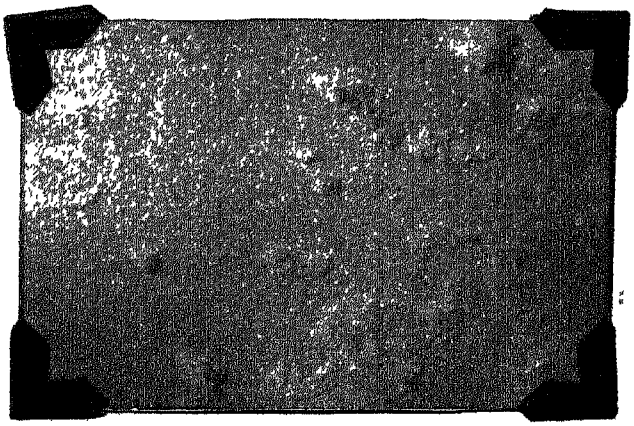

4.709
Magnification = 18064 X

Chapter 6

CONCLUSIONS

The following conclusions can be drawn from this study:

1. Bismuth and silver can be incorporated fairly easily into the glass matrix, during the melting process itself.

2. Fibres can be drawn without much difficulty from all the nine compositions.

3. All the metal containing glasses and glass fibres have a crystalline phase as is evident from TEM, Optical Microscope and x-ray diffraction studies. The crystalline phase is Bismuth in the case of the Bismuth containing glasses and glass fibres and is silver and calcium magnesium silicate in the silver series of glasses and fibres. The base glasses show no evidence of any crystalline phase.

4. The micro-structure in Bismuth containing glasses and glass fibres consists of a distribution of dark spheres in the glassy matrix. The spheres do not consist solely of Bismuth but probably contain some Alkali ions as well. Feeble diffraction spots are obtainable from these spheres and intense spots are obtained on subjecting the spheres to electron bombardment in the TEM. Diffraction spots are more intense in patchy regions.

In the silver glasses and glass fibres, the crystalline phase is not always spherical in shape. Here SAD is obtained from both spherical and patchy regions.

5. Optical microscopic evidence shows glasses 6 and 7 and glass fibres 5, 6 and 7 to be crystallized. The crystalline phase is relatively coarse grained but uniformly distributed in glasses 6 and 7 and is not quite spherical in shape.

In glass fibres 5, 6 and 7 the crystalline phase shows up as streaks along the fibre axis.

6. DTA studies show that the introduction of Ag_2O and Bi_2O_3 into the corresponding base glass compositions results in a lowering of the glass transition temperature.

The lowering is more for the silver glasses than for the Bismuth ones.

These oxides probably act as network modifiers and render the glass network less rigid.

7. The tensile strengths and Young's Modulii of Bismuth containing glasses and glass fibres are higher than the corresponding values for the base glass. Strengthening is attributable mainly to modulus enhancement and flaw size limitation. Rupture Modulii of silver containing glasses are higher than those of the base glass. Here, there is no

modulus enhancement and strengthening is due mainly to flaw size limitation and may be in a certain measure to induced thermo-mechanical compressive stresses.

Strengths of silver containing glass fibres are lower than those of the base glass fibres. This is because the pointed shape of the crystalline phase in these fibres leads to stress concentrating effects.

8. The effect of flaw density and the 'size effect' in metal containing glass fibres is much less than that in the base glass fibres.

9. Fracture surface replicas of metal containing glasses show a much higher degree of surface roughness than those of the base glasses. Replicas of glasses 6 and 7 also show fracture steps; which are a clear indication of the fact that the crack front is interacting with the dispersed particles.

LIST OF REFERENCES

1. T.K. Gupta, J. Mat. Sc., 9, 1585-1589, (1974).

2. D.P.H. Hasselman and R.H. Bulrath, J. Amer. Ceram. Soc. 49, 68-72 (1966).

3. A.A. Griffith, Phil. Trans. R. Soc., London, Ser. A., 221 [4], 163-198, (1920).

4. F.F. Lange, Phil. Mag. 22, [179], 983-992, (1970).

5. K.P. Borom, J.Amer. Ceram. Soc. 60,[1-2], 17-21,(1977).

6. R.H.Doremus and A.L. Turkalo, J.Mat.Sc., 11, Part 1, 903, (1976).

7. D.N. Koshavaram, M.Tech. Thesis, Materials Science Program, IIT Kanpur, Aug. 1978.

8. D. Chakravorty, C.D. Vaidhiari and G.K. Mehta, J. Mat. Sc. 13, 1438-1442, (1978).

9. S. Chakrabarti, M.Tech. Thesis, Materials Science Program, IIT Kanpur, 1979.

10. D. Chakravorty, A.K. Bandyophadyay and T.K. Nagesh, J. Phys. D: Appl. Phys., 10, 2077-2087, (1977).

11. S. Chakrabarti, M.Tech. Thesis, Materials Science Program, IIT Kanpur, 1979.

12. W.J. Thomas, Phys. Chem. Glasses, 1, 1-18, (1960).

13. P. Hing and D.W. McMillan, J. Mat. Sc. 9, 1041-1043, (1973).

Date Slip

This book is to be returned on the date last stamped.

MSP - 1979 - M-VEN - FRA